A PERFORMANCE BOUND FOR NONLINEAR CONTROL SYSTEMS

By

RAFAEL J. FANJUL JR.

A DISSERTATION PRESENTED TO THE GRADUATE SCHOOL
OF THE UNIVERSITY OF FLORIDA IN PARTIAL FULFILLMENT
OF THE REQUIREMENTS FOR THE DEGREE OF
DOCTOR OF PHILOSOPHY

UNIVERSITY OF FLORIDA

1996

To my parents, Rafael James and Estela Linares Fanjul,

my grandmother, Margaret Stewart Fanjul,

my aunt, Sheila Stewart,

and

my nephews, Frankie and Rafi Montalvo

ACKNOWLEDGEMENTS

I would like to express my gratitude to my advisor, Professor Hammer, for his encouragement, guidance and wisdom throughout the course of my studies. Professor Hammer has always found time to discuss my work and for that I am especially thankful.

I am grateful to Professor Crisalle for his many hours of assistance in formulating my research. I wish to thank Professor Schwartz for her help during the early stages of my research. In addition, I would like to thank Professor Anderson and Professor Principe for serving on my committee.

A number of my fellow students have provided both inspiration and advice. In particular, I wish to thank Victor Brennan, Patrick Walker, Aiguo Yan, and Kuo-Huei Yen for their help over the past four-and-a-half years. Finally, I would like to thank Margaret Fanjul Montalvo and Christopher Riffer for editing the manuscript.

TABLE OF CONTENTS

ACKNOWLEDGEMENTS iv

ABSTRACT vii

CHAPTERS

1 INTRODUCTION 1

1.1 Background 4
1.2 Notation 7

2 TERMINOLOGY AND BASICS 8

2.1 Right Fraction Representations and Coprimeness 12
2.2 Generalized Right Inverse 15

3 THE PERFORMANCE BOUND 18

3.1 Causality of Systems 18
3.2 Systems with the Lipschitz Norm 20
3.3 Approximate Right Inverse 22
3.3.1 The Existence Theorem of Best Approximate Right Inverse 24
3.4 The Measure of Right Singularity 27

4 CALCULATION OF THE PERFORMANCE BOUND 30

4.1 The Estimate of the Performance Bound 30
4.2 Practical Implementation Techniques 31
4.3 Permanent Magnet Stepper Motor Model Example 35
4.3.1 Simulation 37
4.3.2 The Estimate of the Performance Bound $\tilde{\mathcal{P}}(\Sigma)$ 39
4.4 Aerodynamic Model Example 44
4.4.1 Simulation 46
4.4.2 The Estimate of the Performance Bound $\tilde{\mathcal{P}}(\Sigma)$ 51
4.5 Multivariable Process Control Model Example 60
4.5.1 Simulation 63
4.5.2 The Estimate of the Performance Bound $\tilde{\mathcal{P}}(\Sigma)$ 65

5 CONCLUSION 73

5.1 Summary 73
5.2 Future Directions 74

REFERENCES 77
BIOGRAPHICAL SKETCH 80

Abstract of Dissertation Presented to the Graduate School
of the University of Florida in Partial Fulfillment of the
Requirements for the Degree of Doctor of Philosophy

A PERFORMANCE BOUND FOR NONLINEAR CONTROL SYSTEMS

By

Rafael J. Fanjul Jr.

December 1996

Chairman: Professor Jacob Hammer
Major Department: Electrical and Computer Engineering

This research focuses on the control of a nonlinear system whose output subject to an additive disturbance. The main interest is in the investigation of controllers that reduce the effect of the disturbance on the system output. Usually, it is not possible to construct a controller that completely eliminates the effects of the disturbance. It is then of interest to find how well the "best" controller can attenuate the effect of the disturbance. The main result of this dissertation is a performance bound, that provides an estimate of the best disturbance attenuation that can be achieved for a given system, using a causal controller that renders the system internally stable.

An approximate right inverse of a nonlinear system Σ is introduced to facilitate the derivation of the performance bound and the development of nonlinear controllers. An approximate right inverse is constructed to be stable and causal for implementation purposes. The difference between an approximate right inverse and a right inverse is that the right inverse may not be both stable and causal. The role

of an approximate right inverse is to approximate a disturbed signal with a signal in the image of the system Σ. An approximate right inverse can be constructed for any system Σ.

The calculation of the performance bound involves an optimization process of finding a global maximum of a non-convex function. For several cases, a nonlinear programming algorithm is developed to handle the optimization. To demonstrate the application of this performance bound, it is calculated for three practical systems:

1. the voltage control of a permanent magnet stepper motor;
2. the longitudinal control of an aircraft; and
3. the multivariable process control of a regulator that regulates the liquid level in a pressurized tank.

CHAPTER 1
INTRODUCTION

Over the last 2 decades, there has been considerable interests in the literature in the derivation of optimal controllers that minimizes the effect of the disturbance on the output of a control system. This dissertation addresses this question for the case of nonlinear systems. The main objective is to derive an estimate of the performance of an optimal controller, by deriving a bound on the effect of the disturbance has on the system output when the optimal controller is used. Using this bound, we can then gauge the performance of suboptimal controller, to see how well they compare to the optimal ones. Suboptimal controllers may be much easier to implement than their optimal counterparts. Thus, our performance bound can be use to find simple controllers whose disturbance attenuation properties are close to those of optimal disturbance attenuating controllers.

The performance bound derived in this dissertation came from the requirement to characterize the performance of a controller that reduces the effect of the disturbance on the output to a minimum. The original work provided is the derivation of the performance bound and nonlinear programming algorithm in how to calculate the performance bound. The application of the performance bound for disturbance attenuation is proposed as future directions.

The basic design problem to which this performance bound relates is the problem of disturbance attenuation for nonlinear control systems. Specifically, this dissertation discusses the following configuration. In the configuration of Figure 1.1, Σ is the nonlinear system to be controlled. C represents an equivalent controller that incorporates all the control elements of the loop. The external (or reference) signal

is denoted by v; the disturbance signal is denoted by d; and the output signal is denoted by z. The closed loop system is required to be internally stable. Internal stability signifies that a configuration can tolerate small disturbances on its external and internal ports (including ports within the equivalent controller C) without losing stability. The equations that describe Figure 1.1 are

$$z = d + y, \quad y = \Sigma u, \quad u = C(v, z). \tag{1.1}$$

In Figure 1.1, Σ_C represents the appropriate equivalent system. This can be expressed in notation

$$z = \Sigma_C(v, d) \tag{1.2}$$

where the output signal z is determined by the signals v and d and depends on the system Σ as well as the equivalent controller C. We would like to reduce as much as possible the effects of d on z. Our bound, which is the attainable performance for control of a nonlinear system whose output is subject to an additive disturbance, provides an estimate of the minimal effect of d on z. Using the estimates of the minimal effect, we can evaluate controllers. The analysis of the dissertation is restricted to the case of discrete-time systems.

The desired response, with or without the disturbance signal for the configuration in Figure 1.1, is $z = \Sigma v$. To null out the disturbance signal, the design of the equivalent controller C would be such that $y = \Sigma u = \Sigma v - d$. Substituting for y in

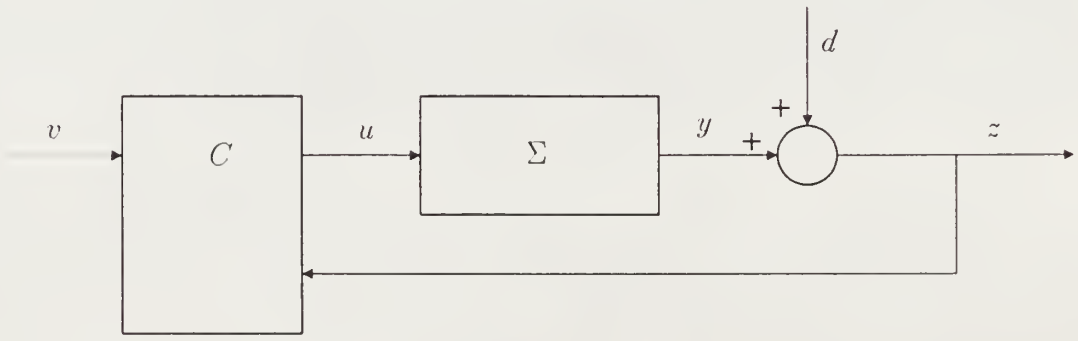

Figure 1.1: The block diagram of Σ_C.

the first equation of (1.1), this yields $z = \Sigma v$ which is our stated goal. For the sake of argument, assume that the system Σ has a stable and causal inverse system Σ^{-1}. The input signal u to the system Σ would then be required to be $u = \Sigma^{-1}(\Sigma v - d)$. The inverse system Σ^{-1} in some cases might not be implementable because it is not stable or it is not causal. For those cases, approximations of the inverse systems would then be used for practical implementation. The approximations will be selected in a manner suited to approximate the signal $\Sigma v - d$ with a signal in the image of Σ.

The composition of the system and its approximate inverse system forms a nearly identity system. For points inside the image of the system Σ, the composition will appear as the identity. For external points, which are points outside the image of the system Σ, the composition will produce a point in the image of Σ that is closest to the external point. Our performance bound is a norm that gauges the closeness of the identity system and a nearly identity system formed from the system Σ and its approximate inverse.

The performance where Σ_C can attain by using our bound is determined by the inherent properties of the system Σ. The bound is directly related to an *approximate inverse*. The role of an approximate inverse is to approximate the signal u with a signal v in the image of Σ. Therefore, the approximate invertibility of the system Σ provides a measure of the ability to match a set S by a subset of the image of the system Σ. A *measure of singularity* is introduced as an indicator of approximate invertibility which is then used to derive the performance bound. To demonstrate the application of this performance bound, it is calculated for three practical systems:

1. the voltage control of a permanent magnet stepper motor;

2. the longitudinal control of an aircraft; and

3. the multivariable process control of a regulator that regulates the liquid level in a pressurized tank.

The dissertation is organized as follows. Chapter 2 contains the basic notions of nonlinear systems including the theory of fraction representation. Chapter 3 discusses an approximate right inverse and the performance bound. Chapter 4 discusses the main results of the dissertation, including calculations of the performance bound for applications. Chapter 5 contains a summary and future directions.

1.1 Background

This section contains a qualitative survey of some topics in nonlinear control that are important to the dissertation. A more technical discussion of these topics is provided in Chapter 2.

The description of Σ_C in Figure 1.1 has its origins in the theory of fraction representation of nonlinear systems. It can be stated that a *right fraction representation* of a nonlinear system Σ is a factorization of Σ into a composition form $\Sigma = PQ^{-1}$, where P and Q are stable systems with Q being invertible. In Hammer [16, 18], tools for a compact and perceptive statement of results were developed for the theory of fraction representation of nonlinear systems. The fraction representation $\Sigma = PQ^{-1}$ is said to be *coprime* when the systems P and Q are right coprime. An attribute of right coprime fraction representation is that every instability of the inverse system Q^{-1} is also an instability of the system Σ; i.e., there is no cancellation of instabilities within the composition PQ^{-1}.

A causal (respectively, strictly causal) system Σ is one where the values of the output sequence Σu up to and including index i (respectively, $i+1$) depend only on the values of the input sequence u up to index i. A system is bicausal if it is causal and if it possesses a causal inverse.

In this dissertation, it is assumed that the system Σ being controlled can be stabilized, that it is strictly causal, and that it possesses a right coprime fraction representation of the form $\Sigma = PQ^{-1}$, with Q being bicausal. The stabilization

assumption on the system Σ is necessary because the closed loop system is required to be internally stable. Strict causality is placed on the system Σ as a handy assumption to certify that the closed loop system is well posed. Strict causality is not an essential condition and it can be replaced with plain causality combined with a well-posedeness requirement. This dissertation relies on stabilization theory which applies only to systems possessing right coprime fraction representations.

A result from [22] gives a simple parameterization of the set of all system responses that can be obtained through internally stable control of a given system. The control scheme to control Σ is shown Figure 1.1. The parameterization provides a clear indication of the effects of the disturbance on the response of the stabilized closed loop system. This result can be summarized as follows. Let $\Sigma = PQ^{-1}$ be a right coprime fraction representation (with a bicausal "denominator" Q) of the system being controlled. Then,

1. For every causal equivalent controller C for which the closed loop system of Figure 1.1 is internally stable, there exists a stable and causal system $\phi(v, d)$ such that

$$\Sigma_C(v, d) = d + P\phi(v, d) = [I + P\phi(v, \cdot)]d \tag{1.3}$$

   where P is the "numerator" of the right coprime fraction representation of Σ and I denotes the identity system.

2. Conversely, for every stable and causal system $\phi(v, d)$, there is an internally stable control configuration around the system Σ for which the equivalent system $\Sigma_C(v, d)$ satisfies $\Sigma_C(v, d) = [I + P\phi(v, \cdot)]d$.

Thus, equation (1.3) provides a complete parameterization of the class of all responses $\{\Sigma_C\}$ that can be obtained by internally stable control of the system Σ, with the stable and causal system ϕ serving as the sole parameter. In other words, for every ϕ, there is an equivalent controller C that internally stabilizes Σ and yields

the response (1.3). Conversely, every equivalent controller C that internally stabilizes Σ generates an explicit ϕ.

On a superficial inspection of (1.3), the attainable performance is prescribed by the "numerator" system P of Σ because it is the only fixed quantity apart from the identity. For a linear time-invariant system, it was shown in [50] that the attainable performance was determined by the location of its right half-plane zeros. For a nonlinear system Σ, the instabilities of P^{-1} (the inverse of the "numerator" system P) would be analogous to the right half-plane zeros of a linear time-invariant system. Using this analogy it could be inferred that the instabilities of P^{-1} would limit performance. The performance bound developed in the dissertation will further confirm this hypothesis.

1.2 Notation

The following notational convention will apply unless otherwise stated.

$\Re^m$	: The set of m-dimensional real vectors.
$S(\Re^m)$	: The set of m-dimensional real vector sequences.
D^λ	: The λ-step shift operator.
$\mathcal{L}(\Sigma) \geq \lambda$	: The system Σ has latency of at least λ.
$\|u\|$	: The ℓ^∞-norm of the sequence u.
$\rho(u)$	: The weighted ℓ^∞-norm of the sequence u.
$\|\Sigma\|$	: The Lipschitz semi-norm of the system Σ.
$\mathcal{B}$	: The set of all stable, causal and recursive systems $\Sigma\colon \mathcal{D} \to S(\Re^p)$ where $\mathcal{D}$ is a bounded subset of $S(\Re^m)$.
$Lip(\mathcal{D}, S(\Re^p))$	: The subset of $\mathcal{B}$ with $\|\Sigma\| < \infty$.
$\|\Sigma\|_{Lip}$	: The Lipschitz norm of the system Σ.
$\varrho_{M_\epsilon}(u, S_2)$	: The distance from any $u \in S_1$ and the set S_2.
$\varrho_\epsilon(S_1, S_2)$	: The maximal distance from any $u \in S_1$ and the set S_2.
$\mathcal{P}(\Sigma)$	: The right singularity of measure of the system Σ.

CHAPTER 2
TERMINOLOGY AND BASICS

This chapter contains a summary of the principal mathematical results which are needed in the dissertation. The presentation is for discrete-time time-invariant nonlinear systems. Almost all the necessary mathematics are contained in [9, 14, 17, 18, 22, 27].

The set of real numbers is denoted by $\Re$. The set of m-dimensional real vectors is denoted by $\Re^m$. The set of all sequences u is denoted by $S(\Re^m)$ where $u = \{u_0, u_1, u_2, \ldots\}$ of m-dimensional real vectors $u_i \in \Re^m$, $i = 0, 1, 2, \ldots$. Given the sequence $u \in S(\Re^m)$, the i^{th} element is denoted by u_i. The set of elements $\{u_i, u_{i+1}, \ldots, u_j\}$ where $j \geq i \geq 0$ is denoted by u_i^j. A *system* Σ, from an input/output perspective, is a map $\Sigma\colon S(\Re^m) \to S(\Re^p)$ which transforms input sequences of m-dimensional real vectors into output sequences of p-dimensional real vectors. The image of a subset $S \subset S(\Re^m)$ through the system Σ is denoted by $\Sigma[S]$. The entire image of system the Σ is denoted by $\operatorname{Im}\Sigma$ where $\operatorname{Im}\Sigma \stackrel{\text{def}}{=} \Sigma[S(\Re^m)]$. Given a system $\Sigma\colon S(\Re^m) \to S(\Re^p)$ and an input sequence $u \in S(\Re^m)$, we denote by $\Sigma u]_i \stackrel{\text{def}}{=} y_i$ the i^{th} element of the output sequence $y = \Sigma u$, and by $y = \Sigma u]_i^j$ the set of elements $\{y_i, y_{i+1}, \ldots, y_j\}$ where $j \geq i \geq 0$ are integers.

There are two kinds of binary operations, addition and composition. For a pair of systems $\Sigma_1, \Sigma_2\colon S(\Re^m) \to S(\Re^p)$, the *sum* is defined, as usual, by $(\Sigma_1 + \Sigma_2)u \stackrel{\text{def}}{=} \Sigma_1 u + \Sigma_2 u$ for all sequences $u \in S(\Re^m)$; the right side of the last formula is the usual elementwise addition of sequences of real vectors. *Composition* is the usual composition of maps.

Definition 2.0.1 *A system* $\Sigma: S(\Re^m) \to S(\Re^p)$ *is* causal *(respectively,* strictly causal*) if it satisfies the following condition. For every integer* $i \geq 0$ *and for every pair of input sequences* $u, v \in S(\Re^m)$ *satisfying* $u_0^i = v_0^i$*, the output sequences satisfy* $\Sigma u]_0^i = \Sigma v]_0^i$ *(respectively,* $\Sigma u]_0^{i+1} = \Sigma v]_0^{i+1}$*).*

A system $M: S(\Re^m) \to S(\Re^m)$ is *bicausal* if it is causal and if it possesses a causal inverse.

A system $\Sigma: S(\Re^m) \to S(\Re^p)$ is called a *recursive system* if there is a pair of integers $\eta, \mu \geq 0$ and a function $f: (\Re^p)^{\eta+1} \times (\Re^m)^{\mu+1} \to \Re^p$ such that, for every input sequence $u \in S(\Re^m)$, the corresponding output sequence $y \stackrel{\text{def}}{=} \Sigma u$ can be computed recursively in the form

$$y_{k+\eta+1} = f(y_k, \ldots, y_{k+\eta}, u_k, \ldots, u_{k+\mu}) \tag{2.1}$$

for all integers $k \geq 0$. The initial conditions $y_0, \ldots, y_\eta$ must of course, be specified and fixed. The function f is called a *recursion function* of Σ. For causality (strict causality), the condition $\eta+1 \geq \mu$ ($\eta \geq \mu$) is placed on system Σ. The class of strictly causal systems include every system $\Sigma: S(\Re^m) \to S(\Re^p)$ that can be represented in the form

$$\begin{aligned} x_{k+1} &= f(x_k, u_k) \\ y_k &= h(x_k), \qquad k = 1, 2, \ldots. \end{aligned} \tag{2.2}$$

Here, $u \in S(\Re^m)$ is the input sequence; $y \in S(\Re^p)$ is the output sequence; and $x \in S(\Re^n)$ is an intermediate sequence of "states." In the case that the maps $f: \Re^n \times \Re^m \to \Re^n$ and $h: \Re^n \to \Re^p$ are continuous, then the system (2.2) constitutes a *continuous realization* of the system Σ.

For a real number $\theta > 0$, the set of all vectors in $\Re^m$ with components in the closed interval $[-\theta, \theta]$ is denoted by $[-\theta, \theta]^m$. The set of all sequences $u \in S(\Re^m)$ with elements u_i belonging to $[-\theta, \theta]^m$ for all integers $i \geq 0$ is denoted by $S(\theta^m)$.

Thus, $S(\theta^m)$ consists of all sequences bounded by θ. It follows then that a system $\Sigma: S(\Re^m) \to S(\Re^p)$ is BIBO (Bounded-Input Bounded-Output)-*stable* if for every real number $\theta > 0$, there exists a real number $M > 0$ such that $\Sigma[S(\theta^m)] \subset S(M^p)$. A sequence $u \in S(\Re^m)$ is said to be *bounded* if there is a real number $\theta > 0$ such that $u \in S(\theta^m)$.

The basic notion of stability that is used in this dissertation is related to continuity with respect to a metric. Two norms are particularly useful in this context to derive a metric: the ℓ^∞-norm and the weighted ℓ^∞-norm. The ℓ^∞-norm is denoted by $|\cdot|$; for a vector $a = (a_1, a_2, \ldots, a_m) \in \Re^m$, it is simply $|a| \stackrel{\text{def}}{=} \max\{|a_1|, |a_2|, \ldots, |a_m|\}$. For a sequence $u \in S(\Re^m)$, the ℓ^∞-norm is given by

$$|u| \stackrel{\text{def}}{=} \sup_{i \geq 0} |u_i|. \tag{2.3}$$

The weighted ℓ^∞-norm is denoted by ρ_ϵ and is given by

$$\rho_\epsilon(u) \stackrel{\text{def}}{=} \sup_{i \geq 0} (1+\epsilon)^{-i} |u_i|, \quad \epsilon > 0 \tag{2.4}$$

for a sequence $u \in S(\Re^m)$. For purposes of this dissertation different values of ϵ will not affect our results; hence, the subscript will be dropped and the weighted ℓ^∞-norm is simply denoted by ρ. The use of the weighted ℓ^∞-norm simplifies mathematical arguments over the ℓ^∞-norm because the bounded set of sequences $S(\theta^m)$ is compact with respect to ρ. The norm ρ induces a metric $\boldsymbol{\rho}$ on a given $S(\Re^m)$, for every pair of elements $u, v \in S(\Re^m)$, by $\boldsymbol{\rho}(u, v) \stackrel{\text{def}}{=} \rho(u - v)$. Formally, the notion of stability employed in this dissertation is as follows.

Definition 2.0.2 *A system $\Sigma: S(\Re^m) \to S(\Re^p)$ is* stable *with respect to the metric $\boldsymbol{\rho}$ if it is BIBO-stable, and if the restriction $\Sigma: S(\alpha^m) \to S(\Re^p)$ is continuous with respect to $\boldsymbol{\rho}$ for every real number $\alpha > 0$.*

Definition 2.0.2 is usually referred to as *input/output stability*. The following concept, which describes a weak form of uniform continuity with respect to the ℓ^∞-norm, plays a fundamental role in stabilization theory (see [17]).

Definition 2.0.3 *A stable system* $\Sigma: S(\Re^m) \to S(\Re^p)$ *is* differentially bounded *if there is a pair of real numbers* $\varepsilon, \theta > 0$ *such that, for every pair of sequences* $u \in S(\Re^m)$ *and* $\nu \in S(\varepsilon^m)$, *one has* $|\Sigma(u+\nu) - \Sigma(u)| \leq \theta$.

So far, only stability properties of individual systems have been mentioned. When several individual systems are combined into a composite system, a stronger notion of stability is required, and it is usually referred to as *internal stability.* Internal stability guarantees desirable stability properties of the composition, and takes into account the effects of various disturbances and noises that may affect the component systems. Consider a composite system $\Sigma^{(s)}$ that consists of s individual systems, labeled $\Sigma^1, \ldots, \Sigma^s$ where $\Sigma^i: S(\Re^{m(i)}) \to S(\Re^{p(i)})$, $i = 1, \ldots, s$. Individual entries in the list $\Sigma^1, \ldots, \Sigma^s$ may represent summers, multipliers, etc. Let $u \in S(\Re^m)$ be the external input sequence of the composite system, and let $y \in S(\Re^p)$ be its output sequence. Let $u^j \in S(\Re^{m(j)})$ be the input sequence of the system Σ^j within the configuration, and let $y^j \in S(\Re^{p(j)})$ be its output sequence. The interconnections among the subsystems are then characterized by a set of equalities $u^i = y^{j(i)}$, which determine to which output each input is connected. The external signal u is now augmented by s new input signals $\eta^i \in S(\Re^{m(i)})$, $i = 1, \ldots, s$, and set $u^i \stackrel{\text{def}}{=} y^{j(i)} + \eta^i$. For each i, the η^i acts as an additive disturbance on the input port of the system Σ^i. The disturbances are all assumed to be bounded by a real number $\delta > 0$, so that in fact $\eta^i \in S(\delta^{m(i)})$, $i = 1, \ldots, s$.

Let $\Sigma^{*s*}: S(\Re^m) \times S(\Re^{m(1)}) \times \cdots \times S(\Re^{m(s)}) \to S(\Re^p) \times S(\Re^{p(1)}) \times \cdots \times S(\Re^{p(s)}): (u, \eta^1, \ldots, \eta^s) \mapsto \Sigma^{*s*}(u, \eta^1, \ldots, \eta^s)$ denote the system induced by the interconnected system $\Sigma^{(s)}$ and the disturbances, having the input signals $u, \eta^1, \ldots, \eta^s$ and the output signals $y, y^1, \ldots, y^s$, respectively.

Definition 2.0.4 *The composite system* $\Sigma^{(s)}$ *is* internally stable *if the system* Σ^{*s*} *is stable in the sense of Definition 2.0.2. The composite system* $\Sigma^{(s)}$ *is* strictly internally stable *if, besides being stable, the system* Σ^{*s*} *is also differentially bounded.*

Definition 2.0.5 *A system* $\Sigma: S(\Re^m) \to S(\Re^p)$ *is* entirely stabilizable *if there is a strictly internally stable control configuration that stabilizes* Σ *over the entire input space* $S(\Re^m)$.

2.1 Right Fraction Representations and Coprimeness

A right fraction representation of a system $\Sigma: S(\Re^m) \to S(\Re^p)$ is determined by three quantities: a subset $S \subset S(\Re^q)$, $q > 0$, called the *factorization space*; and two stable systems $P: S \to S(\Re^p)$ and $Q: S \to S(\Re^m)$, where Q is invertible, such that $\Sigma = PQ^{-1}$. A right fraction representation $\Sigma = PQ^{-1}$ is *coprime* whenever the stable systems P and Q are right coprime according to the following definition ([16, 18]). (Let $G: S_1 \to S_2$ be a map, where $S_1 \subset S(\Re^m)$ and $S_2 \subset S(\Re^n)$ are subsets. For a subset $S \subset S(\Re^n)$, we denote $G^*[S]$ the inverse image of S through G, i.e., the set of all sequences $u \in S_1$ satisfying $Gu \in S$.)

Definition 2.1.1 *Let* $S \subset S(\Re^q)$ *be a subset. Two stable systems* $P: S \to S(\Re^p)$ *and* $Q: S \to S(\Re^m)$ *are* right coprime *whenever the following conditions hold.*

1. *For every real number* $\tau > 0$ *there is a real number* $\theta > 0$ *such that*

$$P^*[S(\tau^p)] \cap Q^*[S(\tau^m)] \subset S(\theta^q).$$

2. *For every real number* $\tau > 0$ *the set* $S \cap S(\tau^q)$ *is a closed subset of* $S(\tau^q)$ *(with respect to the topology induced by* $\boldsymbol{\rho}$*).*

The concept of a homogeneous system is of key importance to the theory of right coprime fraction representations of nonlinear systems. A homogeneous system has the property of being a continuous map whenever its outputs are bounded. The precise definition is as follows.

Definition 2.1.2 *A system* $\Sigma: S(\Re^m) \to S(\Re^p)$ *is a* homogeneous system *if the following holds for every real number* $\alpha > 0$*: for every subset* $S \subset S(\alpha^m)$ *for which*

there exists a real number $\tau > 0$ *satisfying* $\Sigma[S] \subset S(\tau^p)$, *the restriction of* Σ *to the closure* $\overline{S}$ *of* S *in* $S(\alpha^m)$ *is a continuous map* $\Sigma: S \to S(\tau^p)$.

The importance of homogeneous systems to the dissertation is stated in the next two theorems.

Theorem 2.1.3 [17] *An injective system* $\Sigma: S(\Re^m) \to S(\Re^p)$ *has a right coprime fraction representation if and only if it is a homogeneous system.*

Theorem 2.1.4 [17] *Let* $\Sigma: S(\Re^m) \to S(\Re^p)$ *be a recursive system. If* Σ *has a recursive representation* $y_{k+\eta+1} = f(y_k, \ldots, y_{k+\eta}, u_k, \ldots, u_{k+\mu})$ *with a continuous recursion function* f, *then* Σ *is a homogeneous system.*

The following two theorems are important for stabilization theory. Theorem 2.1.5 defines the technical details in the stabilizing system Σ in Figure 2.1 with $\pi = B^{-1}$ and $\varphi = A$. Theorem 2.1.6 uses a basic property or right coprime factorization, which is the denominator system contains the exact information about the instabilities of the system, of right coprime fraction representation for stabilization.

Theorem 2.1.5 [19] *Let* $\Sigma: S(\alpha^m) \to S(\Re^p)$ *be a system with a bounded input space* $S(\alpha^m)$, $\alpha > 0$, *and assume it has a right coprime fraction representation* $\Sigma = PQ^{-1}$, *where* $P: S \to S(\Re^p)$ *and* $Q: S \to S(\alpha^m)$, *and where* $S \subset S(\Re^q)$ *for some integer* $q >$

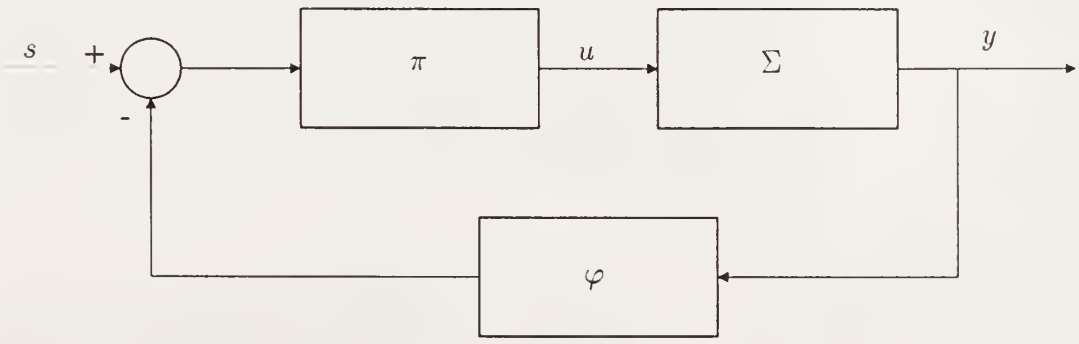

Figure 2.1: The block diagram of $\Sigma_{(\pi,\varphi)}$.

0. *Then, for every stable system* $M: S \to S$ *with a stable inverse system* $M^{-1}: S \to S$, *there exists a pair of stable systems* $A: S(\Re^p) \to S(\Re^q)$ *and* $B: S(\alpha^m) \to S(\Re^q)$ *such that* $AP + BQ = M$.

Theorem 2.1.6 [22] *Let* $\Sigma: S(\Re^m) \to S(\Re^p)$ *be a system having a right coprime fraction representation* $\Sigma = PQ^{-1}$, *where* $P: S \to S(\Re^p)$, $Q: S \to S(\Re^m)$, $S \subset S(\Re^m)$, *and where* Q *is bicausal. Let* $D: S(\Re^r) \to S(\Re^m)$ *be any stable and causal system for which the composition* $\Sigma D: S(\Re^r) \to S(\Re^p)$ *is stable. Then, there is a stable and causal system* $\phi: (\Re^r) \to S$ *such that* $D = Q\phi$.

In Figure 1.1, $\Sigma: S(\Re^m) \to S(\Re^p)$ is a strictly causal system that needs to be controlled. It will be convenient to regard the external input sequence v as a fixed "parameter" while regarding the disturbance d as an external input, i.e., to consider appropriate partial functions. Since no restriction will be placed on v and d, this will have no effect on the validity of the final result. In the same spirit, we shall use the notation

$$\Psi(v)z \stackrel{\text{def}}{=} C(v, z)$$

in which v can be intuitively viewed as a parameter of the system $\Psi(v)$, while z is its input. Control is achieved by a causal nonlinear dynamic controller $C: S(\Re^m) \times S(\Re^p) \to S(\Re^m): (v, z) \mapsto C(v, z)$. For Figure 2.2, $\Psi(v)z \stackrel{\text{def}}{=} C(v, z)$ was defined with the system $\Psi(v): S(\Re^p) \to S(\Re^m): z \mapsto \Psi(v)z = u$. A result of [22] is now stated

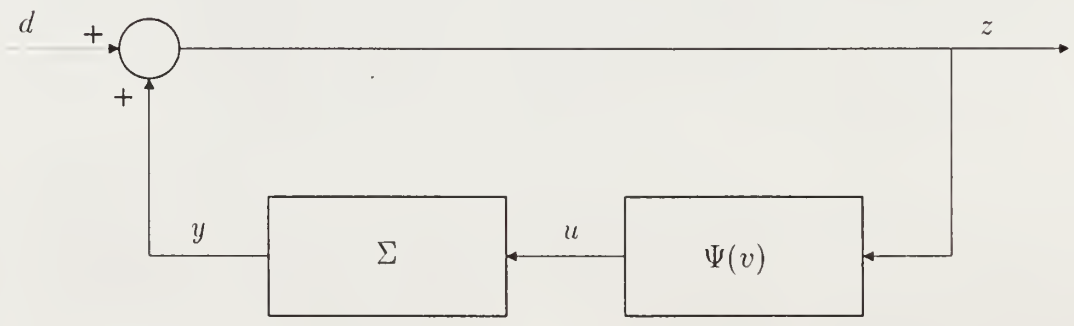

Figure 2.2: The block diagram of $\Sigma_{\Psi(v)}$.

formally in Theorem 2.1.7. which furnishes a parameterization of the class of all systems that can be obtained from a given system Σ by internally stable control.

Theorem 2.1.7 [22] *Let $\Sigma: S(\Re^m) \to S(\Re^p)$ be a strictly causal system having a right coprime fraction representation $\Sigma = PQ^{-1}$ with a bicausal denominator $Q: S(\Re^m) \to S(\Re^m)$. Assume that Σ can be strictly internally stabilized by a controller that admits representation $C_i(s,z) = G^{-1}(z)[s + Tz] = u$. Then, referring to (1.2), the following is true. The class of all input&disturbance/output responses Σ_C that can be achieved through internally stable control of Σ is given by*
$\{\Sigma_C(v,d) = [I + P\phi(v)]d,\ \phi(\cdot): S(\Re^m) \times S(\Re^p) \to S(\Re^m): (v,d) \mapsto \phi(v)d$ *is a stable and causal system*$\}$.

A special case of Theorem 2.1.7 is when the system Σ is stable. In that case, the right coprime factorization of $\Sigma = PQ^{-1}$ can be taken as $P = \Sigma$ and $Q = I$, and the following is obtained.

Corollary 2.1.8 [22] *Let $\Sigma: S(\Re^m) \to S(\Re^p)$ be a strictly causal, stable and differentially bounded system. Then, referring to (1.2), the following is true. The class of all input&disturbance/output responses Σ_C that can be achieved through internally stable control of Σ is given by*
$\{\Sigma_C(v,d) = [I + \Sigma\phi(v)]d,\ \phi(\cdot): S(\Re^m) \times S(\Re^p) \to S(\Re^m): (v,d) \mapsto \phi(v)d$ *is a stable and causal system*$\}$.

2.2 Generalized Right Inverse

For the nonlinear recursive system $\Sigma: S(\Re^m) \to S(\Re^p)$ to possess a right inverse, the system Σ is required to be surjective. By restricting the range of Σ to the image of Σ, a surjective system $\Sigma^r: S(\Re^m) \to \operatorname{Im}\Sigma$ is obtained with its right inverse system $\Sigma^*: \operatorname{Im}\Sigma \to S(\Re^m)$. Let $\Sigma^g: S(Re^p) \to S(\Re^m)$ be any extension of Σ^* from $\operatorname{Im}\Sigma$ to the whole space $S(\Re^p)$. Then, for every element $y \in \operatorname{Im}\Sigma$, it is evident that

$\Sigma\Sigma^g y = \Sigma\Sigma^* y = y$. The system Σ^g is a *generalized right inverse* of the system Σ. The generalized right inverse of system Σ is non-unique when system Σ is not bijective. The next theorem and its corollaries from [14] state that a recursive system has a recursive generalized right inverse.

Theorem 2.2.1 [14] *A recursive system* $\Sigma: S(\Re^m) \to S(\Re^p)$ *has a recursive generalized right inverse* $\Sigma^g: S(\Re^p) \to S(\Re^m)$.

A couple of notes from the proof of Theorem 2.2.1. Let the system $\Sigma^*: \operatorname{Im}\Sigma \to S(\Re^m)$ be the recursive system represented by

$$u_{k+\mu} = g(u_k, \ldots, u_{k+\mu-1}, y_k, \ldots, y_{k+\mu+\eta+1}). \tag{2.5}$$

In order to extend the domain of Σ^* from $\operatorname{Im}\Sigma$ to all $S(\Re^p)$, let $g^e: (\Re^m)^\mu \times (\Re^p)^{\eta+\mu+2} \to \Re^m$ be any extension of the function g. Then, the recursive system $\Sigma^g: S(Re^p) \to S(\Re^m)$ represented by

$$u_{k+\mu} = g^e(u_k, \ldots, u_{k+\mu-1}, y_k, \ldots, y_{k+\mu+\eta+1}) \tag{2.6}$$

is a generalized right inverse of Σ.

Corollary 2.2.2 [14] *Let* $\Sigma: S(\Re^m) \to S(\Re^p)$ *be a recursive isomorphism. Then, its inverse* $\Sigma^{-1}: S(\Re^p) \to S(\Re^m)$ *is also a recursive isomorphism.*

Theorem 2.2.1 cannot be generalized to the case of an arbitrary domain $\mathcal{D}$. Nevertheless, Theorem 2.2.1 can be generalized to the case when the domain $\mathcal{D}$ is in the following particular form. A subset $\mathcal{D} \subset S(\Re^m)$ is *recursive* if there exists an integer ξ and a function σ assigning each point $(\alpha_0, \ldots, \alpha_\xi) \in (\Re^m)^{\xi+1}$ a subset $\sigma(\alpha_0^\xi) \subset \Re^m$ such that $\mathcal{D}$ consists of exactly all sequences $u \in S(\Re^m)$ satisfying $u_{k+\xi+1} \in \sigma(u_k^{k+\xi})$ for all integers k. The function σ is called the *generating function* of $\mathcal{D}$. For instance, if $\Pi: S(\Re^q) \to S(\Re^m)$ is a recursive system, then $\operatorname{Im}\Pi$ is a recursive subset of $S(\Re^m)$.

Corollary 2.2.3 [14] *A recursive system* $\Sigma: \mathcal{D} \to S(\Re^p)$, *where* $\mathcal{D}$ *is a recursive subset of* $S(\Re^m)$, *has a recursive right inverse* $\Sigma^*: \operatorname{Im}\Sigma \to \mathcal{D}$.

CHAPTER 3
THE PERFORMANCE BOUND

This chapter starts by discussing causality of systems and Lipschitz norms which will be useful in establishing the existence theorem of a best approximate right inverse. The performance bound will later be defined as a lower bound for the performance index of the approximate right inverse optimization problem.

3.1 Causality of Systems

Recall a causal system Σ is one for which the values of the output sequence Σu up to and including index i depend only on the values of the input sequence u up to index i. This was precisely defined in Definition 2.0.1.

For an integer λ, the λ-step shift operator is denoted by D^λ, defined, on any sequence u by

$$D^\lambda u]_k \stackrel{\text{def}}{=} u_{k-\lambda} \tag{3.1}$$

for all integer k for which $u_{k-\lambda}$ exists.

Definition 3.1.1 *Let $\Sigma: S_1 \to S_2$ be a system, where $S_1 \subset S(\Re^m)$ and $S_2 \subset S(\Re^p)$. The system Σ has* latency of at least λ *if there is an integer λ such that, for every pair of input sequences $u, v \in S_1$ and for every integer $k \geq 0$, the equality $u_0^k = v_0^k$ implies $\Sigma u]_0^{k+\lambda} = \Sigma v]_0^{k+\lambda}$.*

We write $\mathcal{L}(\Sigma) \geq \lambda$ if the system Σ has latency of at least λ. Intuitively, the latency represents a 'time delay' incurred in the propagation of changes from the input of Σ to the output of Σ. It is a simple consequence of the definition that a system Σ is causal if and only if $\mathcal{L}(\Sigma) \geq 0$, and it is strictly causal if and only if $\mathcal{L}(\Sigma) \geq 1$. From [17], a few simple properties of latency are listed.

Theorem 3.1.2 [17] *Let* $\Sigma_1: S_1 \to S_2$ *and* $\Sigma_2: S_2 \to S_3$, *where* $S_1 \subset S(\Re^m)$, $S_2 \subset D^{\lambda_1}[S(\Re^p)]$ *and* $S_3 \subset D^{\lambda_1+\lambda_2}[S(\Re^q)]$, *be systems, each with a well-defined latency, respectively* $\mathcal{L}(\Sigma_1) \geq \lambda_1$ *and* $\mathcal{L}(\Sigma_2) \geq \lambda_2$. *Under this hypothesis the composition* $\Sigma \stackrel{\text{def}}{=} \Sigma_2\Sigma_1$ *has a well-defined latency, and* $\mathcal{L}(\Sigma) \geq \lambda_1+\lambda_2$. *In particular if* $\lambda_1+\lambda_2 \geq 0$ *then* Σ *is a causal system.*

Theorem 3.1.3 [17] *Let* $\Sigma: S_1 \to S_2$, *where* $S_1 \subset S(\Re^m)$ *and* $S_2 \subset S(\Re^p)$, *be a recursive system with a recursive representation* $y_{k+\eta+1} = f(y_k, \ldots, y_{k+\eta}, u_k, \ldots, u_{k+\mu})$ *(and some fixed initial conditions). Under this hypothesis* Σ *has well-defined latency, and* $\mathcal{L}(\Sigma) \geq \eta + 1 - \mu$.

Theorem 3.1.4 [17] *A system* $\Sigma: S_1 \to S_2$, *where* $S_1 \subset S(\Re^m)$ *and* $S_2 \subset S(\Re^p)$, *has well-defined latency if and only if there exists an integer* λ *such that the system* $D^{-\lambda}\Sigma: S_1 \to D^{-\lambda}[S_2]$ *is a causal system.*

The system $\Sigma: S_1 \to S_2$, where $S_1 \subset S(\Re^m)$ and $S_2 \subset S(\Re^p)$, is a recursive system with a recursive representation $y_{k+\eta+1} = f(y_k, \ldots, y_{k+\eta}, u_k, \ldots, u_{k+\mu})$. By restricting the range of Σ to the image of Σ, we obtain the map $\Sigma^r: S_1 \to \Sigma[S_1]$ which is evidently surjective and possesses a right inverse $\Sigma^*: \Sigma[S_1] \to S_1$ such that $\Sigma\Sigma^* y = y$ for $y \in \Sigma[S_1]$. From Theorem 2.2.1, the system Σ^* is recursive with a recursive representation given by

$$u_{k+\mu} = g(u_k, \ldots, u_{k+\mu-1}, y_k, \ldots, y_{k+\mu+\eta+1}). \tag{2.5}$$

Examining (2.5), $\eta + 1$ shifts are required on the output of a right inverse system Σ^* to guarantee causality, i.e., $\mathcal{L}(D^{(\eta+1)}\Sigma^*) \geq 0$.

Lemma 3.1.5 *Let* $\Sigma: S_1 \to S_2$, *where* $S_1 \subset S(\Re^m)$ *and* $S_2 \subset S(\Re^p)$, *be a recursive system with a recursive representation* $y_{k+\eta+1} = f(y_k, \ldots, y_{k+\eta}, u_k, \ldots, u_{k+\mu})$. *Let* $\Sigma^*: \Sigma[S_1] \to S_1$ *be a right inverse of* Σ *by restricting the range of* Σ *to the image of* Σ *with a recursive representation* $u_{k+\mu} = g(u_k, \ldots, u_{k+\mu-1}, y_k, \ldots, y_{k+\mu+\eta+1})$. *Under this hypothesis the system* Σ *has a* latency of at most $\eta + 1$, *i.e.,* $\mathcal{L}(D^{(\eta+1)}\Sigma^*) \geq 0$.

3.2 Systems with the Lipschitz Norm

In the previous chapter we discussed two norms: the ℓ^∞-norm and the weighted ℓ^∞-norm. We will need to define a new norm for a set of systems that has the convergence property which is that every Cauchy sequence in a compact metric space $(X, \boldsymbol{\rho})$ converges to some point of X. The Lipschitz norm for a set of systems is introduced here because it has the necessary convergence property. The Lipschitz norm will be derived from a semi-norm. The semi-norm definition from [41] is given below.

Definition 3.2.1 *A* semi-norm *on a vector space X is a real-valued function p on X for all x and y in X and all scalars α such that*

1. $p(x+y) \leq p(x) + p(y)$
2. $p(\alpha x) = |\alpha| p(x)$
3. $p(x) \neq 0$ *if* $x \neq 0$.

In this section, we let $(S(\Re^m), \boldsymbol{\rho})$ and $(S(\Re^p), \boldsymbol{\rho})$ be two metric spaces over the set of all sequences of m-dimensional and p-dimensional real vectors. Let $\mathcal{B}$ be the set of all stable, causal, and recursive systems $\Sigma: \mathcal{D} \to S(\Re^p)$ where $\mathcal{D}$ is a bounded subset of $S(\Re^m)$. Introduce an operator $\|\cdot\|: \mathcal{B} \to \Re^+$ defined by

$$\|\Sigma\| \stackrel{\text{def}}{=} \sup_{u_1, u_2 \in \mathcal{D},\, u_1 \neq u_2} \frac{\rho(\Sigma(u_1) - \Sigma(u_2))}{\rho(u_1 - u_2)}. \tag{3.2}$$

The number $\|\Sigma\|$ has the following properties.

Lemma 3.2.2 *If $\Sigma, \Psi \in \mathcal{B}$ and $a \in \Re$, then*

1. $\|\Sigma\| = 0$ *if and only if* Σ *is a constant system on* $\mathcal{D}$;
2. $\|a\Sigma\| = |a| \, \|\Sigma\|$; *and*

3. $\|\Sigma + \Psi\| \leq \|\Sigma\| + \|\Psi\|$.

The number $\|\Sigma\|$ is called the *Lipschitz semi-norm* ([7]) of the system Σ on $\mathcal{D}$. A semi-norm has the property that $\|\Sigma\| = 0$ does not necessarily imply that $\Sigma = 0$. In fact, it can be easily seen that $\|\Sigma\| = 0$ if and only if Σ is a constant system (need not be zero) that maps all sequences from $\mathcal{D}$ to the same sequence in $S(\Re^p)$. The Lipschitz semi-norm is like a derivative bound or gain for all systems in $\mathcal{B}$. Let's define $Lip(\mathcal{D}, S(\Re^p))$ as the subset of $\mathcal{B}$ satisfying $\|\Sigma\| < \infty$.

It is clear that an element Σ of $\mathcal{B}$ is in $Lip(\mathcal{D}, S(\Re^p))$ if and only if there is a number $L \geq 0$ such that

$$\rho(\Sigma(u_1) - \Sigma(u_2)) \leq L\rho(u_1 - u_2)$$

for all $u_1, u_2 \in \mathcal{D}$. Moreover, $\|\Sigma\|$ is the "least" such number L. It is also evident that *a system with the Lipschitz semi-norm is both bounded and continuous on its domain.* The Lipschitz semi-norm will be used to define the boundary of a set from which an approximate right inverse can be chosen. The semi-norm $\|\cdot\|$ can be made into a norm as seen in the following theorem.

Theorem 3.2.3 *Let u_0 be an element of $\mathcal{D}$ and let*

$$\begin{aligned} \|\Sigma\|_{Lip} &\stackrel{\text{def}}{=} \rho(\Sigma(u_0)) + \|\Sigma\| \\ &= \rho(\Sigma(u_0)) + \sup_{u_1, u_2 \in \mathcal{D}, u_1 \neq u_2} \frac{\rho(\Sigma(u_1) - \Sigma(u_2))}{\rho(u_1 - u_2)}, \end{aligned} \tag{3.3}$$

then the number $\|\Sigma\|_{Lip}$ defines a norm for all $\Sigma \in Lip(\mathcal{D}, S(\Re^p))$.

$\|\Sigma\|_{Lip}$ will be called the *Lipschitz norm* ([7]) of the system Σ defined by $u_0 \in \mathcal{D}$. A convenient choice of u_0 is of course $u_0 = \mathbf{0}$ if $\mathbf{0} \in \mathcal{D}$, where note that $\Sigma(\mathbf{0})$ is not zero in general. To prove the theorem, it amounts to showing that $\|\Sigma\|_{Lip} = 0$ implies $\Sigma = \mathbf{0}$, the zero system. This, however, is an immediate consequence of part 1. of Lemma 3.2.2.

Theorem 3.2.4 [7] *The family $Lip(\mathcal{D}, S(\Re^p))$ is a complete metric space under the Lipschitz norm $\|\cdot\|_{Lip}$.*

A complete metric space $(Lip(\mathcal{D}, S(\Re^p)), \|\cdot\|_{Lip})$ has the property that every Cauchy sequence of systems $\{\Sigma_k\}$ converges.

3.3 Approximate Right Inverse

In [50], the concept of an approximate inverse was formulated for linear systems. The problem of disturbance attenuation was addressed with a configuration very similar to Figure 1.1. As a result of [50], the approximate invertibility of the system was shown to be a necessary and sufficient condition for disturbance attenuation. The optimization problem from [50] used the $\mathcal{H}^\infty$-norm $\|\cdot\|_\infty$ and a weighted semi-norm $\|\cdot\|_W$ with the property $\|\cdot\|_W \leq \|\cdot\|_\infty$. The weighted semi-norm has a weighing filter where W will denote a stable and causal system of unit norm such that $\|d\|_W = \|Wd\|_\infty$.

The definition from [50] of an approximate inverse is as follows. The set of all stable, causal, and linear systems is denoted by $\mathcal{C}_S$. For any stable and strictly causal system P, an approximate right inverse of P is any stable and causal system Ψ for which $\|I - P\Psi\|_W < \|I\|_W$. The right singularity measure of P, denoted by $\mu(P)$, is

$$\mu(P) \stackrel{\text{def}}{=} \inf_{\Psi \in \mathcal{C}_S} \|I - P\Psi\|_W. \tag{3.4}$$

In general, $\mu(P)$ is a number in the interval $0 \leq \mu(P) \leq 1$.

For nonlinear systems we cannot define a weighted semi-norm with the with the property $\|\cdot\|_W \leq \|\cdot\|_\infty$. As a result, we cannot use (3.4) to derive a right singularity measure of Σ between 0 and 1. Nevertheless we can define an approximate inverse optimization problem. Let's first review some properties of right inverses for nonlinear systems. In Section 2.2 the generalized right inverse was introduced for a class of recursive systems in the form of (2.1). For systems Σ that are not bijective,

the generalized right inverse of systems Σ are non-unique. For the systems that are bijective, the generalized right inverse is stable but not necessarily causal.

By assumption, the system Σ is strictly causal. This implies $\mathcal{L}(\Sigma) \geq 1$. The *design integer* λ, where $\lambda \geq 0$, is used to characterize the class of approximate right inverse systems that takes in account the latency of Σ. The design integer λ is selected before the optimization process. In the three examples of Chapter 4, the design integer was selected at the minimum latency of Σ, i.e., when $\mathcal{L}(\Sigma) \geq \lambda_1$, the design integer $\lambda = \lambda_1$.

The approximate right inverse optimization problem of the stable, strictly causal and recursive system $\Sigma: \mathcal{D} \rightarrow S(\Re^p)$ with $\mathcal{D}$, a compact subset of $S(\Re^m)$, is shown in Figure 3.1 with $e = [I(u) - D^{-\lambda}\Sigma\Psi(u)]$ where $e \in S(\Re^p)$. The performance index is

$$\inf_{\Psi \in \mathcal{A}} \sup_{u \in S(\alpha^p)} \rho(e) \tag{3.5}$$

where $\mathcal{A}$ is the set of all stable and causal systems $\Psi: S(\alpha^p) \rightarrow S(\Re^m)$. The system Ψ is a stable approximate right inverse of Σ while the best approximant Ψ^* is not guaranteed to be stable. To guarantee stability of the best approximant Ψ^*, the systems Σ and Ψ are chosen from a class of systems $Lip(\mathcal{D}, S(\Re^p))$ and $Lip(S(\alpha^p), S(\Re^m))$, respectively. The set $\mathcal{A}$ has to be compact subset of $Lip(S(\alpha^p), S(\Re^m))$. The next two

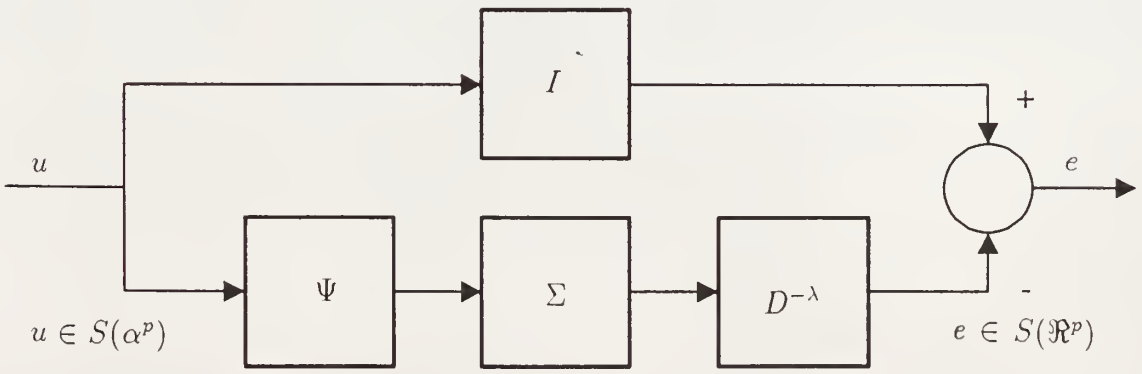

Figure 3.1: The approximate right inverse optimization problem of Σ: inf sup $\rho(e)$.

paragraphs will explain why we need the set $\mathcal{A}$ to be compact to guarantee stability of the best approximant Ψ^*.

Approximation theory is needed to solve the problem of finding a best approximant Ψ^*. In solving the best approximation problem, additional hypotheses are placed to guarantee the existence and uniqueness of the best approximation. Our practical problem is that we need approximate inverses that are stable, causal, and recursive but for now we will take approximate inverses that are only stable and causal. We shall be therefore be interested in a basic existence Theorem 3.3.1, which gives sufficient conditions to guarantee existence of closest point.

Theorem 3.3.1 [6] *Let K denote a compact set in a metric space. To each point p of the space there corresponds a point in K of minimum distance from p.*

In the previous section, the class of systems with the Lipschitz norm was introduced so that we can create a compact set of systems in a metric space. Using the hypothesis of Theorem 3.3.1 as a starting point, we can then prove the existence of best approximate right inverse.

3.3.1 The Existence Theorem of Best Approximate Right Inverse

For clarity, the following sets are defined for this subsection only. Let $\alpha \geq 0$ be a real number. Denote by $Lip(S(\alpha^p), S(\Re^m))$ the set of all stable and casual systems $\Psi: S(\alpha^p) \rightarrow S(\Re^m)$ satisfying $\|\Psi\| < \infty$. Let $\mathcal{D}$ be a compact subset of $S(\Re^m)$ and let $Lip(\mathcal{D}, S(\Re^p))$ be the set of all stable and causal systems $\Sigma: \mathcal{D} \rightarrow S(\Re^p)$ satisfying $\|\Sigma\| < \infty$. Let $G > 0$ be a real number. We denote by $\mathcal{A}_G$ the compact subset $Lip(S(\alpha^p), S(\Re^m))$ given by

$$\mathcal{A}_G = \{\Psi | \Psi \in Lip(S(\alpha^p), S(\Re^m)) \text{ and } \|\Psi\| \leq G\}. \tag{3.6}$$

Theorem 3.3.2 *Let $\Sigma \in Lip(\mathcal{D}, S(\Re^p))$ be a strictly causal and recursive system for a given real number $G > 0$ and for a design integer $\lambda \geq 0$. There is a stable and*

causal system $\Psi^* \in \mathcal{A}_G$ *such that*

$$\sup_{u \in S(\alpha^p)} \rho\left(I(u) - D^{-\lambda}\Sigma\Psi^*(u)\right) \leq \sup_{u \in S(\alpha^p)} \rho\left(I(u) - D^{-\lambda}\Sigma\Psi(u)\right) \tag{3.7}$$

for all $\Psi \in \mathcal{A}_G$.

Proof: The right hand side of (3.7) is a continuous function of Ψ. If we take $\Psi = 0$, then $\sup_{u \in S(\alpha^p)} \rho(I(u) - D^{-\lambda}\Sigma\Psi(u)) = \alpha$. There exists an infimum of the right hand side of (3.7) since it is continuous with respect to Ψ and it is bounded between 0 and α. Let

$$r = \inf_{\Psi \in \mathcal{A}_G} \sup_{u \in S(\alpha^p)} \rho\left(I(u) - D^{-\lambda}\Sigma\Psi(u)\right), \tag{3.8}$$

and suppose that

$$\sup_{u \in S(\alpha^p)} \rho\left(I(u) - D^{-\lambda}\Sigma\Psi_k(u)\right) = r_k, \quad k = 0, 1, 2, \ldots, \tag{3.9}$$

with r_k monotonically decreasing to r. Then, for k sufficiently large

$$\sup_{u \in S(\alpha^p)} \rho\left(I(u) - D^{-\lambda}\Sigma\Psi_k(u)\right) \leq r + 1 \leq M. \tag{3.10}$$

Since the sequences of systems $\{I - D^{-\lambda}\Sigma\Psi_k\}$ are bounded and monotonic, it follows that the sequence of systems $\{I - D^{-\lambda}\Sigma\Psi_k\}$ converges. This implies that for every $\varepsilon > 0$ there exists an integer N such that $l, n \geq N$ implies

$$\sup_{u \in S(\alpha^p)} \rho\left(\left[I(u) - D^{-\lambda}\Sigma\Psi_n(u)\right] - \left[I(u) - D^{-\lambda}\Sigma\Psi_l(u)\right]\right) \leq \varepsilon \tag{3.11}$$

or

$$\sup_{u \in S(\alpha^p)} \rho\left(D^{-\lambda}\Sigma\Psi_n(u) - D^{-\lambda}\Sigma\Psi_l(u)\right) \leq \varepsilon. \tag{3.12}$$

The $Lip(S(\alpha^p), S(\Re^p))$ systems set is a subset of the stable and causal systems $\Gamma: S(\alpha^p) \to S(\Re^p)$ satisfying $\|\Gamma\| < \infty$. The composition of two systems of bounded Lipschitz norm is also a system of bounded Lipschitz norm; hence, for all $\Psi \in Lip(S(\alpha^p), S(\Re^m))$ and a given $\Sigma \in Lip(\mathcal{D}, S(\Re^p))$, the composite system

$\Sigma\Psi \in Lip(S(\alpha^p), S(\Re^p))$. Now we define $f_k \in Lip(S(\alpha^p), S(\Re^p))$ such that $f_k \stackrel{\text{def}}{=} \Sigma\Psi_k$ and rewriting (3.12) we have

$$\|D^{-\lambda} f_n - D^{-\lambda} f_m\|_{Lip} < \varepsilon. \tag{3.13}$$

This establishes $\lim_{k\to\infty} D^{-\lambda} f_k = D^{-\lambda} f^*$ where the system $D^{-\lambda} f^*$ is the limit of the sequence of systems $\{D^{-\lambda} f_k\}$. To translate $D^{-\lambda} f^*$ into a $Lip(S(\alpha^p), S(\Re^p))$ system we get $D^{\lambda}(D^{-\lambda} f^*) = f^*]_{\lambda}^{\infty}$. The system $f^*]_{\lambda}^{\infty}$ has its first λ outputs $y_0, y_1, \ldots, y_{\lambda-1}$ set to zero because they were not used in the convergence of the sequence $\{D^{-\lambda} f_k\}$. It follows by the completeness of $Lip(S(\alpha^p), S(\Re^p))$ that the system $f^*]_{\lambda}^{\infty} \in Lip(S(\alpha^p), S(\Re^p))$.

The sequence of systems $\{D^{-\lambda} f_k\}$ converges to the limit system $D^{-\lambda} f^*$. Therefore, the sequence of systems $\{D^{-\lambda}\Sigma\Psi_k\}$ converges also to the limit system $D^{-\lambda} f^*$. In other words, for every $\varepsilon > 0$ and for all $u \in S(\alpha^m)$, there exists an integer N such that $l, n \geq N$, this implies

$$\sup_{u \in S(\alpha^p)} \rho\left(D^{-\lambda}\Sigma\Psi_n(u) - D^{-\lambda}\Sigma\Psi_l(u)\right) \leq \varepsilon. \tag{3.14}$$

From the properties of a system of bounded Lipschitz norm we can we write

$$\begin{aligned} & \sup_{u \in S(\alpha^p)} \rho\left(D^{-\lambda}\Sigma\Psi_n(u) - D^{-\lambda}\Sigma\Psi_l(u)\right) \\ \leq\ & \|D^{-\lambda}\Sigma\|_{Lip} \sup_{u \in S(\alpha^p)} \rho\left(\Psi_n(u) - \Psi_l(u)\right). \end{aligned} \tag{3.15}$$

We will assume $\|D^{-\lambda}\Sigma\|_{Lip} \neq 0$, which implies that Σ is not the zero system. The sequence of systems $\{\Psi_k\}$ is a continuous mapping from a compact metric space $(S(\alpha^p), \rho)$ into a compact metric space $(\mathcal{D}, \rho)$. Now the sequence of systems $\{\Psi_k\}$ is a sequence in a compact metric space $(\mathcal{A}_G, \|\cdot\|_{Lip})$. Therefore some subsequence of $\{\Psi_k\}$ converges to a system in $\mathcal{A}_G$. Thus we have $\lim_{j\to\infty} \Psi_{k_j} = \Psi^*$ where $\Psi^* \in \mathcal{A}_G$ for the subsequence of systems $\{\Psi_{k_j}\}$.

Now we can define a subsequence of $\{D^{-\lambda} f_k\}$ by $\{D^{-\lambda} f_{k_j}\}$ such that $D^{-\lambda} f_{k_j} \stackrel{\text{def}}{=} D^{-\lambda}\Sigma\Psi_{k_j}$. Every subsequence of $\{D^{-\lambda} f_k\}$ converges to $D^{-\lambda} f^*$ so

$\lim_{j\to\infty} D^{-\lambda} f_{k_j} = D^{-\lambda} f^*$; therefore

$$\lim_{\Psi\to\Psi^*} D^{-\lambda}\Sigma\Psi = D^{-\lambda} f^*. \tag{3.16}$$

The system $\Psi^* \in \mathcal{A}_G$ is best approximate right inverse of the system Σ with optimal sequence of systems $\{\Psi_{k_j}\} \in \mathcal{A}_G$ that converges to Ψ^*. ■

3.4 The Measure of Right Singularity

As has been previously noted, for every pair of elements $u, v \in S(\Re^m)$, the metric $\boldsymbol{\rho}_\epsilon$ is defined

$$\boldsymbol{\rho}_\epsilon(u,v) \stackrel{\text{def}}{=} \sup_{i\geq 0} (1+\epsilon)^{-i} |u_i - v_i|, \quad \epsilon > 0. \tag{3.17}$$

The distance from any $u \in S(\Re^m)$ and the set $S_2 \subset S(\Re^m)$ is defined by the number

$$\varrho_{M_\epsilon}(u, S_2) \stackrel{\text{def}}{=} \inf_{v\in S_2} \boldsymbol{\rho}_\epsilon(u,v). \tag{3.18}$$

We can now define the maximal distance from any $u \in S_1 \subset S(\Re^m)$ and the set S_2 by the number

$$\varrho_\epsilon(S_1, S_2) \stackrel{\text{def}}{=} \sup_{u\in S_1} \varrho_{M_\epsilon}(u, S_2) = \sup_{u\in S_1} \inf_{v\in S_2} \boldsymbol{\rho}_\epsilon(u,v). \tag{3.19}$$

From Theorem 3.3.2, there exists a best approximate right inverse system $\Psi^* \in \mathcal{A}_G$ for a design integer $\lambda \geq 0$ such that the inequality

$$\sup_{u\in S(\alpha^p)} \rho_\epsilon\left(I(u) - D^{-\lambda}\Sigma\Psi^*(u)\right) \leq \sup_{u\in S(\alpha^p)} \rho_\epsilon\left(I(u) - D^{-\lambda}\Sigma\Psi(u)\right) \tag{3.20}$$

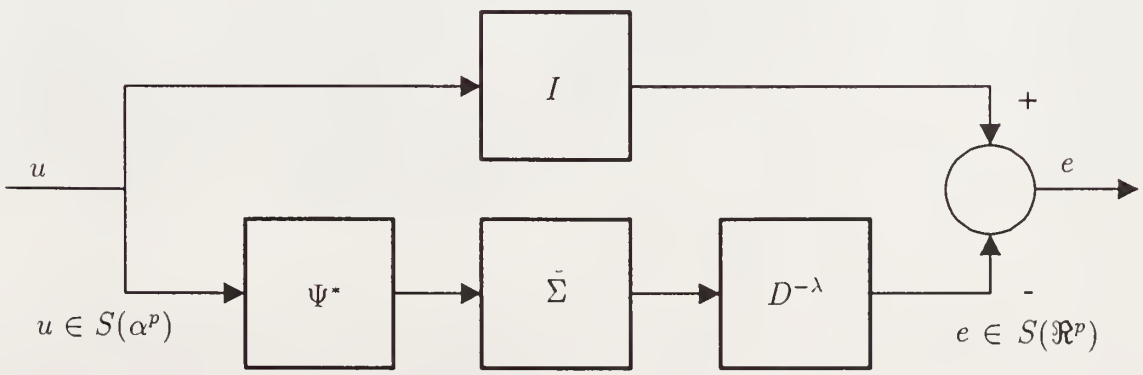

Figure 3.2: The performance bound optimization problem of Σ: $\sup_{u\in S(\alpha^p)} \rho_\epsilon(e)$.

holds for all $\Psi \in \mathcal{A}_G$ and for all $\epsilon > 0$. Using Ψ^* for Ψ with $e = [I(u) - D^{-\lambda}\Sigma\Psi^*(u)]$ in Figure 3.1, Figure 3.2 represents the performance bound optimization problem of the causal and recursive system $\Sigma \in Lip(\mathcal{D}, S(\Re^p))$, where the performance index is

$$\sup_{u \in S(\alpha^p)} \rho_\epsilon(e) \tag{3.21}$$

where $e \in S(\Re^p)$. Now we want to put a lower bound on the term $\sup_{u \in S(\alpha^p)} \rho_\epsilon(e) = \sup_{u \in S(\alpha^p)} \rho_\epsilon(I(u) - D^{-\lambda}\Sigma\Psi^*(u))$. Using (3.18) and (3.19) we can write

$$\begin{aligned} \sup_{u \in S(\alpha^p)} \rho_\epsilon \left(I(u) - D^{-\lambda}\Sigma\Psi^*(u)\right) &= \sup_{u \in S(\alpha^p)} \varrho_{M_\epsilon} \left(u, D^{-\lambda}\Sigma\Psi^*[S(\alpha^p)]\right) \\ &= \varrho_\epsilon \left(S(\alpha^p), D^{-\lambda}\Sigma\Psi^*[S(\alpha^p)]\right) \\ &\geq \varrho_\epsilon \left(S(\alpha^p), D^{-\lambda}\mathrm{Im}\,\Sigma\right). \end{aligned} \tag{3.22}$$

Note that even if $\mathrm{Im}\,\Sigma$ is unbounded, $\varrho_\epsilon \left(S(\alpha^p), D^{-\lambda}\mathrm{Im}\,\Sigma\right)$ is bounded since the first operand of $\varrho_\epsilon(\cdot,\cdot)$, $S(\alpha^p)$, is bounded.

Definition 3.4.1 *For any system $\Sigma \in Lip(\mathcal{D}, S(\Re^p))$ that is a strictly causal recursive of the system (2.1), the* right singularity measure, *denoted by $\mathcal{P}(\Sigma)$, for a real $\alpha > 0$ and a design integer $\lambda \geq 0$ is*

$$\mathcal{P}(\Sigma) \stackrel{\text{def}}{=} \varrho_\epsilon \left(S(\alpha^p),\ D^{-\lambda}\mathrm{Im}\,\Sigma\right). \tag{3.23}$$

The *performance bound* is finally defined as the right singularity measure $\mathcal{P}(\Sigma)$. It provides a measure of the ability to match a set by subset of the image of a system as seen in (3.23). The performance bound came from the requirement to provide an estimate of the minimal effect of the disturbance signal d on the output signal z of Figure 1.1. By assumption the system $\Sigma: \mathcal{D} \to S(\Re^p)$ is stable where $\mathcal{D}$ is a compact subset of $S(\Re^m)$. In that case, the right coprime factorization of $\Sigma = PQ^{-1}$ can be taken as $P = \Sigma$ and $Q = I$ where $I: \mathcal{D} \to \mathcal{D}$, the identity system, and $P: \mathcal{D} \to \Sigma[\mathcal{D}]$.

When the system $\Sigma: S(\alpha^m) \to S(\Re^p)$ is unstable, the right coprime factorization of $\Sigma = PQ^{-1}$ is taken as $P: S \to \Sigma[S(\alpha^m)]$ and $Q: S \to S(\alpha^m)$ where $S \subset S(\Re^m)$

and Q is bicausal. From Theorem 2.1.5, any stable and bicausal system $M: S \rightarrow S$ with a stable inverse system $M^{-1}: S \rightarrow S$ can be selected, so there exists a pair of stable systems $A: S(\Re^p) \rightarrow S(\Re^m)$ and $B: S(\alpha^m) \rightarrow S(\Re^m)$ such that $AP + BQ = M$. The stabilization of Σ can be seen in Figure 2.1 with $\pi = B^{-1}$ and $\varphi = A$. The closed loop response of the stabilization is PM^{-1}. Now M can be selected as the identity system $I: S \rightarrow S$. The factorization space S can be taken as $S(\alpha^m)$ and [21] describes the construction of the stabilizing controllers that yield the factorization space of $S(\alpha^m)$. As a result the closed loop response is $P: S(\alpha^m) \rightarrow \Sigma[S(\alpha^m)]$.

The preceding paragraphs illustrate that the "numerator" system P directly drives the performance bound by the image of its system Σ. The image of Σ for discrete-time nonlinear systems is analogous to the right half-plane zeros of linear continuous-time systems. Both of these quantities are fixed and cannot be altered by feedback. Now we can use the performance bound for systems of practical origin.

CHAPTER 4
CALCULATION OF THE PERFORMANCE BOUND

4.1 The Estimate of the Performance Bound

It turns out that the calculation of the right singularity measure $\mathcal{P}(\Sigma)$ for nonlinear systems is rather laborious. We develop in this section an estimate $\tilde{\mathcal{P}}(\Sigma)$ of $\mathcal{P}(\Sigma)$ which is easier to calculate. This estimate satisfies

$$\mathcal{P}(\Sigma) \leq \tilde{\mathcal{P}}(\Sigma). \tag{4.1}$$

From Theorem 3.3.2, there exists a best approximate right inverse system $\Psi^* \in \mathcal{A}_G$ such that the inequality

$$\sup_{u \in S(\alpha^p)} \rho_\epsilon \left(I(u) - D^{-\lambda} \Sigma \Psi^*(u) \right) \leq \sup_{u \in S(\alpha^p)} \rho_\epsilon \left(I(u) - D^{-\lambda} \Sigma \Psi(u) \right) \tag{3.20}$$

holds for all $\Psi \in \mathcal{A}_G$ and for a design integer $\lambda \geq 0$. Theorem 3.3.2 demonstrates the existence of a best approximate right inverse system but does not provide the construction of a best approximate right inverse system.

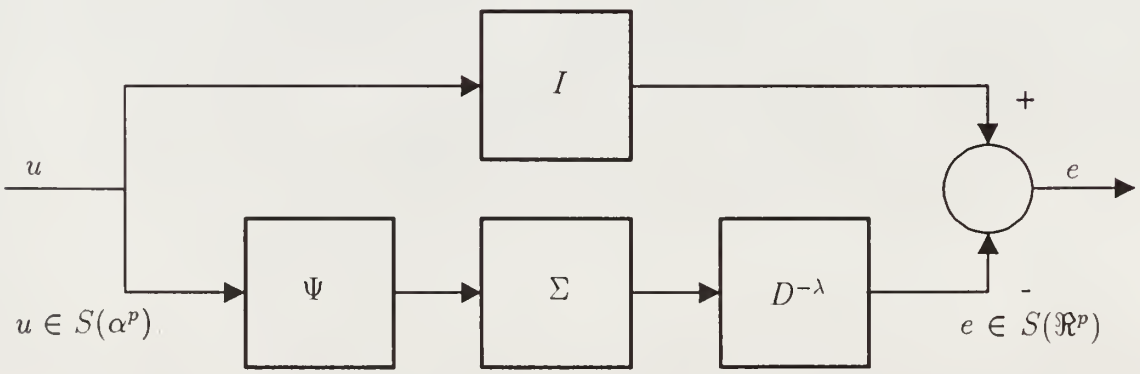

Figure 4.1: The estimate of the performance bound optimization problem of the system Σ with an approximate right inverse system Ψ: $\tilde{\mathcal{P}}(\Sigma) = \sup_{u \in S(\alpha^p)} \rho_\epsilon(e)$.

Using a causal approximate right inverse system $\Psi \in Lip(S(\alpha^p), S(\Re^m))$ for a given design integer $\lambda \geq 0$ from Figure 3.1, Figure 4.1, with $e = [I(u) - D^{-\lambda}\Sigma\Psi(u)]$, represents the estimate of the performance bound optimization problem of the causal and recursive system $\Sigma \in Lip(\mathcal{D}, S(\Re^p))$, where the performance index is

$$\sup_{u \in S(\alpha^p)} \rho_\epsilon(e) \tag{4.2}$$

where $e \in S(\Re^p)$. Now we want to express the term $\sup_{u \in S(\alpha^p)} \rho_\epsilon(e) = \sup_{u \in S(\alpha^p)} \rho_\epsilon (I(u) - D^{-\lambda}\Sigma\Psi(u))$ using the operator $\varrho_\epsilon(\cdot, \cdot)$. Using (3.18) and (3.19) we can write

$$\begin{aligned} \sup_{u \in S(\alpha^p)} \rho_\epsilon \left(I(u) - D^{-\lambda}\Sigma\Psi(u) \right) &= \sup_{u \in S(\alpha^p)} \varrho_{M_\epsilon} \left(u, D^{-\lambda}\Sigma\Psi[S(\alpha^p)] \right) \\ &= \varrho_\epsilon \left(S(\alpha^p), D^{-\lambda}\Sigma\Psi[S(\alpha^p)] \right). \end{aligned} \tag{4.3}$$

Definition 4.1.1 *For any system $\Sigma \in Lip(\mathcal{D}, S(\Re^p))$ that is strictly causal and recursive, an* estimate of the performance bound, *denoted by $\tilde{\mathcal{P}}(\Sigma)$, given real $\alpha > 0$ and design integer $\lambda \geq 0$, is given by*

$$\tilde{\mathcal{P}}(\Sigma) \stackrel{\text{def}}{=} \varrho_\epsilon \left(S(\alpha^p), D^{-\lambda}\Sigma\Psi[S(\alpha^p)] \right), \tag{4.4}$$

where $\Psi \in Lip(S(\alpha^p), S(\Re^m))$ is a causal approximate right inverse system.

4.2 Practical Implementation Techniques

For the applications presented here, we will be interested in the response of the systems over a finite interval of time, say for a discrete set $[0, T]$, where $T > 0$ is a fixed integer. Let $C_T(\Re^n)$ be the set of all functions $h: [0, T] \to \Re^n$. Denote by $|h| \stackrel{\text{def}}{=} \sup_{i \in [0,T]} |h(i)|$, the ℓ^∞-norm on $C_T(\Re^n)$ and by $\rho_\epsilon(h) \stackrel{\text{def}}{=} \sup_{i \in [0,T]} (1+\epsilon)^{-i} |h(i)|$, for $\epsilon > 0$, the norm ρ_ϵ on $C_T(\Re^n)$. Let $h \in C_T(\Re^n)$ be any function. Then

$$\sup_{i \in [0,T]} (1+\epsilon)^{-i} |h(i)| \leq \sup_{i \in [0,T]} |h(i)|$$

and

$$(1+\epsilon)^T \sup_{i \in [0,T]} (1+\epsilon)^{-i} |h(i)| = \sup_{i \in [0,T]} (1+\epsilon)^{T-i} |h(i)| \geq \sup_{i \in [0,T]} |h(i)|,$$

so that

$$\rho_\epsilon(h) \leq |h| \leq (1+\epsilon)^T \rho_\epsilon(h) \quad \text{and} \quad (1+\epsilon)^{-T}|h| \leq \rho_\epsilon(h) \leq |h| \tag{4.5}$$

on $C_T(\Re^n)$. These inequalities imply the equivalence of the norms $|\cdot|$ and $\rho_\epsilon(\cdot)$ on $C_T(\Re^n)$. We will use the ℓ^∞-norm for its simplicity in the calculation of the estimate of the performance bound $\tilde{\mathcal{P}}(\Sigma)$ (so the norms $|\cdot|$ and $\rho_\epsilon(\cdot)$ are interchangeable over finite intervals of time).

For the mathematical analysis presented in Chapter 2 and Chapter 3, the signals of interest are always bounded. For implementation purposes, the maximum peak deviation of the input signal, $\max_{i\geq 0}|\Delta u_i|$ where $\Delta u_i = u_{i+1} - u_i$ is limited. To limit the maximum peak deviation, the signals are transformed by using a discrete-time lowpass filter. A new family of sequences, denoted by $S_{\Omega_{LP}}(\alpha)$, is formed by using a second order discrete-time lowpass filter with a cutoff frequency Ω_{LP} in rad/sec on $S(\alpha)$. The transformation between $S(\alpha)$ and $S_{\Omega_{LP}}(\alpha)$ is bijective since the lowpass filter is one-to-one and the image of the lowpass filter is $S_{\Omega_{LP}}(\alpha)$. Thus, the transformed space $S_{\Omega_{LP}}(\alpha)$ is isomorphic to the input space $S(\alpha)$.

The alternate definitions of $\tilde{\mathcal{P}}(\Sigma)$ are given in (4.3) and using the ℓ^∞-norm (for $\epsilon = 0$) we get

$$\tilde{\mathcal{P}}(\Sigma) = \sup_{u\in S(\alpha^p)} \left| I(u) - D^{-\lambda}\Sigma\Psi(u) \right| = \sup_{u\in S(\alpha^p)} \varrho_{M_0}\left(u, D^{-\lambda}\Sigma\Psi[S(\alpha^p)]\right). \tag{4.6}$$

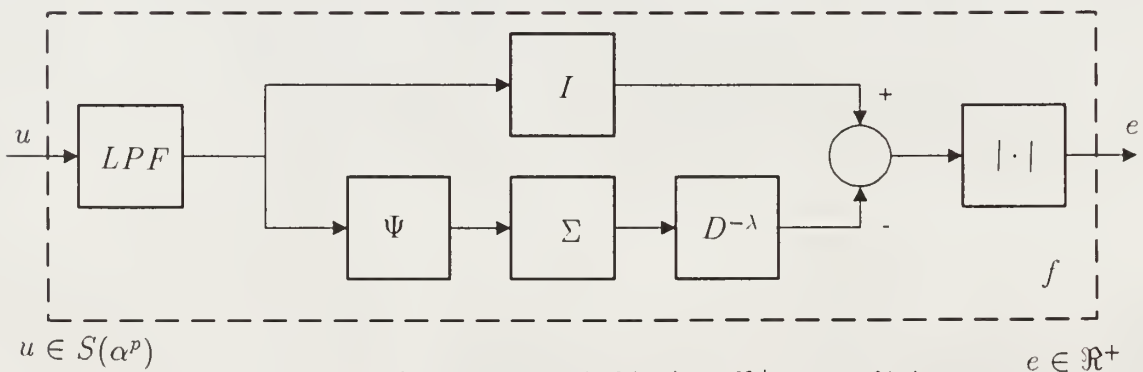

Figure 4.2: The Function $f: S(\alpha^p) \to \Re^+: u \mapsto f(u)$.

Define a function $f: S(\alpha^p) \rightarrow \Re^+$ that incorporates the lowpass filter, as displayed in Figure 4.2, such that

$$\tilde{\mathcal{P}}(\Sigma) = \sup_{u \in S(\alpha^p)} f(u), \tag{4.7}$$

where the function f is defined as follows

$$f(u) \stackrel{\text{def}}{=} \left| I\left(LPF(u)\right) - D^{-\lambda}\Sigma\Psi\left(LPF(u)\right) \right|. \tag{4.8}$$

The parameters of the function f are the system Σ, an approximate inverse system Ψ, the design integer λ, the optimization set $S(\alpha^p)$, and the lowpass filter cutoff frequency Ω_{LP}. The function f must also satisfy $f(u) = \varrho_{M_0}(u,\, D^{-\lambda}\Sigma\Psi[S_{\Omega_{LP}}(\alpha^p)])$ where $\varrho_{M_0}(\cdot,\cdot)$ is defined in (3.18). It then follows that $f(\cdot)$ is a convex function when its input or optimization set $S(\alpha^p)$ and the image set $\Sigma\Psi[S_{\Omega_{LP}}(\alpha^p)]$ are convex since ϱ_{M_0} is a distance function from a point in the optimization set to the image set. The distance function ϱ_{M_0} by its construction is a convex function. In practice, the image set is not convex; however, studying the optimization problem of finding a global maximum of a convex function will give us insight to the non-convex optimization problem.

Unlike the minimization of a convex function, once a local maximum has been found there is, more or less by definition, no local information to tell you how to proceed to a higher local maximum. In particular, there is no local criterion for deciding whether a given local maximum is really the global maximum. Hence, maximizing a convex function is usually a much harder task than minimizing a convex function. Theorem 4.2.1 shows that a convex function achieves a maximum over a compact polyhedral set at an extreme point.

Theorem 4.2.1 [3] *Let $g: S(\Re^p) \rightarrow \Re$ be a convex function, and let S be a nonempty compact polyhedral set in $S(\Re^p)$. For the problem of maximizing $g(u)$ subject to $u \in S$, there is an optimal solution, $\bar{u}$, where $\bar{u}$ is an extreme point of S such that $g(\bar{u}) \geq g(u)$ for all $u \in S$.*

Using Theorem 4.2.1, he global maximum of $f(u)$ maybe found by evaluating all the extreme points of $S(\alpha^p)$ and finding the maximum on this set. For example, if we have a one-dimensional set of sequences which is a finite length of 250 elements, the number of extreme points, and hence the number of evaluations of f, would be $2^{250} = 1.8903 \times 10^{75}$. This procedure is laborious as far as computation is concerned. Although the image set S is non-convex, the property that the optimization set is convex is enough to suspect that global maximum would be found on an extreme point of the optimization set. If we take an interior point u_i from the optimization set which is a nonempty compact polyhedral set and form a neighborhood $N_{r_i}(u_i)$ of radius r_i, then we can find a $u_{i+1} \in N_{r_i}(u_i)$ such that $\varrho_{M_0}(u_{i+1}, S) > \varrho_{M_0}(u_i, S)$ and u_{i+1} is closer to the boundary than u_i. The radius r_i of a neighborhood $N_{r_i}(u_i)$ is selected so that we do not accumulate in an interior local maximum. Since the optimization set is convex and ϱ_{M_0} is a distance function, the sequence $\{u_i\}$ will converge to a point on the boundary. Therefore, the global maximum will be on the boundary. For simulation purposes, the global maximum is assumed to be an extreme point.

The three systems of practical origin that have been selected for investigation are all fourth order nonlinear systems. Each of the systems has a distinct memoryless nonlinear subsystem. These subsystems represent, respectively, dead-zones, position constraints, and rate constraints for the problems: permanent magnet stepper motor model example, multivariable process control model example, and aerodynamic model example. Nonlinear programming is used to calculate the estimate of the performance bound. The algorithms that are developed take advantage of the traits of each of the nonlinear systems and of the finite bandwidth of the input signal space. A useful trait of a system is a property that would help reduce the region of optimization in the search for a global maximum. It will be shown in the next sections that the computation is not as laborious as previously conjectured.

4.3 Permanent Magnet Stepper Motor Model Example

This section is concerned with voltage control of a permanent magnet (PM) stepper motor. This example comes from [5], wherein the authors developed a model-based control law using exact linearization implemented on an industrial setup.

The PM stepper motor model consists of a slotted stator with two phases and a permanent magnet rotor. One side of the rotor is a north pole, and the other side is a south pole. The teeth on each side of the rotor are out of alignment by a tooth-width. The equations of motion for the PM stepper motor model are given by:

$$\frac{di_a}{dt} = \frac{1}{L}[v_a - Ri_a + K_m\omega\sin(N_r\theta)] \tag{4.9}$$

$$\frac{di_b}{dt} = \frac{1}{L}[v_b - Ri_b - K_m\omega\cos(N_r\theta)] \tag{4.10}$$

$$\frac{d\omega}{dt} = \frac{1}{J}[-K_m i_a\sin(N_r\theta) + K_m i_b\cos(N_r\theta) - B\omega] \tag{4.11}$$

$$\frac{d\theta}{dt} = \omega \tag{4.12}$$

where v_a, v_b and i_a, i_b are the voltages and currents in phases A and B, respectively. Further, ω is the rotor (angular) speed, θ is the rotor (angular) position, B is the viscous friction coefficient, J is the combined inertia of the motor and the translation table, K_m is the motor torque constant, R is the resistance of the phase winding, L is the inductance of the phase winding, and N_r is the number of rotor teeth. Table 4.1 shows the values of the stepper motor parameters used in [5].

Table 4.1: The PM Stepper Motor Model Parameters

Parameter	Value
L	1.5 mH
R	0.55 Ω
J	4.5×10^{-5} kg·m^2
K_m	0.19 N·m/A
N_r	50
B	8.0×10^{-4} N·m·s/rad

For the PM stepper motor model, there is an appropriate nonlinear coordinate transformation which is known as the direct-quadrature (DQ) transformation. The DQ transformation for the phase voltages and currents is defined as follows:

$$\begin{bmatrix} v_d \\ v_q \end{bmatrix} \stackrel{\text{def}}{=} \begin{bmatrix} \cos(N_r\theta) & \sin(N_r\theta) \\ -\sin(N_r\theta) & \cos(N_r\theta) \end{bmatrix} \begin{bmatrix} v_a \\ v_b \end{bmatrix} \tag{4.13}$$

$$\begin{bmatrix} i_d \\ i_q \end{bmatrix} \stackrel{\text{def}}{=} \begin{bmatrix} \cos(N_r\theta) & \sin(N_r\theta) \\ -\sin(N_r\theta) & \cos(N_r\theta) \end{bmatrix} \begin{bmatrix} i_a \\ i_b \end{bmatrix}. \tag{4.14}$$

The direct current i_d corresponds to the component of the stator magnetic field along the axis of the rotor magnetic field, while the quadrature current i_q corresponds to the orthogonal component. The application of the DQ transformation to the original system equations (4.9) through (4.12) yields:

$$\frac{di_d}{dt} = \frac{1}{L}\left[v_d - Ri_d + N_r L\omega i_q\right] \tag{4.15}$$

$$\frac{di_q}{dt} = \frac{1}{L}\left[v_q - Ri_q - N_r L\omega i_d - K_m\omega\right] \tag{4.16}$$

$$\frac{d\omega}{dt} = \frac{1}{J}\left[K_m i_q - B\omega\right] \tag{4.17}$$

$$\frac{d\theta}{dt} = \omega \tag{4.18}$$

where v_d is the direct voltage, v_q is the quadrature voltage, i_d is the direct current, i_q is the quadrature current, ω is the angular velocity, and θ is the angular position.

The quadrature component i_q of the current produces torque while the direct component i_d does not produce any torque. However, in order to attain higher speeds, it is necessary to apply a negative direct current in order to cancel the effect of the back-emf of the motor which results from the "back-emf" term $K_m\omega$ in (4.16). The direct current i_d will be forced to be negative by the correct choice direct voltage v_d. The optimal lead-angle approach is used in [5] to properly choose v_d which becomes a nonlinear function of the states. The equations of motion are discretized using first order Euler integration. Let $x_k = [i_{d_k}\ i_{q_k}\ \omega_k\ \theta_k]'$. Equations (4.15) through (4.18)

take the following form:

$$x_{k+1} = f(x_k) + g(x_k) \cdot v_{q_k} \tag{4.19}$$

$$\omega_k = \begin{bmatrix} 0 & 0 & 1 & 0 \end{bmatrix} \cdot x_k, \tag{4.20}$$

where $x_k \in \Re^4$, and f, g are vector fields on $\Re^4$.

The analytical expression for the input dead-zone is

$$v_{q_k} = DZ(v_{Cq_k}) = \begin{cases} v_{Cq_k} - 1 & \text{if} \quad v_{Cq_k} \geq 1 \\ 0 & \text{if} \quad -1 < v_{Cq_k} < 1 \\ v_{Cq_k} + 1 & \text{if} \quad v_{Cq_k} \leq -1. \end{cases} \tag{4.21}$$

The system $\Sigma: \mathcal{D} \rightarrow S(\Re) : v_{Cq} \mapsto \omega$, where $\mathcal{D} \subset S(\Re)$, is the composition of the equations of motion with the dead-zone for which v_{Cq} is the quadrature voltage command. Figure 4.3 shows the block diagram of the system Σ.

4.3.1 Simulation

The signal of interest is the angular velocity signal ω. It is assumed that all signals of interest start at rest (i.e., $\omega_n = 0$ for all $n \leq n_0$). In one of the applications presented in [5], the desired speed trajectory required the motor to go from to zero to 1350 RPM in 10 ms with a sample rate of 10 kHz. The bandwidth of ω was set to 50 Hz. The rise time was about 10.6 ms and the absolute bound of $|\omega| \leq 1350$ RPM was imposed.

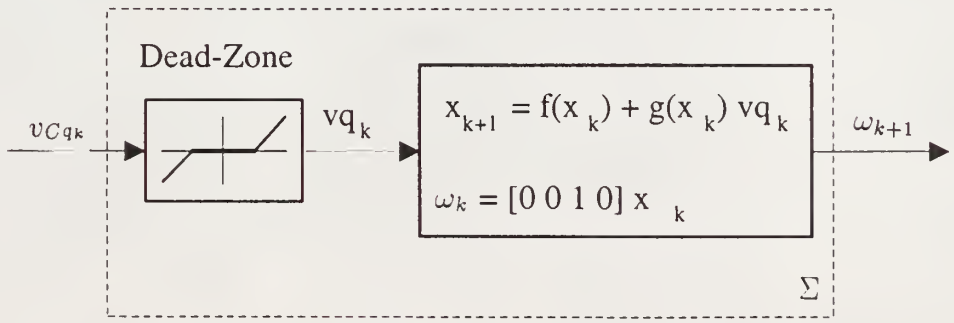

Figure 4.3: The block diagram of the system $\Sigma: \mathcal{D} \rightarrow S(\Re) : v_{Cq} \mapsto \omega$ for the PM Stepper Motor Model Example.

The block diagram of an approximate right inverse system $\Psi: S_{2\pi \cdot 50}(\alpha) \rightarrow S(\Re) : \omega_C \mapsto v_{q\text{inv}}$ is shown in Figure 4.4. The first block calculates the raw quadrature voltage v'_{q_k} for a given angular velocity command ω_{C_k}. The analytical expression for the continuous dead-zone inverse (CDI) is given by

$$v_{q\text{inv}_k} = CDI(v'_{q_k}) = \begin{cases} v'_{q_k} + 1 & \text{if} \quad v'_{q_k} \geq \frac{1}{G-1} \\ G \cdot v'_{q_k} & \text{if} \quad -\frac{1}{G-1} < v'_{q_k} < \frac{1}{G-1} \\ v'_{q_k} - 1 & \text{if} \quad v'_{q_k} \leq -\frac{1}{G-1} \end{cases} . \tag{4.22}$$

Here $G = \|CDI(\cdot)\|$ represents the Lipschitz semi-norm of the CDI system. The range of G is $1 < G < \infty$. In the CDI block, the voltage quadrature command $v_{q\text{inv}_k}$ is determined by using (4.22) on the raw quadrature voltage v'_{q_k}. The voltage quadrature command $v_{q\text{inv}_k}$ is then used to update the states x_{inv_k} of the system Ψ.

Two integrations of v_q are required to reach ω. This results in the discretized model of at least a two step delay. Therefore, $\mathcal{L}(\Sigma) \geq 2$. From Figure 4.4 it follows that $\mathcal{L}(\Psi) \geq 0$. Theorem 3.1.2 applied to the composite system $\Sigma\Psi: S_{2\pi \cdot 50}(\alpha) \rightarrow S(\Re) : \omega_C \mapsto \omega$ yields $\mathcal{L}(\Sigma\Psi) \geq 2$. For the simulation, $g(x_k) = [0 \ \frac{1}{L}\Delta t \ 0 \ 0]' \neq 0$ in (4.19) for all $v_{C_q} \in \mathcal{D}$ and a given x_0. The design integer is taken as $\lambda = 2$ for an approximate right inverse system Ψ.

For the simulation of 40 milli-seconds, a sampling period of 100 micro-seconds yields a sequence of 400 points. In the previous section, the global maximum was

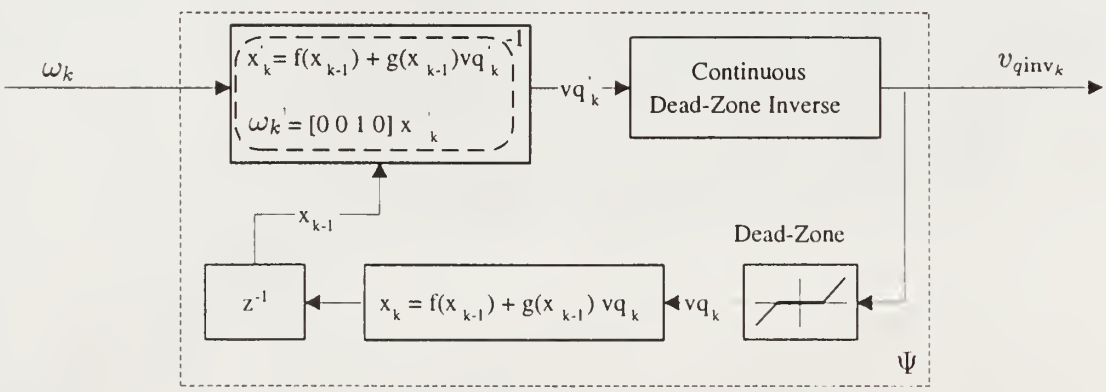

Figure 4.4: The block diagram of an approximate right inverse system $\Psi: S_{2\pi \cdot 50}(\alpha) \rightarrow S(\Re) : \omega_C \mapsto v_{q\text{inv}}$ for the PM Stepper Motor Model Example.

shown to be on the boundary. For simulation purposes, the global maximum is assumed to be an extreme point. The pre-filtered binary random sequences have only the values ± 1350 RPM, the extreme points of $S(1350)$. Table 4.2 shows the Monte Carlo results for 4 different system gains G of the CDI system: 2, 10, 100 and 1000, where the error $|\omega_C - D^{-2}\Sigma\Psi(\omega_C)|$ is evaluated for each of the sequences. As can be seen from Table 4.2, as $G \to \infty$, the error $|\omega_C - D^{-2}\Sigma\Psi(\omega_C)| \to 0$ in a linear fashion. For the limiting case as $G \to \infty$, an approximate right inverse system Ψ is not continuous. However, the performance bound $\mathcal{P}(\Sigma)$ appears to be directly proportional to the system gain G. This observation will be proven true in the following subsection.

From Table 4.2, the maximum value of $|\omega_C - D^{-2}\Sigma\Psi(\omega_C)|$, for $G = 10$ rad/sec, is 0.02686. This corresponds to the 18^{th} sequence in the Monte Carlo run. In the following subsection we will calculate the estimate of the performance bound $\tilde{\mathcal{P}}(\Sigma)$ over the optimization set $S_{2\pi\cdot 50}(1350)$. A first estimate is $\tilde{\mathcal{P}}(\Sigma) \geq 0.02686$. In Figure 4.5, the 18^{th} sequence for ω_C, the filtered square wave, is plotted with the response sequence $\Sigma\Psi(\omega_C)$, without the D^{-2} shift since the errors are less than 0.01% of the magnitude of the signal. The absolute angular velocity error sequence is plotted in Figure 4.6. The quadrature voltage v_q and the absolute quadrature voltage error, $|v'_{q_k} - v_{q_k}|$, are plotted in Figure 4.7 and Figure 4.8, respectively. Note, that Figure 4.6 and Figure 4.8 appear to be the same figure but of different scales.

4.3.2 The Estimate of the Performance Bound $\tilde{\mathcal{P}}(\Sigma)$

In this section, we will find an estimate of the performance bound $\tilde{\mathcal{P}}(\Sigma)$ for the voltage control problem of a PM stepper motor by using the optimization definition as follows:

$$\tilde{\mathcal{P}}(\Sigma) = \sup_{\omega_C \in S_{2\pi\cdot 50}(1350)} \left|\omega_C - D^{-2}\Sigma\Psi(\omega_C)\right| \tag{4.23}$$

Table 4.2: Family of Sequences, $S_{2\pi\cdot 50}(1350)$, Comparison

	Approximate Right Inverse Error $\lvert\omega_C - D^{-2}\Sigma\Psi(\omega_C)\rvert$			
Sequence	Gain $G = 2$	Gain $G = 10$	Gain $G = 100$	Gain $G = 1000$
1	0.1339	0.02628	0.001151	0.0002244
2	0.1341	0.02588	0.001021	0.0000000
3	0.1342	0.02510	0.001979	0.0001157
4	0.1343	0.02546	0.001346	0.0000000
5	0.1332	0.02623	0.001882	0.0000000
6	0.1336	0.02631	0.000332	0.0000000
7	0.1343	0.02652	0.002509	0.0000000
8	0.1340	0.02608	0.000279	0.0000000
9	0.1341	0.02659	0.001415	0.0000000
10	0.1326	0.02628	0.001764	0.0000000
11	0.1343	0.02641	0.001312	0.0002664
12	0.1339	0.02650	0.002210	0.0000549
13	0.1344	0.02617	0.000710	0.0000000
14	0.1332	0.02537	0.002150	0.0000000
15	0.1334	0.02670	0.002611	0.0000000
16	0.1328	0.02683	0.002629	0.0000000
17	0.1334	0.02662	0.002360	0.0001910
18	0.1336	0.02686	0.001415	0.0000000
19	0.1341	0.02619	0.002322	0.0000000
20	0.1341	0.02636	0.002085	0.0000224
21	0.1337	0.02680	0.002059	0.0000000
22	0.1342	0.02615	0.002300	0.0002322
23	0.1337	0.02464	0.000000	0.0000000
24	0.1343	0.02566	0.001393	0.0000000
25	0.1342	0.02677	0.002103	0.0002603
max	0.1344	0.02686	0.002629	0.0002664

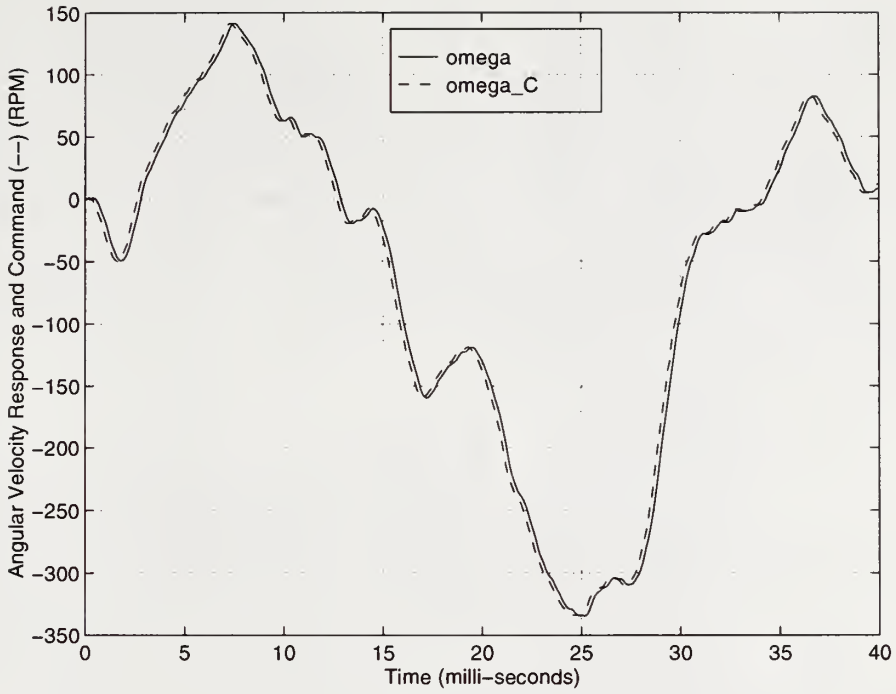

Figure 4.5: The angular velocity response $\omega = \Sigma\Psi(\omega_C)$ and the command $\omega_C \in S_{2\pi\cdot 50}(1350)$ with system gain $G = 10$ are shown for the 18^{th} sequence in the Monte Carlo run.

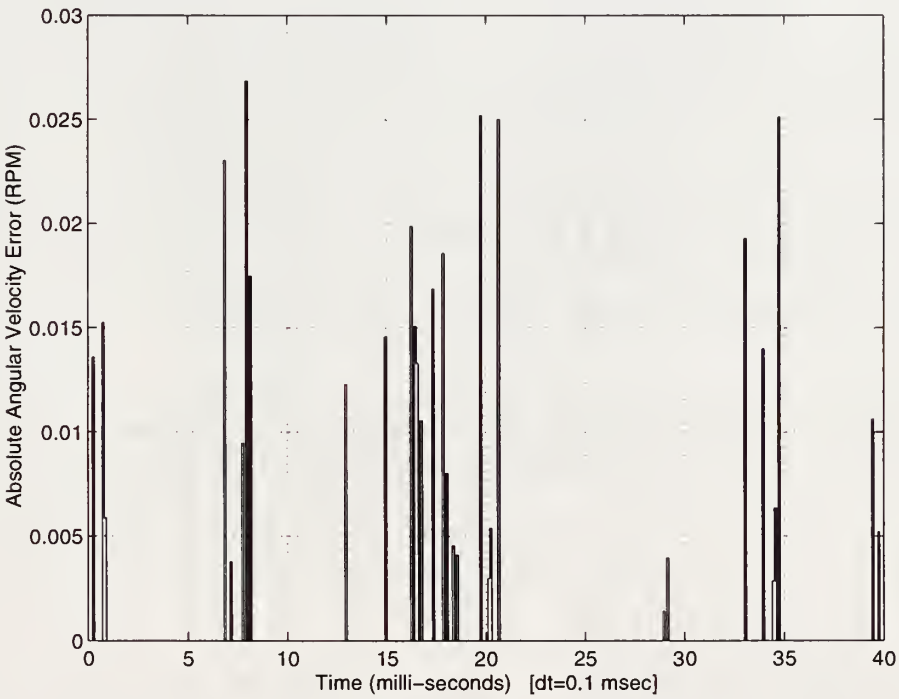

Figure 4.6: The absolute angular velocity error, $|\omega_{C_k} - D^{-2}\Sigma\Psi(\omega_{C_k})|$, is shown for the 18^{th} sequence in the Monte Carlo run of $q_C \in S_{2\pi\cdot 50}(1350)$ with system gain $G = 10$ where $|\omega_C - D^{-2}\Sigma\Psi(\omega_C)| = 0.02686$.

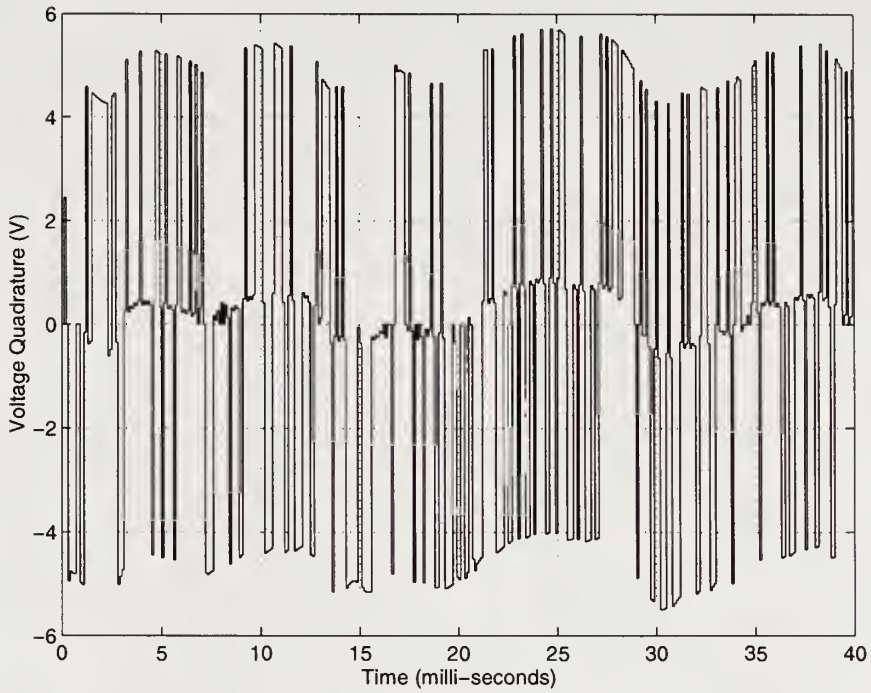

Figure 4.7: The quadrature voltage v_q is shown for the 18^{th} sequence in the Monte Carlo run of $\omega_C \in S_{2\pi\cdot 50}(1350)$ with system gain $G = 10$.

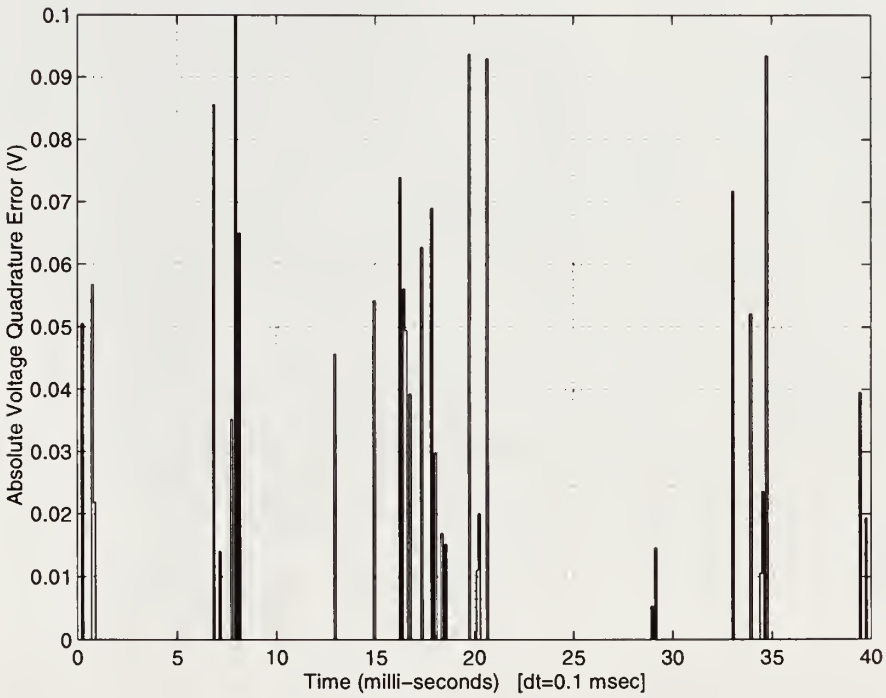

Figure 4.8: The absolute quadrature voltage error, $|v'_{q_k} - v_{q_k}|$, is shown for the 18^{th} sequence in the Monte Carlo run of $\omega_C \in S_{2\pi\cdot 50}(1350)$ with system gain $G = 10$ where $|v'_q - v_q| = 0.0993$.

where the system Σ and an approximate right inverse system Ψ are illustrated in Figure 4.3 and Figure 4.4, respectively.

The first block of Figure 4.4 calculates the raw quadrature voltage v'_{q_k} for a given angular velocity command ω_{C_k}. In the CDI block, the voltage quadrature command $v_{q\text{inv}_k}$ is determined by using (4.22) on the raw quadrature voltage v'_{q_k}. In Figure 4.3 ($v_{Cq_k} = v_{q\text{inv}_k}$), the quadrature voltage v_{q_k} is the output of the DZ block by using (4.21). The composition of (4.22) and (4.21) yields

$$v_{q_k} = DZ\left(CDI\left(v'_{q_k}\right)\right) = \begin{cases} v'_{q_k} & \text{if} \quad v'_{q_k} \geq \frac{1}{G-1} \\ G \cdot v'_{q_k} - 1 & \text{if} \quad \frac{1}{G} < v'_{q_k} < \frac{1}{G-1} \\ 0 & \text{if} \quad -\frac{1}{G} \leq v'_{q_k} \leq \frac{1}{G} \\ G \cdot v'_{q_k} + 1 & \text{if} \quad -\frac{1}{G-1} < v'_{q_k} < -\frac{1}{G} \\ v'_{q_k} & \text{if} \quad v'_{q_k} \leq -\frac{1}{G-1}. \end{cases} \tag{4.24}$$

It follows then that for $v'_{q_k} = \pm\frac{1}{G}$,

$$\sup_{v'_q \in S(\Re)} \left|v'_q - v_q\right| = \sup_{v'_q \in S(\Re)} \left|v'_q - DZ\left(CDI\left(v'_{q_k}\right)\right)\right| = \frac{1}{G}. \tag{4.25}$$

For $G = 10$, $\frac{1}{G} = 0.1$, and this is consistent with Figure 4.8 where $|v'_q - v_q| = 0.09993 \leq \frac{1}{G}$.

The maximum quadrature voltage error occurs when the magnitude of the raw quadrature voltage $|v'_{q_k}| = \frac{1}{G}$. Since there is a feedback loop inside an approximate inverse system Ψ, the quadrature voltage errors are not accumulative with respect to the angular velocity errors. Evaluating the right hand side of (4.23) with $|v'_{q_k}| = \frac{1}{G}$ will give us the estimate of the performance bound which requires two integrations of the errors as follows:

$$\begin{aligned} |\Delta v_{q_k}| &= \frac{1}{G} \quad \text{at } |v'_{q_k}| = \frac{1}{G} \\ |\Delta i_{q_{k+1}}| &= \frac{1}{G \cdot L}\Delta t \\ |\Delta \omega_{q_{k+2}}| &= \frac{60}{2\pi}\frac{K_m}{G \cdot L \cdot J}\Delta t^2 \end{aligned}$$

or

$$\tilde{\mathcal{P}}(\Sigma) = \frac{60}{2\pi}\frac{K_m}{G \cdot L \cdot J}\Delta t^2. \tag{4.26}$$

Using the optimization set $\omega_C \in S_{2\pi \cdot 50}(1350)$, and for $G = 10$, this yields $\tilde{\mathcal{P}}(\Sigma) = 0.02688$. The estimate is 0.00002 higher than the value from Table 4.2 of 0.02686. The estimate of the performance bound $\tilde{\mathcal{P}}(\Sigma)$ is directly proportional to the system gain G. Figure 4.6 is a scaling of Figure 4.8 by a factor of $\frac{60}{2\pi}\frac{K_m}{L \cdot J}\Delta t^2$. In this example, we have found a closed form solution for an estimate of the performance bound given by $\tilde{\mathcal{P}}(\Sigma)$ which was verified by simulation. In the next 2 examples, nonlinear programming algorithms will be used to calculate $\tilde{\mathcal{P}}(\Sigma)$.

4.4 Aerodynamic Model Example

This section will provide an example of the performance bound calculation for the longitudinal control of an aircraft. Control of pitch attitude of an aircraft can be achieved by deflecting all or portion of either a forward or aft tail surface. The derivation of the equations of motion of the aircraft with the assumption that the roll rate, yaw rate and y-velocity component in the body-axes frame are all zero is found in [4]. These equations are:

$$\dot{u} = \frac{1}{\mathrm{m}}\left[X\left(u, w, q, \delta\right) + T - \mathrm{mg}\sin(\theta)\right] - wq \tag{4.27}$$

$$\dot{v} = \frac{1}{\mathrm{m}}\left[Z\left(u, w, q, \delta\right) + \mathrm{mg}\cos(\theta)\right] + uq \tag{4.28}$$

$$\dot{q} = M\left(u, w, q, \theta, \delta\right)/\mathrm{I}_{yy} \tag{4.29}$$

$$\dot{\theta} = q \tag{4.30}$$

where u and w are the body-axis x-velocity component and the body-axis z-velocity component, respectively. The body-axis pitch rate and the Euler pitch angle are given by q and θ, respectively. The longitudinal control input or elevator deflection is given by δ. X and Z are the aerodynamic forces and M is aerodynamic moment. The following are constants: T, thrust; m, mass; g, gravity; and I_{yy}, moment of inertia. The aerodynamic forces and moments are represented by the means of the

aerodynamic stability coefficients as seen below:

$$\begin{aligned}
\alpha &= \arctan(w/u) \\
\dot{\alpha} &= \frac{1}{u^2}\left(\cos(\alpha)\right)^2\left(\dot{w}u - w\dot{u}\right) \\
Q &= \frac{1}{2}\rho\left(u^2 + w^2\right) \\
L &= \left(C_L + C_{L_\alpha}\alpha + C_{L_q}q + C_{L_\delta}\delta\right)QS \\
D &= \left(C_D + C_{D_\alpha}\alpha\right)QS \\
X &= L\sin(\alpha) - D\cos(\alpha) \qquad (4.31) \\
Z &= -L\cos(\alpha) - D\sin(\alpha) \qquad (4.32) \\
M &= \left(C_m + C_{m_\alpha}\alpha + C_{m_{\dot{\alpha}}}\dot{\alpha} + C_{m_q}q + C_{m_\delta}\delta\right)QS\bar{c}. \qquad (4.33)
\end{aligned}$$

Here α and $\dot{\alpha}$ are the angle of attack and the angle of attack rate, respectively. Q is the dynamic pressure. The aerodynamic moment, M, and the aerodynamic forces, X and Z, are directly proportional to t he dynamic pressure. L and D are the aerodynamic forces in the wind axes which are known as lift and drag . The following are constants: S, the wing reference area and $\bar{c}$, the wing mean aerodynamic cord.

Table 4.3: The Aerodynamic Model Parameters

Parameter	Value	Parameter	Value
m	1247.390 kg	C_D	0.05
T	1600 N	C_{D_α}	0.33
g	9.81 m·s^{-2}	C_L	0.41
I_{yy}	4066 kg·m^2	C_{L_α}	4.44
ρ	1.225 kg·m^{-3}	C_{L_q}	$3.8{\cdot}\bar{c}/(2u_0)$
S	17.094 m^2	C_{L_δ}	0.355
$\bar{c}$	1.737 m	C_{m_α}	-0.683
u_0	53.8931 m·s^{-1}	$C_{m_{\dot{\alpha}}}$	$-4.36{\cdot}\bar{c}/(2u_0)$
v_0	-0.0931634 m·s^{-1}	C_{m_q}	$-9.96{\cdot}\bar{c}/(2u_0)$
q_0	0 rad·s^{-1}	C_{m_δ}	-0.923
θ_0	0 rad		
δ_{-1}	0.00128510 rad		

The reference geometry, mass characteristics, and aerodynamic characteristics of the general aviation airplane: NAVION were taken from Appendix B of the

reference [33]. The values of the parameters are shown in Table 4.3. The equations of motion are discretized using second order Runge-Kutta integration. Let $x_k = [u_k \; v_k \; q_k \; \theta_k]'$. Equations (4.27) through (4.30) take the following form:

$$x_{k+1} = f(x_k) + g(x_k) \cdot \delta_k \tag{4.34}$$

$$q_k = \begin{bmatrix} 0 & 0 & 1 & 0 \end{bmatrix} \cdot x_k \tag{4.35}$$

where $x_k \in \Re^4$ and f, g are vector fields on $\Re^4$.

The actuator has a first-order response modelled by $G(s) = 10/(s+10)$ which has rate constraints of 15 deg/sec and position constraints of 15 deg. The system $\Sigma: \mathcal{D} \rightarrow S(\Re) : \delta_C \mapsto q$, where $\mathcal{D} \subset S(\Re)$, is the composition of the equations of motion with the actuator dynamics for which δ_C is the elevator deflection command. Figure 4.9 shows the block diagram of the system Σ.

4.4.1 Simulation

The signal of interest is the pitch rate signal q. It is assumed that all signals of interest start at rest (i.e., $q_n = 0$ for all $n \leq n_0$). The absolute bound of $|q| \leq 1.15$ deg/sec was imposed so that after 10 seconds of flight, the aircraft will always be within its parameters of good flight conditions. Typical pitch rate commands are generated by the longitudinal autopilot. The altitude hold mode and the mach hold mode have time constants of approximately 100 milli-seconds ([4]). This corresponds to a restriction on bandwidth of q to be approximately 10 rad/sec.

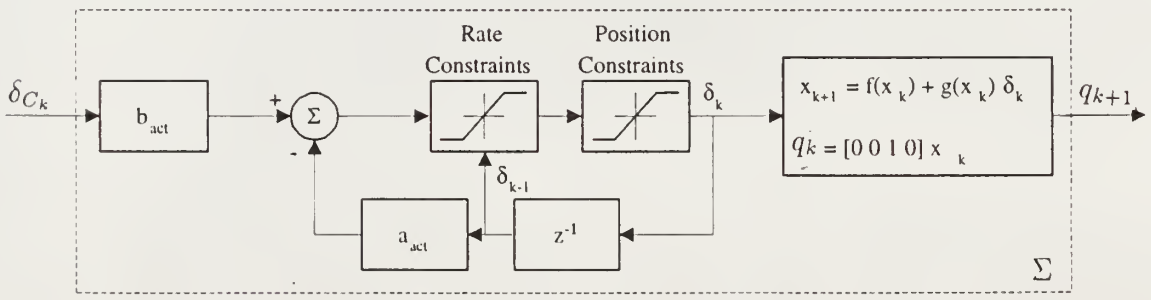

Figure 4.9: The block diagram of the system $\Sigma: \mathcal{D} \rightarrow S(\Re) : \delta_C \mapsto q$ for the Aerodynamic Model Example.

The block diagram of an approximate right inverse system $\Psi: S_{\Omega_{LP}}(\alpha) \rightarrow S(\Re) : q_C \mapsto \delta_{\text{inv}}$ is shown in Figure 4.10. The first block calculates the raw elevator deflection δ'_k for a given pitch rate command q_{C_k}. In the limiting logic block, the elevator deflection command δ_{inv} is determined by first using the constraints on the raw elevator deflection δ'_k and then using the inverse actuator dynamics. The elevator deflection command δ_{inv} is then used to update the states x_{inv} of the system Ψ.

One step delay of δ_C is required to reach q. Therefore, $\mathcal{L}(\Sigma) \geq 1$. From Figure 4.10 it follows that $\mathcal{L}(\Psi) \geq 0$. Theorem 3.1.2 applied to the composite system $\Sigma\Psi: S_{\Omega_{LP}}(\alpha) \rightarrow S(\Re) : q_C \mapsto q$ yields $\mathcal{L}(\Sigma\Psi) \geq 1$. For the considered flight conditions, $g(x_k) \neq 0$ in (4.34) for all $\delta_C \in \mathcal{D}$ and a given x_0. The design integer is taken as $\lambda = 1$ for an approximate right inverse system Ψ.

For a simulation of 10 seconds, a sampling period of 40 milli-seconds yields a sequence of 250 points. The pre-filtered binary random sequences have only the values ± 1.15 deg/sec because we are only interested in the extreme points of $S(1.15)$. Table 4.4 shows the Monte Carlo results for 3 different cutoff frequencies Ω_{LP}: 10, 15, and 20 rad/sec, where the error $|q_C - D^{-1}\Sigma\Psi(q_C)|$ is evaluated for each of the sequences. For practical purposes, as can be seen from Table 4.4, the system $\Psi: S_{10}(1.15) \rightarrow S(\Re)$ is a right inverse of the system Σ.

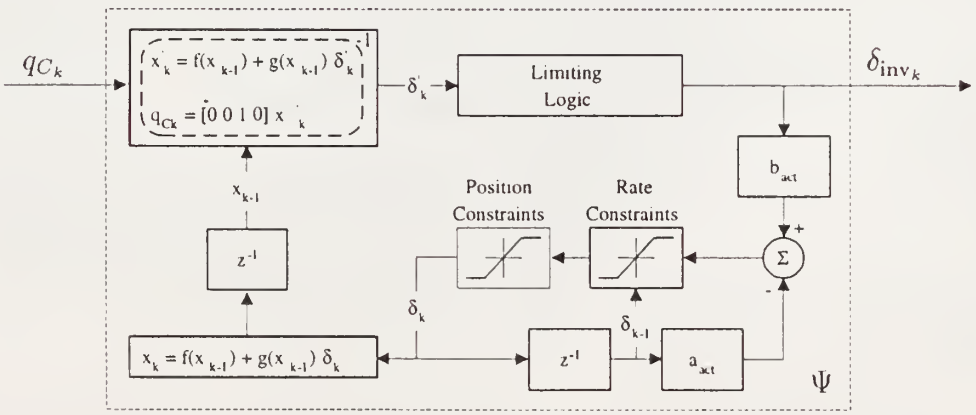

Figure 4.10: The block diagram of an approximate right inverse system $\Psi: S_{\Omega_{LP}}(\alpha) \rightarrow S(\Re) : q_C \mapsto \delta_{\text{inv}}$ for the Aerodynamic Model Example.

Table 4.4: Family of Sequences, $S_{\Omega_{LP}}(1.15)$, Comparison

	Approximate Right Inverse Error $\lvert q_C - D^{-1}\Sigma\Psi(q_C)\rvert$		
Sequence	Ω_{LP} = 10 rad/sec	Ω_{LP} = 15 rad/sec	Ω_{LP} = 20 rad/sec
1	4.996E-16	0.9075	1.353
2	4.163E-16	1.7650	2.265
3	3.331E-16	0.4226	1.553
4	2.776E-16	0.3620	1.121
5	3.608E-16	0.5654	1.592
6	3.331E-16	0.4446	1.356
7	3.331E-16	1.4340	2.153
8	2.498E-16	0.9444	1.788
9	3.331E-16	0.6539	1.896
10	4.441E-16	1.2530	1.931
11	2.220E-16	1.2270	2.121
12	5.551E-16	0.9812	1.371
13	4.996E-16	0.7821	1.471
14	5.551E-16	0.7177	1.488
15	4.441E-16	0.6425	1.351
16	4.441E-16	0.7448	1.602
17	5.551E-16	0.4841	1.454
18	4.996E-16	0.4835	1.586
19	4.441E-16	0.6658	1.585
20	3.331E-16	0.7861	1.675
21	3.608E-16	0.5702	1.544
22	3.331E-16	0.6071	1.809
23	3.886E-16	0.6047	1.635
24	3.053E-16	0.4456	1.797
25	4.441E-16	0.9205	1.413
max	5.551E-16	1.7650	2.265

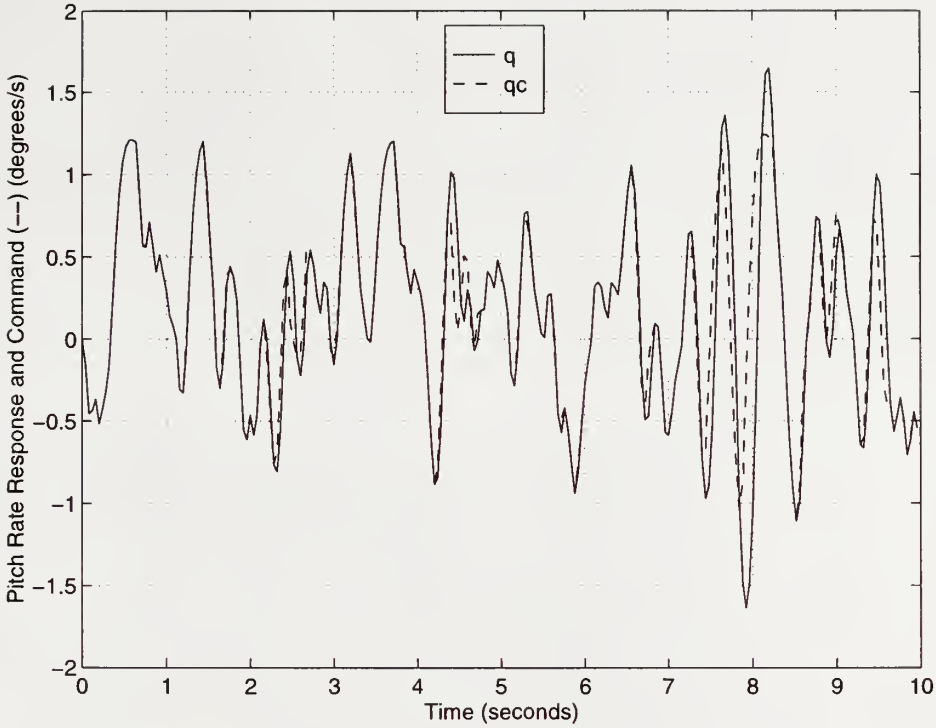

Figure 4.11: The shifted pitch rate response $q = D^{-1}\Sigma\Psi(q_C)$ and the command $q_C \in S_{15}(1.15)$ are shown for the 2^{nd} sequence in the Monte Carlo run.

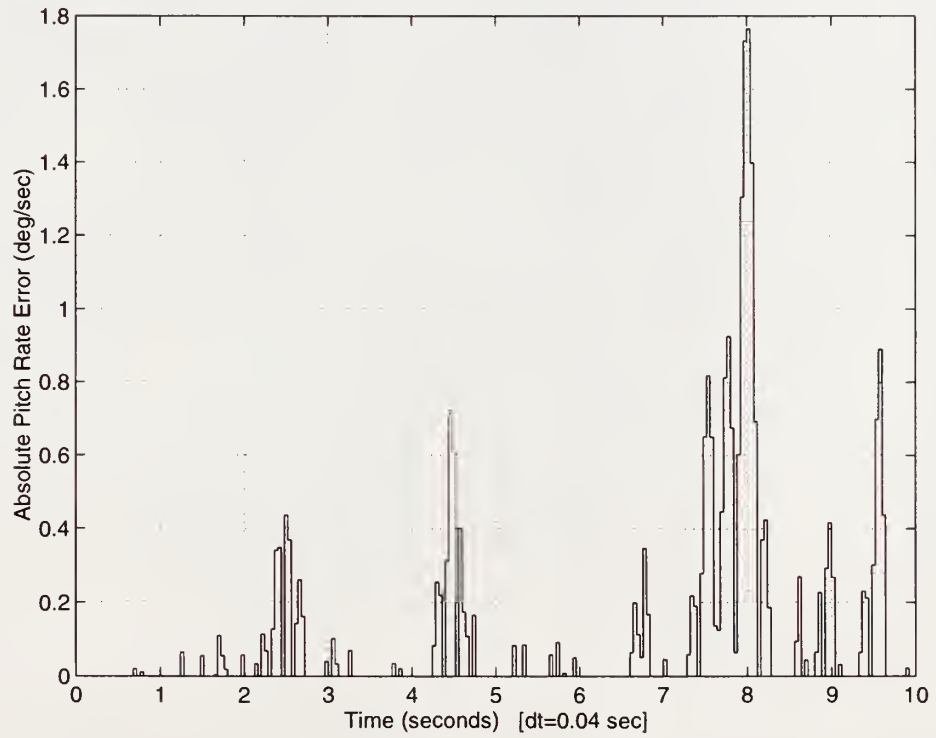

Figure 4.12: The absolute pitch rate error, $|q_{C_k} - D^{-1}\Sigma\Psi(q_{C_k})|$, is shown for the 2^{nd} sequence in the Monte Carlo run of $q_C \in S_{15}(1.15)$ where $|q_C - D^{-1}\Sigma\Psi(q_C)| = 1.765$.

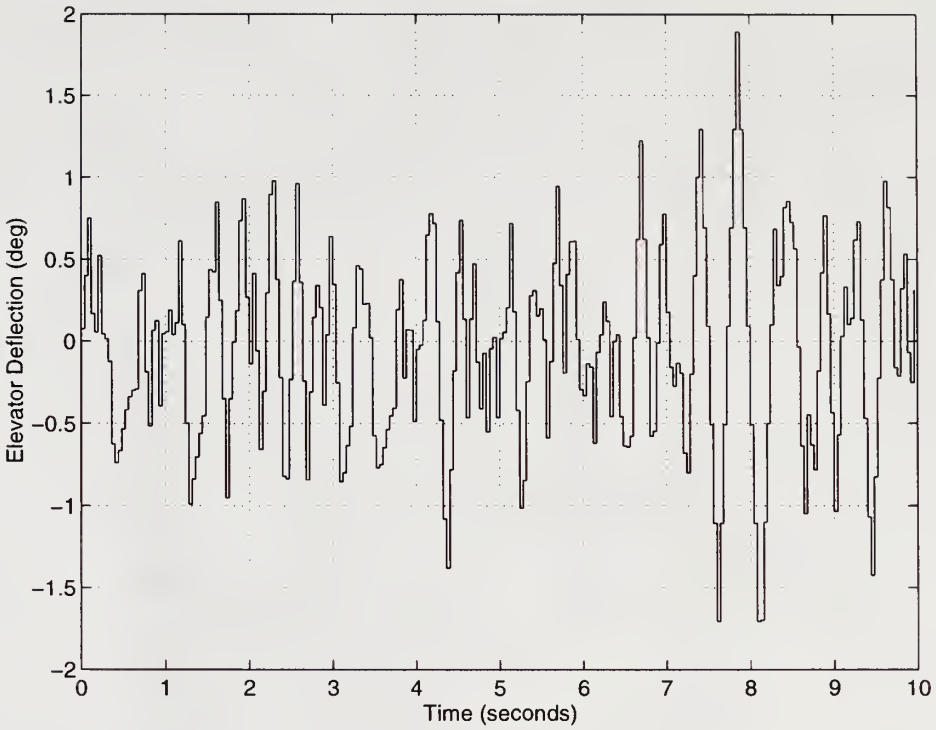

Figure 4.13: The elevator deflection δ is shown for the 2^{nd} sequence in the Monte Carlo run of $q_C \in S_{15}(1.15)$.

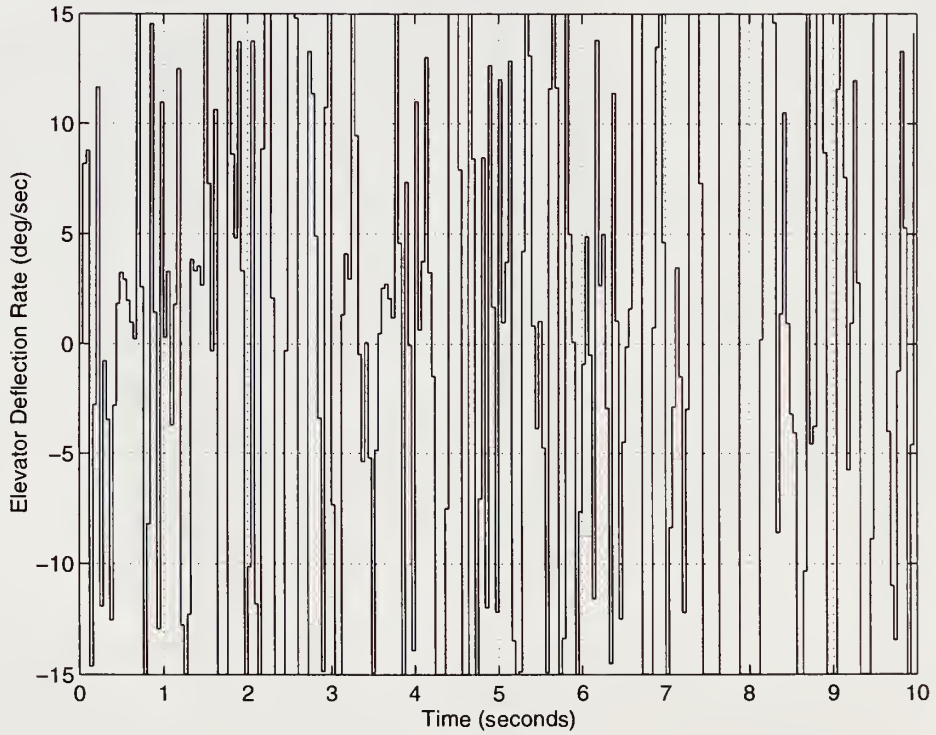

Figure 4.14: The elevator deflection rate $\dot{\delta}$ is shown for the the 2^{nd} sequence in the Monte Carlo run of $q_C \in S_{15}(1.15)$.

From Table 4.4, the maximum value of $|q_C - D^{-1}\Sigma\Psi(q_C)|$ for $\Omega_{LP} = 15$ rad/sec is 1.765. This corresponds to the 2^{nd} sequence in the Monte Carlo run. In the following subsection we will calculate the estimate of the performance bound $\tilde{\mathcal{P}}(\Sigma)$ over the optimization set $S_{15}(1.15)$. A first estimate is $\tilde{\mathcal{P}}(\Sigma) \geq 1.765$. In Figure 4.11, the 2^{nd} sequence of q_C, the filtered square wave, is plotted with the corresponding shifted sequence $\Sigma\Psi(q_C)$ which is shifted one step to the left by 40 milli-seconds. The absolute pitch rate error sequence is plotted in Figure 4.12. The elevator deflection δ and elevator deflection rate $\dot{\delta}$ are plotted in Figure 4.13 and Figure 4.14, respectively. As can be seen from Figure 4.12, the maximum error occurs at 8.0 seconds. Examining the plots between 7 and 8 seconds reveals that the pitch rate response is not keeping up with the pitch rate command. The elevator deflection is never position constrained but is rate constrained from 7.44 to 8.12 seconds for a total of 680 milli-seconds. As seen from this example, when we increase the bandwidth of the pitch rate command from 10 to 15 rad/sec, the rate constraints become effective and thus the measure of right singularity is increased.

4.4.2 The Estimate of the Performance Bound $\tilde{\mathcal{P}}(\Sigma)$

In this section, we will find an estimate of the performance bound $\tilde{\mathcal{P}}(\Sigma)$ for the longitudinal control problem of an aircraft by using the optimization definition as follows:

$$\tilde{\mathcal{P}}(\Sigma) = \sup_{q_C \in S_{15}(1.15)} \left| q_C - D^{-1}\Sigma\Psi(q_C) \right| \tag{4.36}$$

where the system Σ and an approximate right inverse system Ψ are illustrated in Figure 4.9 and Figure 4.10, respectively. The discussion following Theorem 4.2.1 in Section 4.2 suggests that the maximum of the right hand side of (4.36) is found by evaluating all extreme points and then finding the maximum. In Section 4.4.1, 25 random extreme points out of possible 2^{250} (1.8903×10^{75}) extreme points were evaluated with the conclusion $\tilde{\mathcal{P}}(\Sigma) \geq 1.765$.

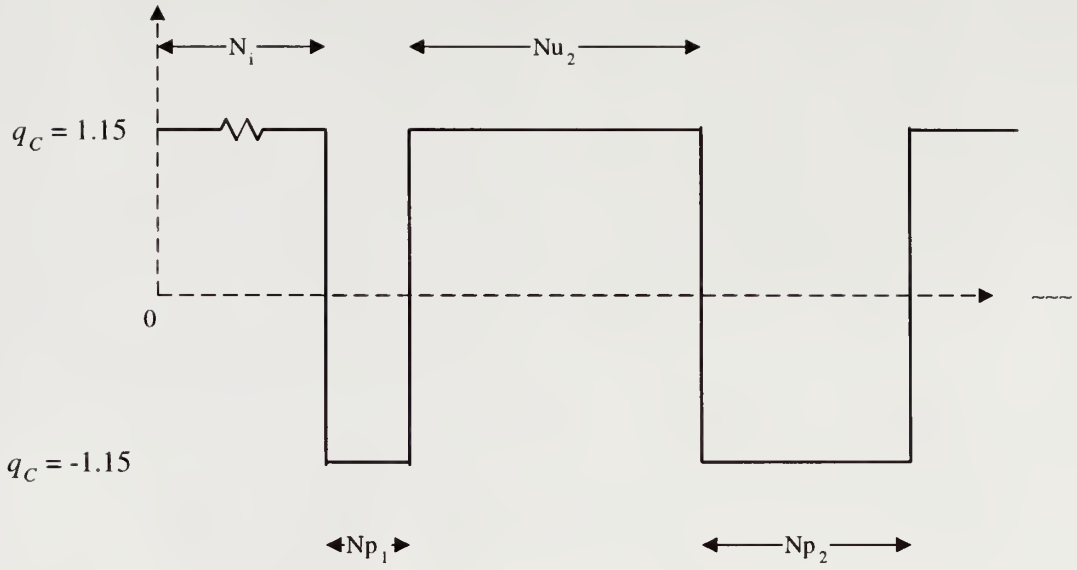

Figure 4.15: Signal Construction's Nomenclature.

It is time to take advantage of the traits of the system. The first block of Figure 4.10 calculates the raw elevator deflection δ'_k for a given pitch rate command q_{C_k}. In mathematical terms it is solving for δ'_k in the following equations:

$$M'_k = \mathrm{I}_{yy}\frac{(q_{C_k} - q_{k-1})}{\Delta t} \tag{4.37}$$

$$M'_k = \Big(C_m + C_{m_\alpha}\alpha_{k-1} + C_{m_q}q_{k-1} + C_{m_{\dot\alpha}}\dot\alpha\,(u_{k-1}, w_{k-1}, \delta'_k) + C_{m_\delta}\delta'_k\Big)Q_{k-1}S\bar{c}. \tag{4.38}$$

As can be seen from (4.38), the raw aerodynamic moment M'_k is affine with respect to the dynamic pressure Q_{k-1}. It turns out that it is also affine with respect to the raw elevator deflection δ'_k. Thus, δ'_k is inversely proportional to Q_{k-1} and decreasing dynamic pressure causes the elevator deflection to increase. This increases the likelihood for the elevator deflection to be rate constrained. Therefore, the optimization region of (4.36) can be reduced to a subset of $S_{15}(1.15)$ which contains a lower than initial dynamic pressure after a period of flight. A pitch-up command, say a command $q_C = 1.15$ deg/sec for at least 2 seconds after initialization, will decrease the dynamic pressure.

Two problems of maximization of convex functions are:

1. Once a local maximum has been found. There is no local information to tell you how to proceed to a higher local maximum.

2. There is no local criterion for deciding whether a given local maximum is really the global maximum.

These features are also applicable to the maximization of non-convex function since its maximum for simulation purposes will be an extreme point. The signal construction and the grid search method will be techniques used to find a higher local maximum to get around the first problems. These two methods are explained in the following paragraphs. After an extensive search for the signal that maximizes (4.36) and an appropriate exiting condition, we can say that we have qualitatively found the global maximum. This alleviates the second problem.

The signal construction will always be done in the pre-filtered space $S(1.15)$ with out any loss of generality since the pre-filtered space $S(1.15)$ is isomorphic to the filtered space $S_{15}(1.15)$. The baseline signal will be $q_C = 1.15$ deg/sec for the entire simulation of 10 seconds. The construction of the signals begins with a pulse $q_C = -1.15$ for Np_1 steps and starting at N_1 steps. An optimization takes place over N_1 and Np_1. The signal construction's nomenclature is shown in Figure 4.15. A second pulse is constructed with Nu_2 steps at $q_C = 1.15$ and Np_2 steps at $q_C = -1.15$. The optimization takes place over N_2, Nu_2, and Np_2 with Np_1 fixed. This procedures continues until the $(i+1)$-th pulse optimization does not produce higher maxima.

A signal with i pulses has $2i$ parameters, $(N_i, Np_1, \ldots, Np_i, Nu_2, \ldots, Nu_i)$. In the search grid method the starting parameter N_i (see Figure 4.15) of the pulse train is still optimized over its range. The other $2i-1$ parameters $(Np_1, \ldots, Np_i, Nu_2, \ldots, Nu_i)$ are varied over a selected range. The selected range is based on the available

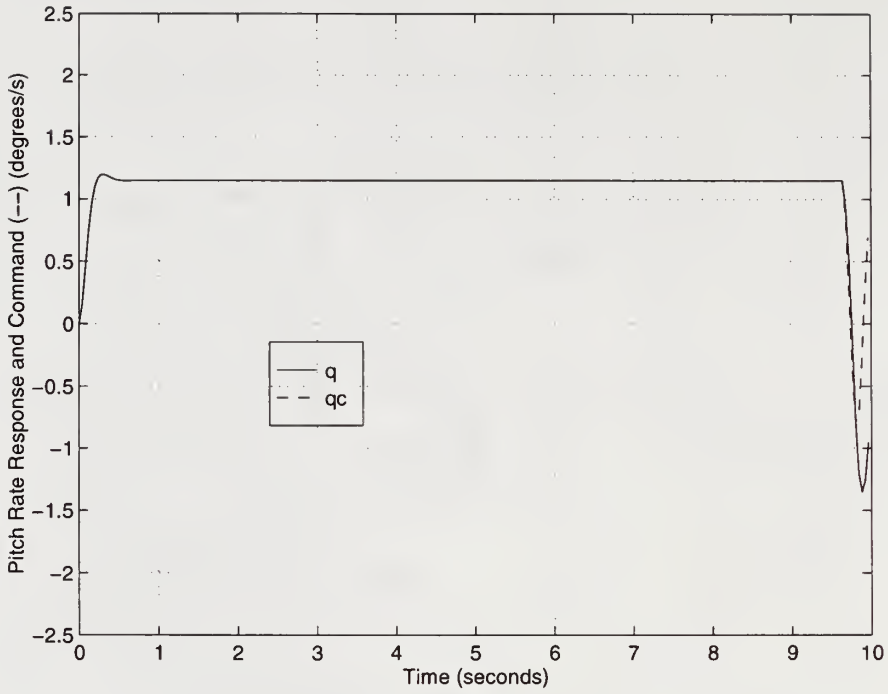

Figure 4.16: The shifted pitch rate response $q = D^{-1}\Sigma\Psi(q_C)$ and the command $q_C \in S_{15}(1.15)$ are shown for the first pulse optimization ($N_1 = 242$, $Np_1 = 4$).

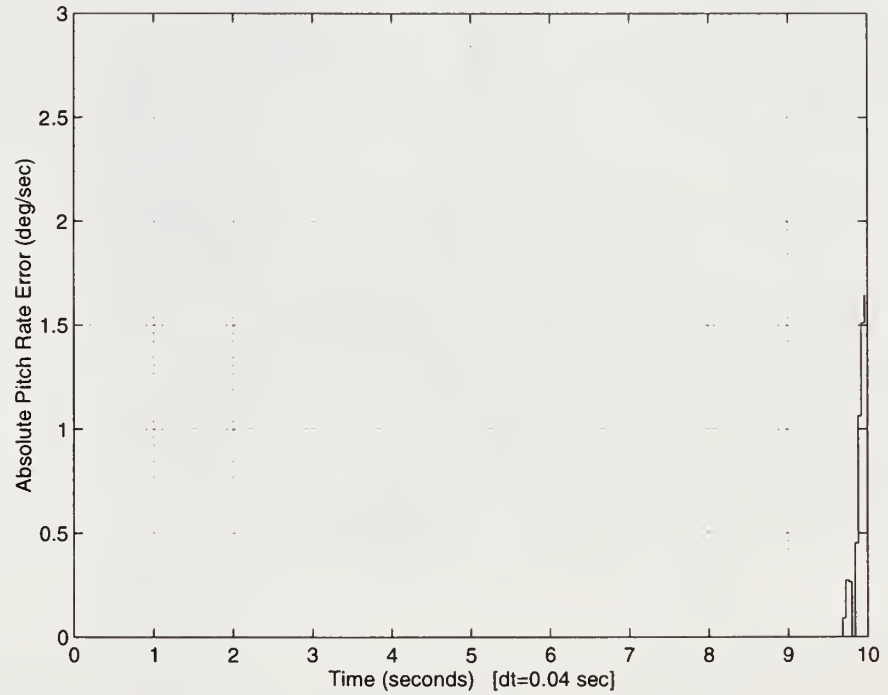

Figure 4.17: The absolute pitch rate error, $|q_{C_k} - D^{-1}\Sigma\Psi(q_{C_k})|$, is shown for the first pulse optimization ($N_1 = 242$, $Np_1 = 4$) of $q_C \in S_{15}(1.15)$ where $|q_C - D^{-1}\Sigma\Psi(q_C)| = 1.646$.

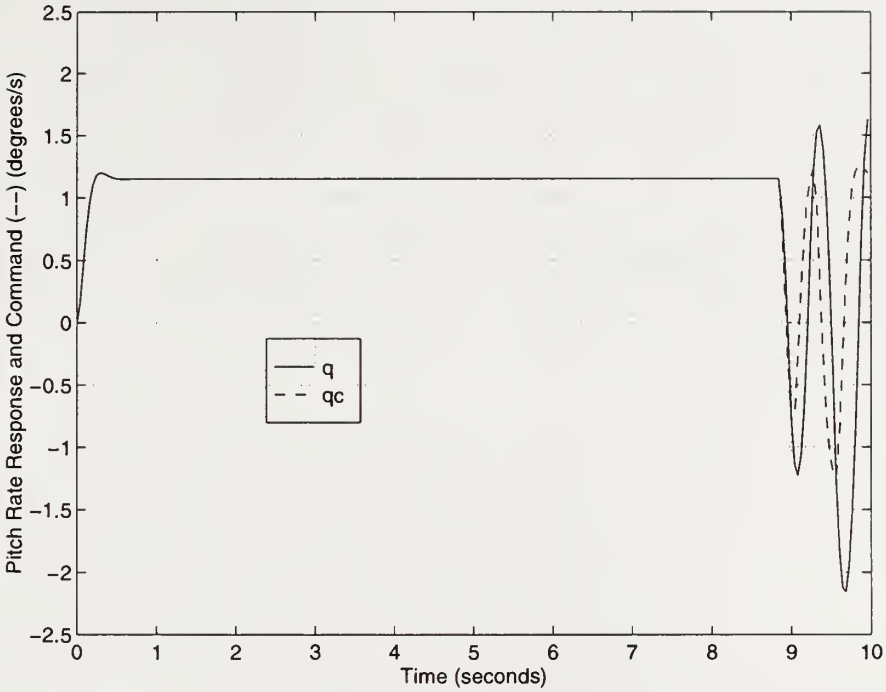

Figure 4.18: The shifted pitch rate response $q = D^{-1}\Sigma\Psi(q_C)$ and the command $q_C \in S_{15}(1.15)$ are shown for the second pulse optimization ($N_2 = 222$, $Nu_2 = 7$, $Np_2 = 7$).

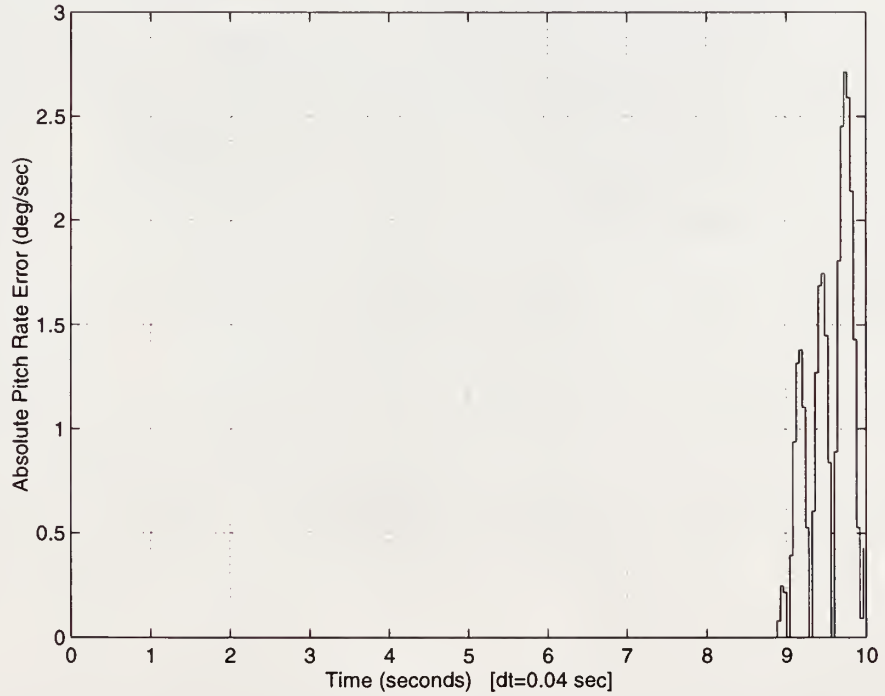

Figure 4.19: The absolute pitch rate error, $|q_{C_k} - D^{-1}\Sigma\Psi(q_{C_k})|$, is shown for the second pulse optimization ($N_2 = 222$, $Nu_2 = 7$, $Np_2 = 7$) of $q_C \in S_{15}(1.15)$ where $|q_C - D^{-1}\Sigma\Psi(q_C)| = 2.713$.

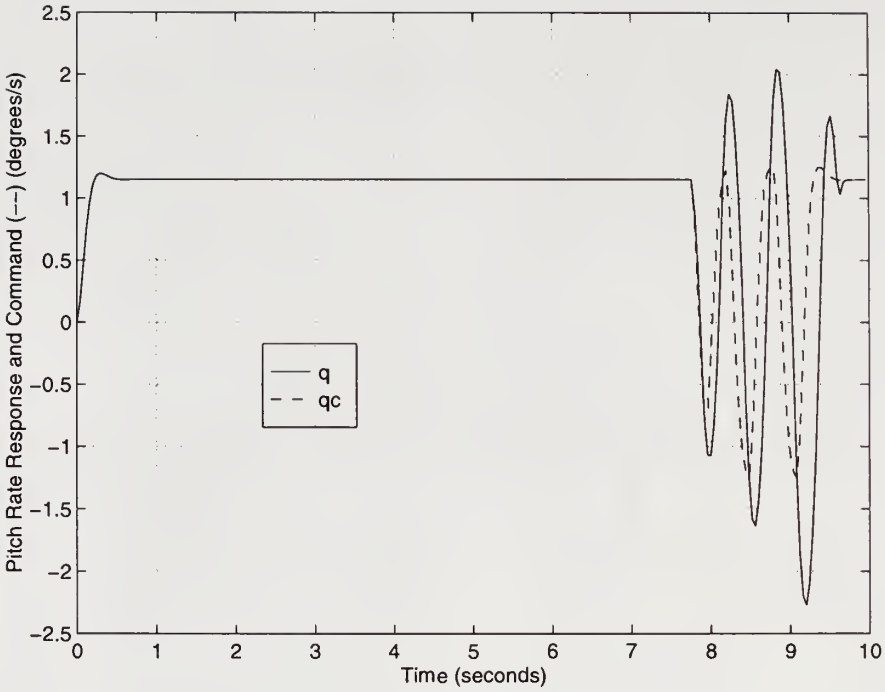

Figure 4.20: The shifted pitch rate response $q = D^{-1}\Sigma\Psi(q_C)$ and the command $q_C \in S_{15}(1.15)$ are shown for the third pulse optimization ($N_3 = 195$, $Nu_3 = 8$, $Np_3 = 7$).

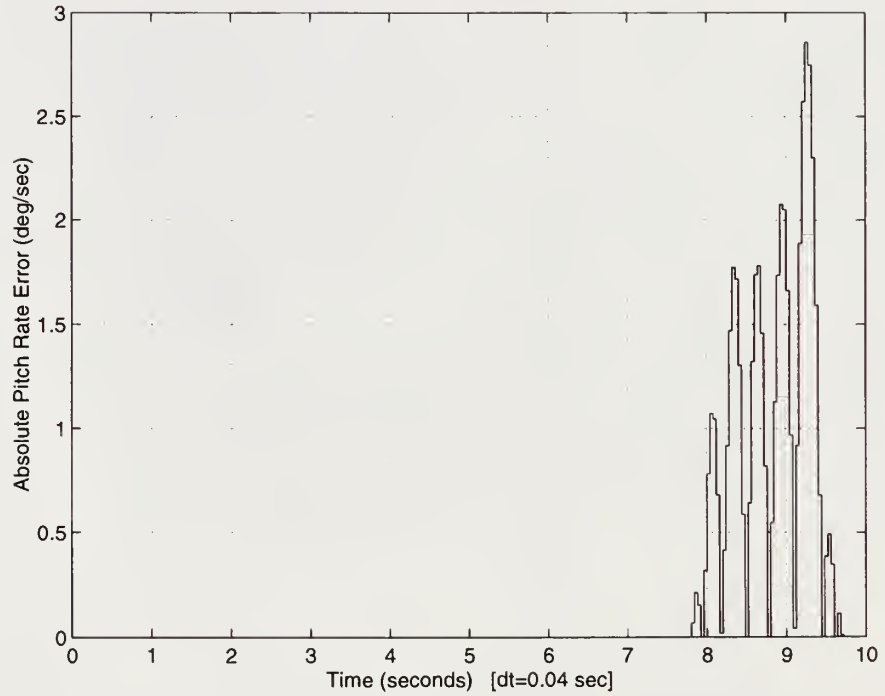

Figure 4.21: The absolute pitch rate error, $|q_{C_k} - D^{-1}\Sigma\Psi(q_{C_k})|$, is shown for the third pulse optimization ($N_3 = 195$, $Nu_3 = 8$, $Np_3 = 7$) of $q_C \in S_{15}(1.15)$ where $|q_C - D^{-1}\Sigma\Psi(q_C)| = 2.856$.

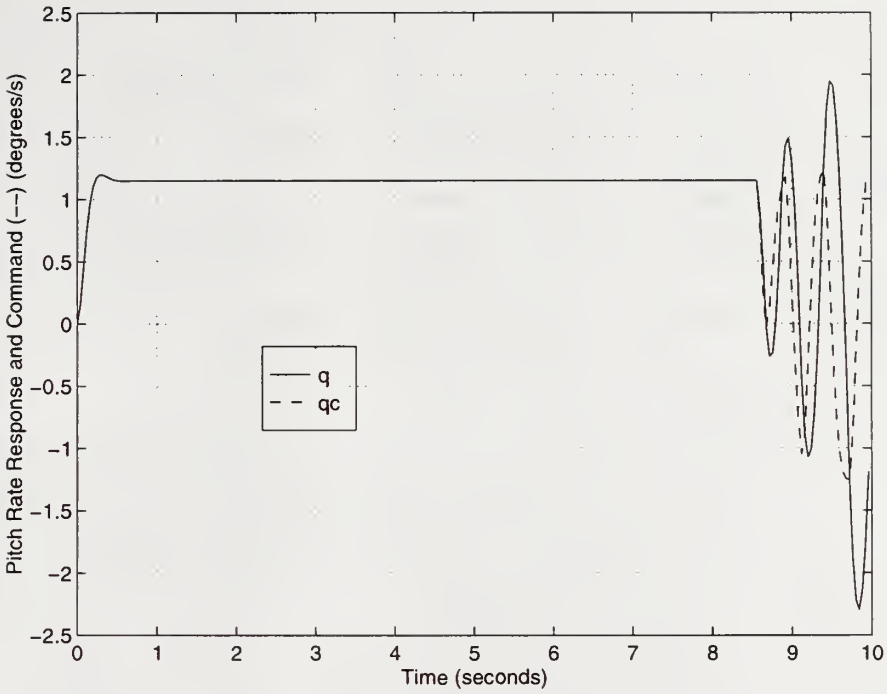

Figure 4.22: The shifted pitch rate response $q = D^{-1}\Sigma\Psi(q_C)$ and the command $q_C \in S_{15}(1.15)$ are shown for the search grid method optimization ($N_3 = 215$, $Np_1 = 2$, $Nu_2 = 7$, $Np_2 = 5$, $Nu_3 = 7$, $Np_3 = 8$).

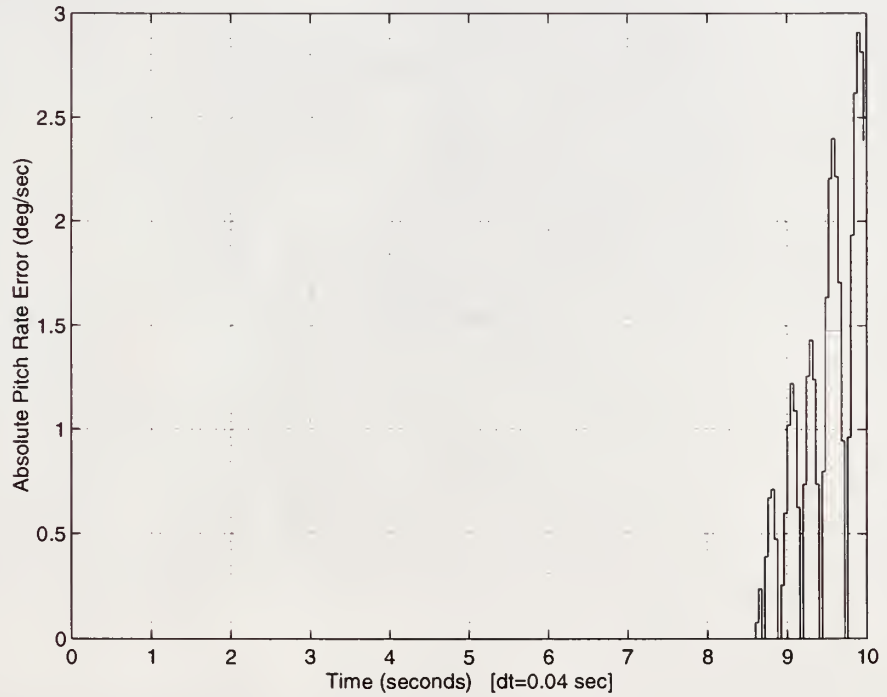

Figure 4.23: The absolute pitch rate error, $|q_{C_k} - D^{-1}\Sigma\Psi(q_{C_k})|$, is shown for the search grid method optimization ($N_3 = 215$, $Np_1 = 2$, $Nu_2 = 7$, $Np_2 = 5$, $Nu_3 = 7$, $Np_3 = 8$) of $q_C \in S_{15}(1.15)$ where $\tilde{\mathcal{P}}(\Sigma) = 2.908$.

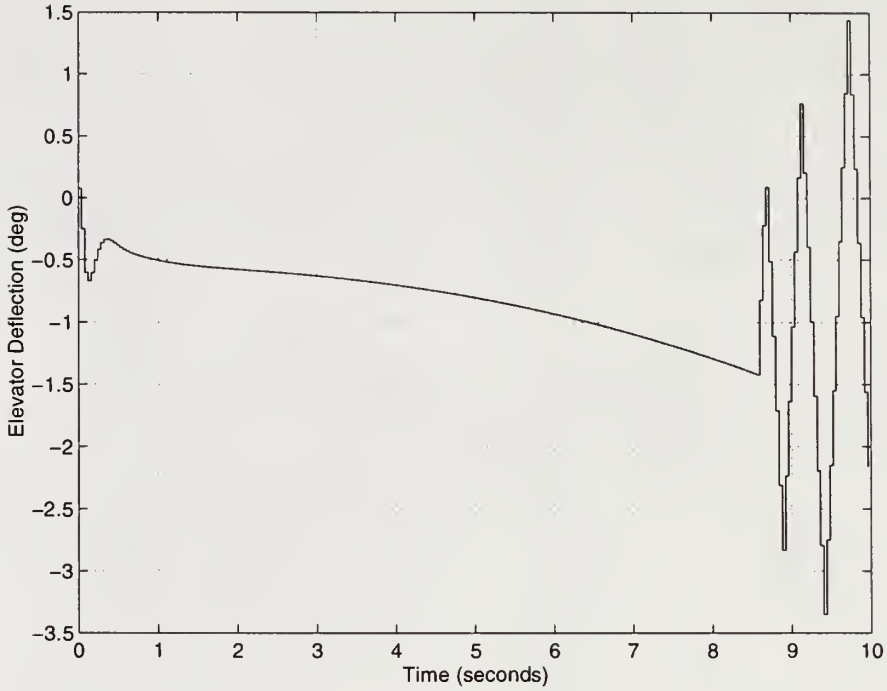

Figure 4.24: The elevator deflection δ is shown for the search grid method optimization ($N_3 = 215$, $Np_1 = 2$, $Nu_2 = 7$, $Np_2 = 5$, $Nu_3 = 7$, $Np_3 = 8$) of $q_C \in S_{15}(1.15)$.

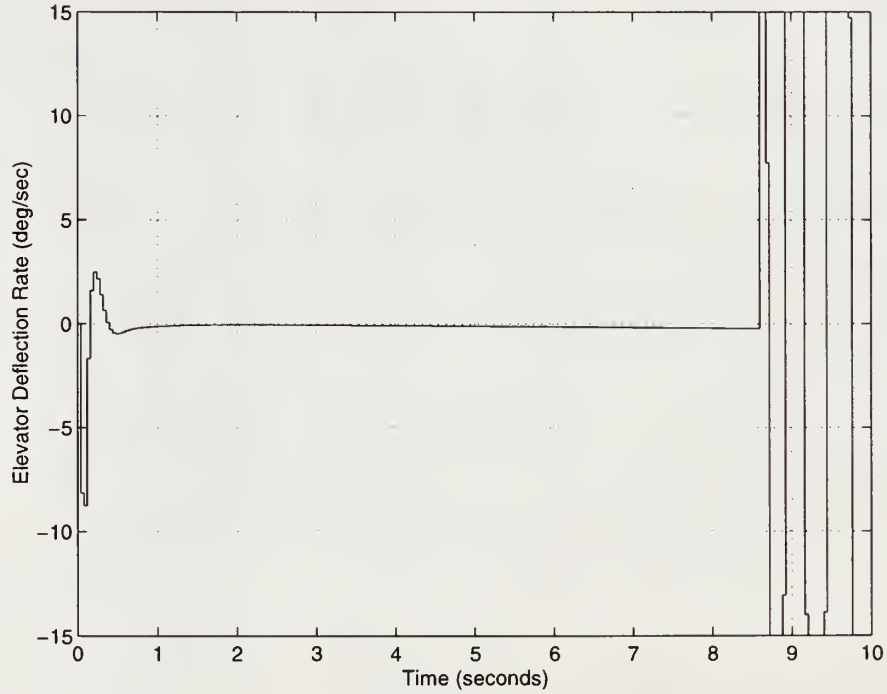

Figure 4.25: The elevator deflection rate $\dot{\delta}$ is shown for the the search grid method optimization ($N_3 = 215$, $Np_1 = 2$, $Nu_2 = 7$, $Np_2 = 5$, $Nu_3 = 7$, $Np_3 = 8$) of $q_C \in S_{15}(1.15)$.

computing power. All points in the selected range are evaluated and then the maximum is found. The maximum of the search grid method is qualitatively the global maximum provided that the selected range is suitable.

The results of the nonlinear programming algorithm, which is the integration of the signal construction and the grid search method, are shown in Table 4.5 and Figures 4.16–4.25. Figure 4.16 and Figure 4.17 represent the first pulse optimization with plots of the sequences q_C, $D^{-1}\Sigma\Psi(q_C)$ and $|q_{C_k} - D^{-1}\Sigma\Psi(q_{C_k})|$. Figure 4.18 and Figure 4.19 represent the second pulse optimization with plots of the sequences q_C, $D^{-1}\Sigma\Psi(q_C)$ and $|q_{C_k} - D^{-1}\Sigma\Psi(q_{C_k})|$. Figure 4.20 and Figure 4.21 represent the third pulse optimization with plots of the sequences q_C, $D^{-1}\Sigma\Psi(q_C)$ and $|q_{C_k} - D^{-1}\Sigma\Psi(q_{C_k})|$.

The third pulse optimization parameters are $(Np_1, Nu_2, Np_2, Nu_3, Np_3) = (4, 7, 7, 8, 7)$. The search grid was taken to be $(2{:}6, 5{:}9, 5{:}9, 6{:}10, 5{:}9)$ which yields 3125 grid points that have to be optimized over the variable N_3. The result of the search grid method and the estimate of the performance bound are:

$$\begin{aligned} (N_3, Np_1, Nu_2, Np_2, Nu_3, Np_3) &= (215,\ 2,\ 7,\ 5,\ 7,\ 8) \\ \hat{\mathcal{P}}(\Sigma) &= 2.908. \end{aligned}$$

The search grid sequence of $q_C \in S_{15}(1.15)$ is examined. In Figure 4.22, the sequence q_C, the filtered square wave, is plotted with the corresponding shifted sequence $\Sigma\Psi(q_C)$ which is shifted one step to the left by 40 milli-seconds. The absolute pitch rate error sequence is plotted in Figure 4.23. The elevator deflection δ and elevator deflection rate $\dot{\delta}$ are plotted in Figure 4.24 and Figure 4.25, respectively. As can be seen from Figure 4.23, the maximum error occurs at 9.88 seconds. Examining the plots between 8.6 and 10 seconds reveals that the pitch rate response does not keep up with the pitch rate command. The elevator deflection is never position

constrained but is rate constrained for a total 1.2 seconds out of the last 1.4 seconds of simulation.

Table 4.5: The Estimate of the Performance Bound $\tilde{\mathcal{P}}(\Sigma)$ for the Aerodynamic Model Example

Optimization Method	Parameters $(N_i, Np_1, Nu_2, Np_2, Nu_3, Np_3)$	$\lvert q_C - D^{-1}\Sigma\Psi(q_C)\rvert$ for $q_C \in S_{15}(1.15)$
First Pulse	$(242, 4)$	1.646
Second Pulse	$(222, 4, 7, 7)$	2.713
Third Pulse	$(195, 4, 7, 7, 8, 7)$	2.856
Search Grid	$(215, 2, 7, 5, 7, 8)$	2.908
$\tilde{\mathcal{P}}(\Sigma) = 2.908$		

4.5 Multivariable Process Control Model Example

This section is concerned with multivariable control of a plant consisting of a cylindrical tank containing a water column pressurized by air. This example comes from [10, 11] wherein the authors developed a multivariable predictive control strategy with a variable receding horizon.

The process control model consists of a cylindrical tank which contains a water column pressurized by air. Figure 4.26 is a simplified process diagram. A centrifugal pump feeds water into the tank through the pneumatic valve 1, and a compressor feeds air through the pneumatic valve 2. Liquid can drain from the tank through the manual valve 3 while air can exit through the relief valve 4. Measurements of the process output—the height of the liquid column y_1 and the gauge pressure of the enclosed air y_2—are obtained by means of pressure transducers. Valves 1 and 2 are manipulated through electro-pneumatic transducers by voltage signals u_1 and u_2. The height of the tank is 105 cm and the diameter is 7.5 cm.

The dynamics of the process control model can be described in terms of four states. Let x_1 denote the liquid-level height [m], x_2 the air pressure inside the column

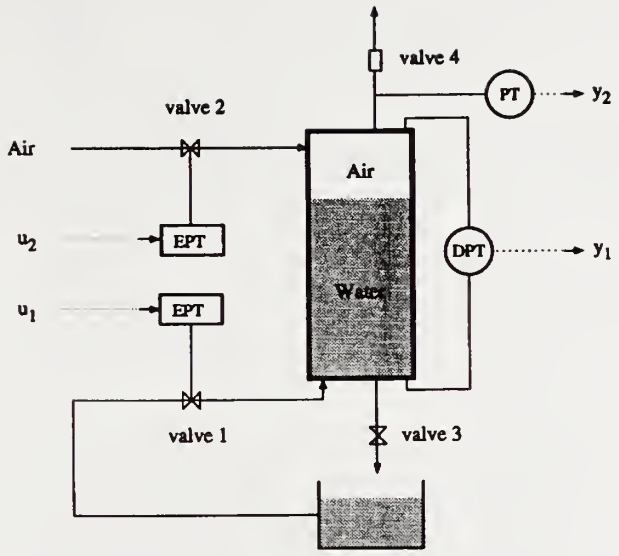

Figure 4.26: The Multivariable Process Control Model with inputs: valve signals u_1 and u_2; with outputs: liquid level y_1 and the air pressure y_2.

[bar gauge], x_3 the opening of water valve 1 (lift) [dimensionless], and x_4 the opening of air valve 2 (lift) [dimensionless]. The equations of motion of the process control model are given by:

$$\dot{x}_1 = \frac{1}{\mathrm{S}}(q_{lf} - q_{ld}) \tag{4.39}$$

$$\dot{x}_2 = \frac{1 + x_2}{\mathrm{S}(L - x_1)}[(q_{lf} - q_{ld}) + (q_{gf} - q_{gd})] \tag{4.40}$$

$$\dot{x}_3 = \frac{1}{\tau_l}(g_l u_1 - x_3) \tag{4.41}$$

$$\dot{x}_4 = \frac{1}{\tau_g}(g_g u_2 - x_4) \tag{4.42}$$

where L is the height of the column and S is the cross-sectional area of the column. The volumetric flow rates of the liquid feed and liquid discharge streams are represented by the variables q_{lf} and q_{ld}, respectively; and the gas feed and gas discharge rates by the variables q_{gf} and q_{gd}, respectively.

The liquid and air flow rates are modeled using a steady-state relationships appropriate for the square-root and equal-percentage characteristics of the valves

used in the process control model:

$$q_{lf} = x_3 K_{lf} \sqrt{p_{lf} - x_2 - \rho_l G(x_1 + \Delta L')} \tag{4.43}$$

$$q_{ld} = x_{ld} K_{ld} \sqrt{x_2 + \rho_l G(x_1 + \Delta L'')} \tag{4.44}$$

$$q_{gf} = x_4 K_{gf} (p_{gf} - x_2)^{0.65} \tag{4.45}$$

$$q_{gd} = K_{gd} \sqrt{x_2} \tag{4.46}$$

where the constants K_{ij} represent the valve coefficients, G is the acceleration of gravity, ρ_l is density of the liquid, p_{gf} is the inlet pressure of the air, p_{lf} is the inlet pressure of the liquid, $\Delta L'$ is the height difference between valve 1 and the bottom of the column, and $\Delta L''$ is the height difference between valve 3 and the bottom of the column. Specific values and definitions of all the multivariable process control model parameters are given in Table 4.6. The states and inputs must satisfy the constraints

$$\begin{bmatrix} 0 \\ 0 \\ 0 \\ 0 \end{bmatrix} \leq \begin{bmatrix} x_1 \\ x_2 \\ x_3 \\ x_4 \end{bmatrix} \leq \begin{bmatrix} \bar{x}_1 \\ \bar{x}_2 \\ 1 \\ 1 \end{bmatrix}, \qquad \begin{bmatrix} 0 \\ 0 \end{bmatrix} \leq \begin{bmatrix} u_1 \\ u_2 \end{bmatrix} \leq \begin{bmatrix} \bar{u}_1 \\ \bar{u}_2 \end{bmatrix} \tag{4.47}$$

where $\bar{u}_1 = \bar{u}_2 = 10$[V] (the maximum signal voltage) and $\bar{x}_1$ and $\bar{x}_2$ are bounds established by the user. The bounds of the output vector are identical to those of the states x_1 and x_2 because $y_1 = x_1$ and $y_2 = x_2$.

Table 4.6: The Multivariable Process Control Model Parameters

Parameter	Value	Parameter	Value
S	0.0043 m^2	K_{ld}	4.0×10^{-4} $m^3 \cdot s^{-1} \cdot \sqrt{bar}$
L	1.05 m	K_{lf}	6.9×10^{-4} $m^3 \cdot s^{-1} \cdot \sqrt{bar}$
$\Delta L'$	0.16 m	K_{gd}	9.8×10^{-4} $m^3 \cdot s^{-1} \cdot \sqrt{bar}$
$\Delta L''$	0.40 m	K_{gf}	3.1×10^{-4} $m^3 \cdot s^{-1} \cdot \sqrt{bar}$
p_{lf}	0.5 bar	τ_l	1.5 s
ρ_l	1.0×10^3 $kg \cdot m^{-3}$	g_l	0.1 V^{-1}
p_{gf}	0.4 bar	τ_g	0.3 s
		g_g	0.1 V^{-1}

The equations of motion are discretized using first order Euler integration. Let $x_k = [x_{1_k}\ x_{2_k}\ x_{3_k}\ x_{4_k}]'$. Equations (4.39) through (4.42) take the following form:

$$x_{k+1} = f(x_k) + \begin{bmatrix} g_1(x_k) & g_2(x_k) \end{bmatrix} \cdot \begin{bmatrix} u_{1_k} \\ u_{2_k} \end{bmatrix} \tag{4.48}$$

$$\begin{bmatrix} y_{1_k} \\ y_{2_k} \end{bmatrix} = \begin{bmatrix} 1 & 0 & 0 & 0 \\ 0 & 1 & 0 & 0 \end{bmatrix} \cdot x_k \tag{4.49}$$

where $x_k \in \Re^4$, and f, g_1, g_2 are vector fields on $\Re^4$. The system $\Sigma: \mathcal{D} \rightarrow S(\Re^2)$: $u_C \mapsto y$ of interest, where $\mathcal{D} \subset S(\Re^2)$, is the composition of the equations of motion with the input/states constraints for which u_C is the voltage command signals u_1 and u_2. Figure 4.27 shows the block diagram of the system Σ.

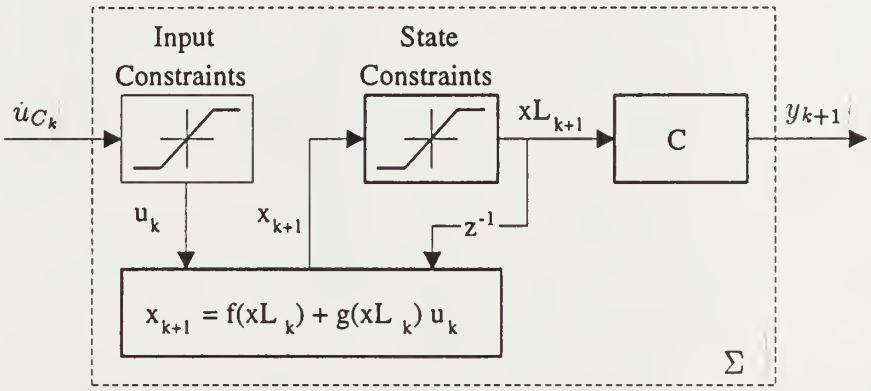

Figure 4.27: The block diagram of the system $\Sigma: \mathcal{D} \rightarrow S(\Re^2)$: $u_C \mapsto y$ for the Multivariable Process Control Model Example.

4.5.1 Simulation

The signals of interest are the liquid-level height y_1 and the gauge pressure y_2 of the enclosed air. The bounds of (4.47) have been set to $\bar{x}_1 = 0.75$ m and $\bar{x}_2 = 0.30$ bar. It is assumed that all signals of interest start at their midpoints (i.e., $y_{1_n} = 0.375$ m and $y_{2_n} = 0.15$ bar for all $n \leq n_0$). From [11], the time constant of the liquid-level y_1 (under zero gauge-pressure of air) varies from 50–70 s and the time constant of the air pressure y_2 is 1.3 s. The bandwidth of y_1 was set at 0.3 rad/sec to stress an approximate right inverse system Ψ while the bandwidth of y_2 was set at 1/1.3 rad/sec.

The set $\mathcal{D}_S \subset S(\Re^2)$ is defined with initial conditions $y_{1_i} = 0.375$ and $y_{2_i} = 0.15$ for all $i \leq 0$, and with $|y_{1_i} - 0.375| \leq 0.357$ and $|y_{2_i} - 0.15| \leq 0.1428$, for all $i > 0$. The domain $\mathcal{D}_\Psi \subset S(\Re^2)$ of an approximate right inverse system Ψ takes the sequences of $\mathcal{D}_S$'s components 1 and 2 that are passed through a second order discrete-time low pass filter with cutoff frequencies 0.3 and 1/1.3 rad/sec, respectively. The outputs of the filters 1 and 2 are then clipped by $[0.0, 0.75]$ and $[0.0, 0.30]$, respectively.

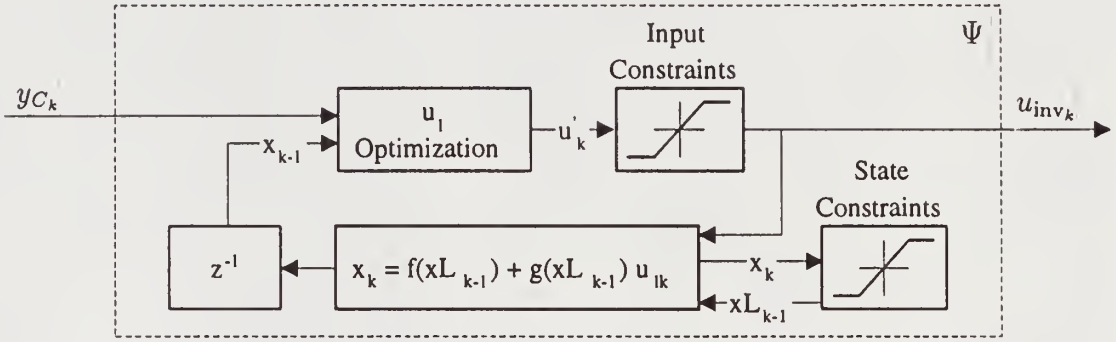

Figure 4.28: The block diagram of an approximate right inverse system $\Psi: \mathcal{D}_\Psi \rightarrow S(\Re^2) : y_C \mapsto u_{\text{inv}}$ with design integer $\lambda = 2$ for the Multivariable Process Control Model Example.

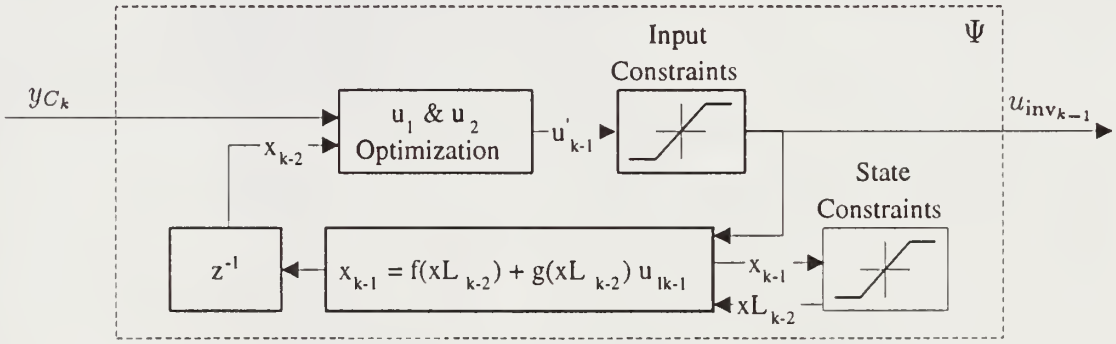

Figure 4.29: The block diagram of an approximate right inverse system $\Psi: \mathcal{D}_\Psi \rightarrow S(\Re^2) : y_C \mapsto u_{\text{inv}}$ with design integer $\lambda = 3$ for the Multivariable Process Control Model Example.

The block diagrams of approximate right inverse systems $\Psi: \mathcal{D}_\Psi \rightarrow S(\Re^2)$: $y_C \mapsto u_{\text{inv}}$ with design integers $\lambda = 2$ and $\lambda = 3$ are shown in Figure 4.28 and

Figure 4.29, respectively. Two integrations of u_1 are required to reach y_1 and similarly for u_2 and y_2. Two integrations of u_1 are also required to reach y_2 but three integrations of u_2 are required to reach y_1.

For the design integer $\lambda = 2$ case, the system Ψ is causal. The u_1 optimization block in Figure 4.28 optimizes u_{1_k} to give a minimum value of $|y_{C_k} - D^{-2}\Sigma\Psi(y_{C_k})|$ each step. For the design integer $\lambda = 3$ case, the system Ψ is strictly causal. The u_1 and u_2 optimization block in Figure 4.29 optimizes u_{1_k} and u_{2_k} to give a minimum value of $|y_{C_k} - D^{-3}\Sigma\Psi(y_{C_k})|$ each step. The procedure involves undertaking a u_{2_k} optimization if the u_{1_k} optimization fails so as to reduce the error $|y_{C_k} - D^{-3}\Sigma\Psi(y_{C_k})|$. The signal u_{2_k} is optimized to give a minimum value of $|y_{C_{k+1}} - D^{-3}\Sigma\Psi(y_{C_{k+1}})|$ provided the result does not augment the error $|y_{C_k} - D^{-3}\Sigma\Psi(y_{C_k})|$.

For the simulation of 60 seconds, a sampling period of 150 milli-seconds yields a two-dimensional sequence of 400 points. The pre-filtered binary random sequences $\{y_{1C_k}\}$ only have values of 0.018, 0.0732 m for $k \geq 1$, and the pre-filtered binary random sequences $\{y_{2C_k}\}$ only have values of 0.0072, 0.2928 bar for $k \geq 1$ because we are only interested in extreme points of $\mathcal{D}_S$. Table 4.7 shows the Monte Carlo results for 2 different design integers λ of the system Ψ: $\lambda = 2$ and $\lambda = 3$ where the error $|y_C - D^{-\lambda}\Sigma\Psi(y_C)|$ is evaluated for each of the sequences. Also included in Table 4.7 is the average number of floating point operations (flops) per Monte Carlo sequence run for the u_1 optimization block and for the u_1 and u_2 optimization block. On the average the u_1 and u_2 optimization subroutine requires $3\times$ greater the number of flops as the u_1 optimization subroutine, but a single execution of the u_1 and u_2 subroutine can require $4^+\times$ greater the number of flops than the u_1 subroutine.

4.5.2 The Estimate of the Performance Bound $\tilde{\mathcal{P}}(\Sigma)$

In this section, we will find an estimate of the performance bound $\tilde{\mathcal{P}}(\Sigma)$ for the multivariable process control problem of a regulator that regulates the liquid level

Table 4.7: Family of Sequences, $\mathcal{D}_\Psi$, Comparison

	Error $\lvert y_C - D^{-\lambda}\Sigma\Psi(y_C)\rvert$		Average Number of Flops	
Sequence	$\lambda = 2$	$\lambda = 3$	$\lambda = 2$	$\lambda = 3$
1	0.02481	0.02190	137.0	367.8
2	0.03742	0.03138	140.3	449.3
3	0.01584	0.01506	142.5	396.0
4	0.05440	0.04699	150.0	432.7
5	0.02408	0.02255	135.5	447.5
6	0.02064	0.01732	137.3	441.0
7	0.02147	0.01917	136.1	379.4
8	0.02613	0.02389	140.9	426.5
9	0.01185	0.01124	135.5	401.5
10	0.00601	0.00589	139.7	374.2
11	0.02080	0.02089	144.9	459.0
12	0.03080	0.02840	137.0	439.1
13	0.01270	0.01113	139.1	404.9
14	0.02746	0.02446	135.5	456.5
15	0.03962	0.03634	144.0	513.7
16	0.02189	0.01942	140.3	413.9
17	0.01852	0.01713	134.6	454.2
18	0.01745	0.01819	136.1	467.9
19	0.01757	0.01527	138.5	441.9
20	0.01637	0.01393	143.1	399.8
21	0.03920	0.03406	144.6	435.2
22	0.03529	0.02838	138.2	418.2
23	0.01935	0.01764	140.9	464.1
24	0.01943	0.01733	138.5	420.2
25	0.01594	0.01466	139.4	393.5
max	0.0544	0.04699	150.0	513.7
min			134.6	367.8
mean			139.6	427.9
st dev			3.703	33.90

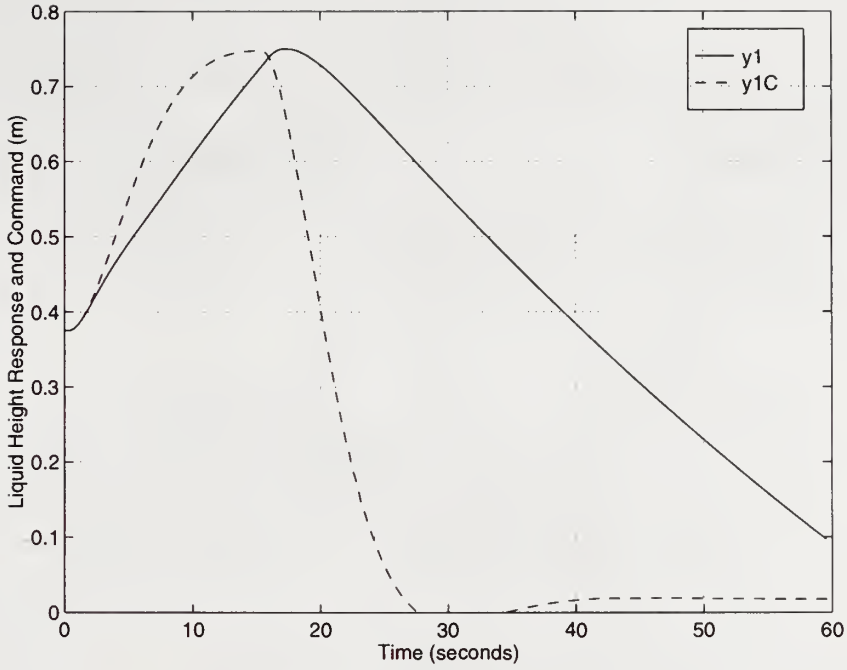

Figure 4.30: For $\lambda = 2$, the liquid height response $y_1 = D^{-2}\Sigma\Psi(y_{1C})$ and the command $y_{1C} \in \mathcal{D}_\Psi$ are shown for the square wave optimization ($N_{1_1} = 104$, $N_{1_2} = 103$).

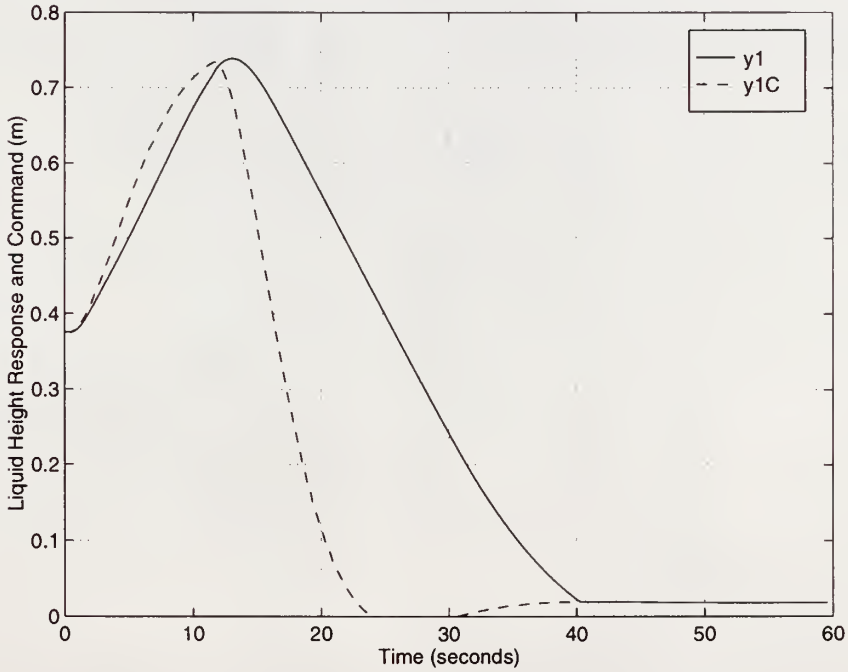

Figure 4.31: For $\lambda = 3$, the liquid height response $y_1 = D^{-3}\Sigma\Psi(y_{1C})$ and the command $y_{1C} \in \mathcal{D}_\Psi$ are shown for the square wave optimization ($N_{1_1} = 78$, $N_{1_2} = 73$).

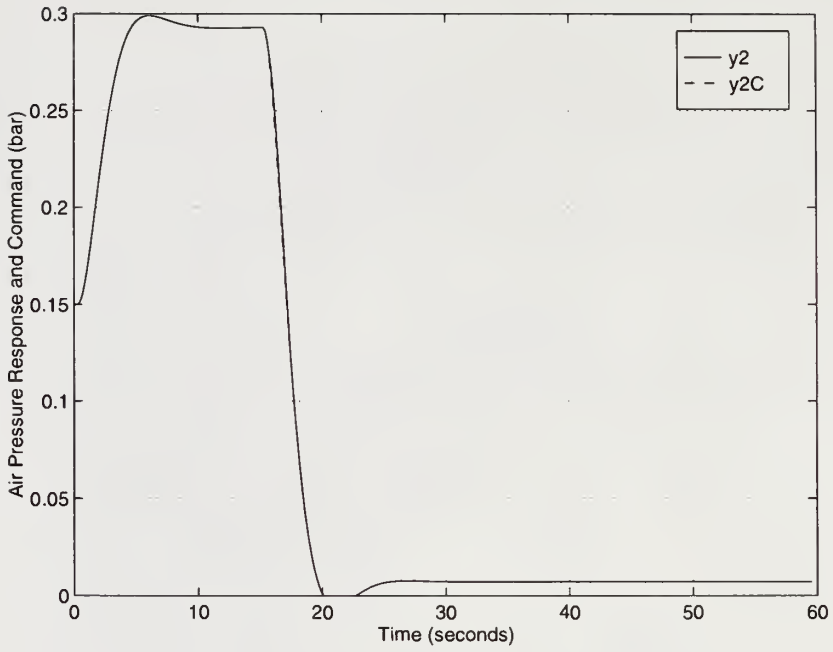

Figure 4.32: For $\lambda = 2$, the air pressure response $y_2 = D^{-2}\Sigma\Psi(y_{2C})$ and the command $y_{2C} \in \mathcal{D}_\Psi$ are shown for the square wave optimization ($N_{1_1} = 104$, $N_{1_2} = 103$).

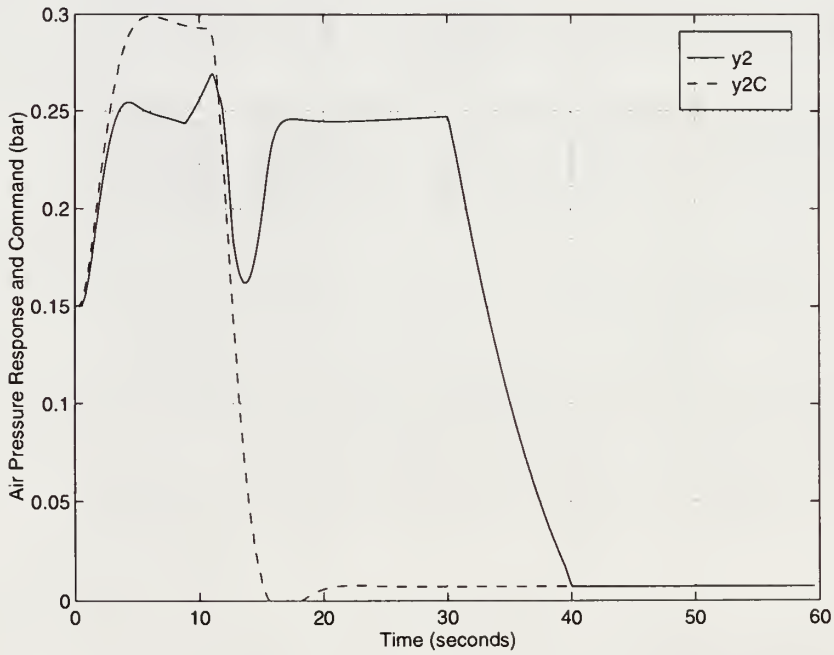

Figure 4.33: For $\lambda = 3$, the air pressure response $y_2 = D^{-3}\Sigma\Psi(y_{2C})$ and the command $y_{2C} \in \mathcal{D}_\Psi$ are shown for the square wave optimization ($N_{1_1} = 78$, $N_{1_2} = 73$).

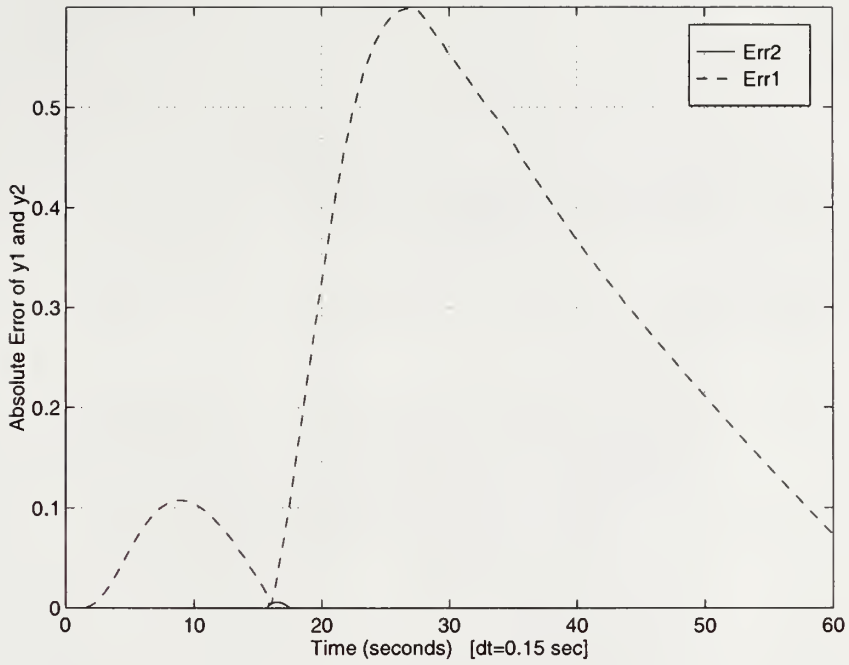

Figure 4.34: For $\lambda = 2$, the absolute errors, $|y_{1C_k} - D^{-2}\Sigma\Psi(y_{1C_k})|$ and $|y_{2C_k} - D^{-2}\Sigma\Psi(y_{2C_k})|$, are shown for the square wave optimization ($N_{1_1} = 104$, $N_{1_2} = 103$) of $y_C \in \mathcal{D}_\Psi$ where $\tilde{\mathcal{P}}(\Sigma) = 0.5983$ and $|y_{2C} - D^{-2}\Sigma\Psi(y_{2C})| = 0.0059$.

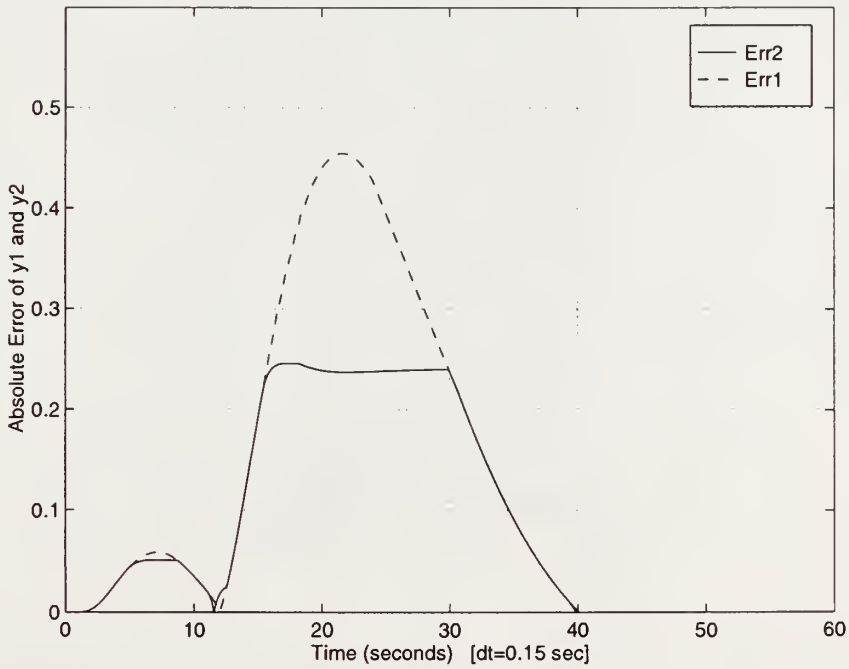

Figure 4.35: For $\lambda = 3$, the absolute errors, $|y_{1C_k} - D^{-3}\Sigma\Psi(y_{1C_k})|$ and $|y_{2C_k} - D^{-3}\Sigma\Psi(y_{2C_k})|$, are shown for the square wave optimization ($N_{1_1} = 78$, $N_{1_2} = 73$) of $y_C \in \mathcal{D}_\Psi$ where $\tilde{\mathcal{P}}(\Sigma) = 0.4544$ and $|y_{2C} - D^{-3}\Sigma\Psi(y_{2C})| = 0.2495$.

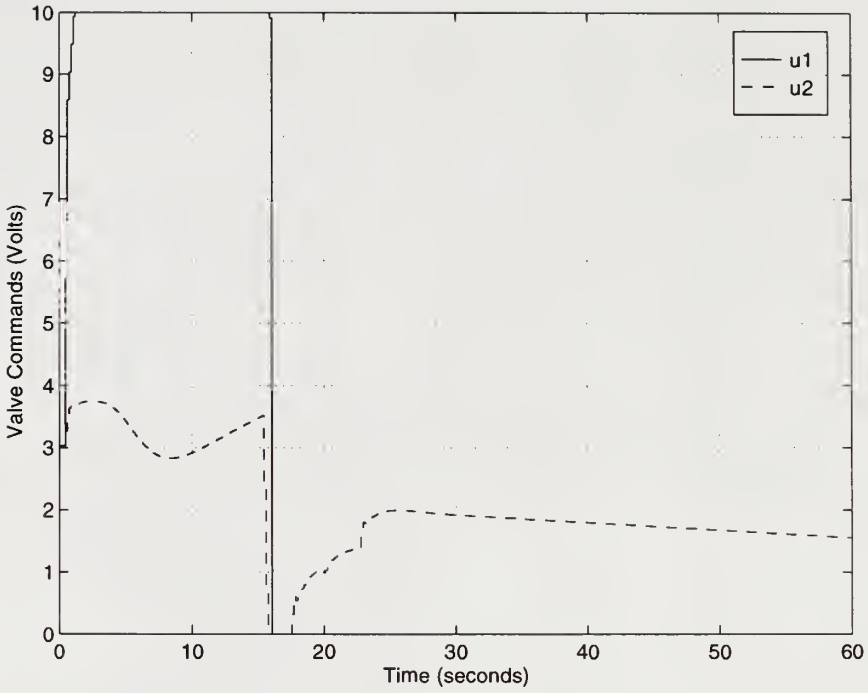

Figure 4.36: For $\lambda = 2$, the valve commands u_1 and u_2 are shown for the square wave optimization ($N_{1_1} = 104$, $N_{1_2} = 103$) of $y_C \in \mathcal{D}_\Psi$.

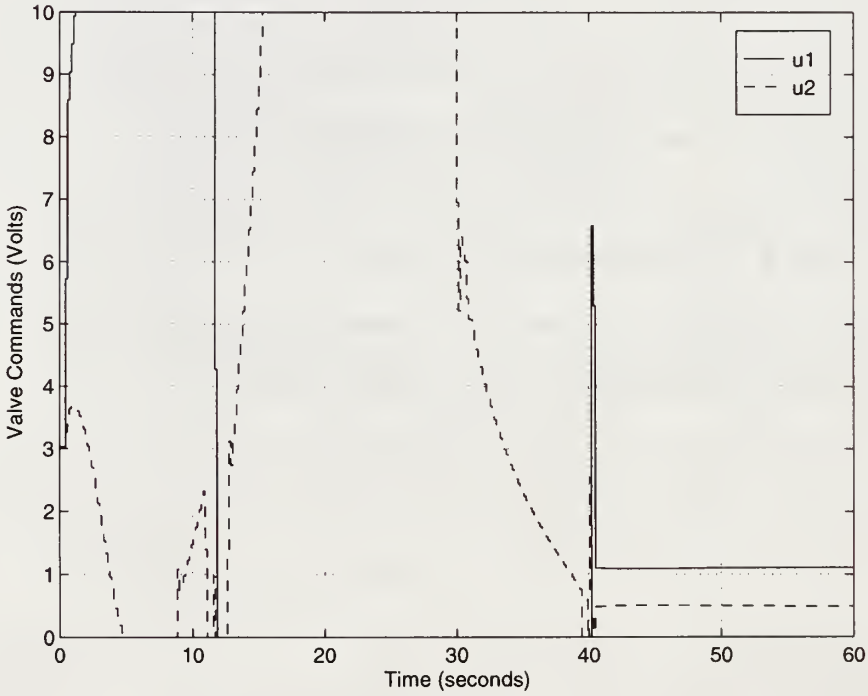

Figure 4.37: For $\lambda = 3$, the valve commands u_1 and u_2 are shown for the square wave optimization ($N_{1_1} = 78$, $N_{1_2} = 73$) of $y_C \in \mathcal{D}_\Psi$.

in a pressurized tank by using the optimization definition as follows:

$$\tilde{\mathcal{P}}(\Sigma) = \sup_{y_C \in \mathcal{D}_\Psi} \left| y_C - D^{-\lambda}\Sigma\Psi(y_C) \right| \tag{4.50}$$

where the system Σ and an approximate right inverse system Ψ with design integers λ: 2 and 3 are illustrated in Figure 4.27, Figure 4.28, and Figure 4.29, respectively.

In Section 4.4.2, a nonlinear programming algorithm was developed to calculate the estimate of the performance bound $\tilde{\mathcal{P}}(\Sigma)$. It exploits the traits of the system. Due to the sluggishness of the liquid height response, only one transition was needed from high to low in both components of the signal y_C. The transition is at N_{1_1} steps for y_{1C} and N_{1_2} steps for y_{2C}. The results of the nonlinear programming algorithm are shown in Table 4.8 and Figures 4.30–4.37.

Table 4.8: The Estimate of the Performance Bound $\tilde{\mathcal{P}}(\Sigma)$ for the Multivariable Process Control Model Example

Design Integer	Parameters (N_{1_1}, N_{1_2})	$\lvert y_C - D^{-\lambda}\Sigma\Psi(y_C)\rvert$ for $y_C \in \mathcal{D}_\Psi$
$\lambda = 2$	$(104, 103)$	$\tilde{\mathcal{P}}(\Sigma) = 0.5983$
$\lambda = 3$	$(78, 73)$	$\tilde{\mathcal{P}}(\Sigma) = 0.4544$

Figure 4.30 and Figure 4.31 represent the optimal liquid height response and command for $\lambda = 2$ and $\lambda = 3$, respectively. The u_1 and u_2 subroutine improves the liquid height response for $\lambda = 3$, at the expense of the air pressure response. Figure 4.32 and Figure 4.33 represent the optimal air pressure response and command for $\lambda = 2$ and $\lambda = 3$, respectively. The u_1 and u_2 subroutine increases the air pressure to help drain the tank while the u_1 subroutine is operating with near zero gauge pressure on y_1 which has a time constant between 50–70 s.

The optimal absolute error sequences are plotted in Figure 4.34 and Figure 4.35 for $\lambda = 2$ and $\lambda = 3$, respectively. In the u_1 & u_2 subroutine, the signal u_{2_k}

is optimized to give a minimum value of $|y_{C_{k+1}} - D^{-3}\Sigma\Psi(y_{C_{k+1}})|$ provided the error $|y_{C_k} - D^{-3}\Sigma\Psi(y_{C_k})|$ does not augment. In the process, the error $|y_{2C_k} - D^{-3}\Sigma\Psi(y_{2C_k})|$ is augmented but never above the value of the error $|y_{1C_k} - D^{-3}\Sigma\Psi(y_{1C_k})|$ which is evident in Figure 4.35. The optimal valve commands u_1 and u_2 are plotted in Figure 4.36 and Figure 4.37 for $\lambda = 2$ and $\lambda = 3$, respectively. For $\lambda = 2$, the signal u_1 is constrained throughout most of the simulation while for $\lambda = 3$ the signal u_2, which influences y_1 in three steps, is optimally used to reduce the error $|y_{1C_k} - D^{-3}\Sigma\Psi(y_{1C_k})|$.

CHAPTER 5
CONCLUSION

5.1 Summary

This dissertation presents new results for the problem of disturbance attenuation for nonlinear control systems. Of primary significance is the derivation of a performance bound that provides a measure of the ability to match a set by subset of the image of a system. Our bound arose from the desire of providing an estimate of the minimal effect of the disturbance signal d on the output signal z of Figure 1.1.

It turns out that the calculation of the performance bound is rather laborious because its definition (Definition 3.4.1) uses $\mathrm{Im}\,\Sigma$. In practice, we will find an estimate of the performance bound that uses an approximate right inverse system in its calculation instead of $\mathrm{Im}\,\Sigma$. The estimate of the performance bound involves an optimization problem which relates to finding a global maximum of a non-convex function. Nonlinear programming is used to calculate the estimate of the performance bound.

Three systems of practical origin were selected for the analysis of the performance bound. In the PM stepper motor example, a closed form estimate of the performance bound was found which was verified by simulation. In the aerodynamic model example, a nonlinear programming algorithm was determined to compute the estimate of the performance bound. The multivariable process model example provided us insight into how different design integers can influence the estimate of the performance bound.

5.2 Future Directions

The results of this dissertation serve to enhance many of the tools used to obtain the optimal controller for nonlinear control systems. In the process of completing one particular objective, other promising areas frequently appear as directions for additional research. One of the more intriguing of such areas emerging from this work is the derivation of a bound that handles constant bias disturbances.

Referring to Figure 1.1, and using the parameterization (1.3) with the assumption that the system Σ is stable (i.e., $P = \Sigma$ and $Q = I$), we get

$$\Sigma_C(v, d) = d + \Sigma\phi(v, d). \tag{5.1}$$

The stable and causal system ϕ is selected such that

$$\phi(v, d) = \Psi\left(\Sigma v - d\right) \tag{5.2}$$

where Ψ is an approximate right inverse system. All that is needed to define a performance bound is an optimization set. In this case, the optimization set is the image of $[\Sigma v - d]$ where the domain of $[\Sigma v - d]$ is a bounded set. The performance bound is given by

$$\mathcal{P}(\Sigma) = \varrho_\epsilon\left(\mathrm{Im}\,[\Sigma v - d],\ D^{-\lambda}\mathrm{Im}\,\Sigma\right). \tag{5.3}$$

The bound of (5.3) is a theoretical estimate of the minimal effect of the disturbance d on the output z.

Let's use $\lambda = 0$ initially in the bound optimization problem. Note that there is another λ associated with the approximate inverse optimization problem. Both are equal for most applications. In this application the design integer λ will be associated with an approximate inverse and $\lambda \geq 0$. Now we need to modify our definition of the norm ρ_ϵ for the bound. For a sequence $u \in S(\Re^m)$ and for a $j \geq 0$, the norm $\rho_{\epsilon,j}$ is defined

$$\rho_{\epsilon,j}(u) \stackrel{\text{def}}{=} \sup_{i \geq j} (1+\epsilon)^{-i}\,|u_i|, \quad \epsilon > 0. \tag{5.4}$$

The class of disturbances is a constant bias; i.e., the magnitude of the disturbance is unknown, but it is constant (i.e., a step disturbance). Let us define our performance bound for $\lambda = 0$, denoted by $\mathcal{R}(\Sigma)$, such that

$$\mathcal{R}(\Sigma) \stackrel{\text{def}}{=} \inf \sup \rho_{\epsilon,\lambda} \left(d + \Sigma\phi(v,d) - \Sigma v \right) \tag{5.5}$$

where Σv is our desired response. The supremum is over the input signal space and the infimum is over the stable and causal systems ϕ. The stable and causal system ϕ can be chosen as

$$\phi(v,d) = \Psi \left(D^{-\lambda}\Sigma v - d \right) \tag{5.6}$$

where the design integer $\lambda \geq 0$ of an approximate right inverse system Ψ is the least latency of the system Σ.

It will be shown that the bound $\mathcal{R}(\Sigma)$ is well suited for a constant bias disturbance d. If the system Ψ were a right inverse of the system Σ, then $\Sigma\Psi = D^{\lambda}I$. Let us substitute (5.6) into (5.5), we get

$$\begin{aligned}
\mathcal{R}(\Sigma) &= \sup \rho_{\epsilon,\lambda} \left(d + \Sigma\Psi \left(D^{-\lambda}\Sigma v - d \right) - \Sigma v \right) \\
&= \sup \rho_{\epsilon,\lambda} \left(d + D^{\lambda} I \left(D^{-\lambda}\Sigma v - d \right) - \Sigma v \right) \\
&= \sup \rho_{\epsilon,\lambda} \left(d + \left(\Sigma v - D^{\lambda} d \right) - \Sigma v \right) \\
&= \sup \rho_{\epsilon,\lambda} \left(d - D^{\lambda} d \right) \\
\mathcal{R}(\Sigma) &= 0
\end{aligned}$$

where the supremum is taken over the input signal space.

The bound $\mathcal{R}(\Sigma)$ can be calculated using techniques of Chapter 4. The optimization set is the image of $[D^{-\lambda}\Sigma v - d]$ where the domain of $[D^{-\lambda}\Sigma v - d]$ is a bounded set. For the PM stepper motor example, the estimate of the performance bound $\tilde{\mathcal{P}}(\Sigma)$ of (4.26) turns out to be the performance bound $\mathcal{R}(\Sigma)$ because the performance bound for this problem is independent of the optimization set. Thus

$$\mathcal{R}(\Sigma) = \frac{60}{2\pi} \frac{K_m}{G \cdot L \cdot J} \Delta t^2 \tag{5.7}$$

for the PM stepper motor example.

Throughout this dissertation, no new results were found for the design of the equivalent controller C of Figure 1.1 because the results from [22] were sufficient. In this emerging area of of deriving a performance bound $\mathcal{R}(\Sigma)$ to handle a constant bias, attention should be given to the controllers that implement the new control laws. There will be other performance requirements in addition to the bound requirement, and so the performance index will be augmented to include additional variables.

REFERENCES

[1] M. A. Armstrong, *Basic Topology.* New York: Springer-Verlag, 1983.

[2] K. J. Åstrom and B. J. Wittenmark, *Adaptive Control*, Second Edition. New York: Addison-Wesley Publishing Company, 1995.

[3] M. S. Bazaraa, H. D. Sherali and C. M. Shetty, *Nonlinear Programming: Theory and Algorithms.* New York: John Wiley & Sons, Inc., 1993.

[4] J. H. Blakelock, *Automatic Control of Aircraft and Missiles*, Second Edition. New York: John Wiley & Sons, Inc., 1991.

[5] M. Bodson, J. N. Chiasson, R. T. Novotnak and R. B. Rekowski, "High-performance nonlinear feedback control of a permanent magnet stepper motor", *IEEE Transactions on Control Systems Technology*, Vol. 1, No. 1, pp. 5–14, 1993.

[6] E. W. Cheney, *Introduction to Approximation Theory*, Second Edition. New York: Chelsea Publishing Company, 1982.

[7] R. J. P. de Figueiredo and G. Chen, *Nonlinear Feedback Control Systems: an Operator Theory Approach.* New York: Academic Press, Inc., 1993.

[8] C. A. Desoer and W. S. Chan, "The feedback interconnection of lumped linear time-invariant system", *Journal of The Franklin Institute*, Vol. 300, No. 5 & 6, pp. 335–351, 1975.

[9] D. S. Dummit and R. M. Foote, *Abstract Algebra.* Englewood Cliffs, NJ: Prentice Hall, 1991.

[10] M. A. Eggiman, O. D. Crisalle and R. Longchamp, "A linear-programming predictive controller with variable horizon" in *Proc. 1992 Amer. Contr. Conf.*, Chicago, IL, pp. 1568–1575, 1992.

[11] M. A. Eggiman, O. D. Crisalle and R. Longchamp, "Design of a multivariable linear-programming predictive controller with variable receding horizon" submitted for publication in *Journal of Process Control.*

[12] B. Etkin, *Dynamics of Flight: Stability and Control.* New York: John Wiley & Sons, Inc., 1982.

[13] M. W. Hirsch and S. Smale, *Differential Equations, Dynamical Systems and Linear Alegebra.* New York: Academic Press, Inc., 1974.

[14] J. Hammer, "Nonlinear systems: stability and rationality", *International Journal of Control*, Vol. 40, No. 1, pp. 1–35, 1984.

[15] J. Hammer, "On nonlinear systems, additive feedback, and rationality", *International Journal of Control*, Vol. 40, No. 5, pp. 953–969, 1984.

[16] J. Hammer, "Nonlinear systems, stabilization and coprimeness", *International Journal of Control*, Vol. 42, No. 1, pp. 1–20, 1985.

[17] J. Hammer, "Stabilization of nonlinear systems", *International Journal of Control*, Vol. 44, No. 5, pp. 1349–1381, 1986.

[18] J. Hammer, "Fraction representation of nonlinear systems: a simplified approach", *International Journal of Control*, Vol. 46, No. 2, pp. 455–472, 1987.

[19] J. Hammer, "Assignment of dynamics for nonlinear recursive feedback systems", *International Journal of Control*, Vol. 48, No. 3, pp. 1183–1212, 1988.

[20] J. Hammer, "Robust stabilization of nonlinear systems", *International Journal of Control*, Vol. 49, No. 2, pp. 629–653, 1989.

[21] J. Hammer, "Fraction representations of nonlinear systems and non-additive state feedback", *International Journal of Control*, Vol. 50, No. 5, pp. 1981–1990, 1989.

[22] J. Hammer, "Internally stable nonlinear systems with disturbance: A parameterization", *IEEE Transactions on Automatic Control*, Vol. 39, No. 2, pp. 300–314, 1994.

[23] A. Isidori, *Nonlinear Control Systems*, Third Edition. New York: Springer-Verlag, 1995.

[24] T. Kenjo, *Stepping motors and their microprocessor control.* New York: Oxford University Press, 1984.

[25] H. K. Khalil, *Nonlinear Systems*, Second Edition. New York: Macmillan Publishing Company, 1996.

[26] A. N. Kolmogorov and S. V. Fomin, *Introductory Real Analysis.* New York: Dover Publications, Inc., 1975.

[27] K. Kuratowski, *Introduction to Set Theory and Topology.* New York: Pergamon Press, 1972.

[28] S. Mac Lane and G. Birkhoff, *Algebra*, Third Edition. New York: Chelsea Publishing Company, 1993.

[29] O. L. Mangasarian, *Nonlinear Programming.* Philadelphia: Society for Industrial and Applied Mathematics, 1994.

[30] D. McLean, *Automatic Flight Control Systems.* Englewood Cliffs, NJ: Prentice Hall, 1990.

[31] D. McRuer, I. Ashkenas and D. Graham, *Aircraft Dynamics and Automatic Control.* Princeton, NJ: Princeton University Press, 1973.

[32] J. R. Munkres, *Topology: A First Course.* Englewood Cliffs, NJ: Prentice Hall, 1975.

[33] R. C. Nelson, *Flight Stability and Automatic Control.* New York: McGraw-Hill, Inc., 1989.

[34] H. Nijmeijer and A. J. van der Schaft, *Nonlinear Dynamical Control Systems.* New York: Springer-Verlag, 1990.

[35] R. J. Norris, *Analysis of multivariable control systems in the presence of structured uncertainties.* Ph.D. thesis, University of Florida, Gainesville, 1990.

[36] A. D. B. Paice and J. B. Moore "Robust stabilization of nonlinear plants via left coprime factorizations", *Systems & Control Letters*, Vol. 15, No. 2, pp. 125–135, 1990.

[37] T. J. Rivlin, *An Introduction to the Approximation of Functions.* New York: Dover Publications, Inc., 1969.

[38] R. T. Rockafellar, *Convex Analysis.* Princeton, NJ: Princeton University Press, 1970.

[39] H. H. Rosenbrock, *State-space and Multivariable Theory.* New York: John Wiley & Sons, Inc., 1970.

[40] H. L. Royden, *Real Analysis.* New York: The Macmillan Company, 1963.

[41] W. Rudin, *Functional Analysis.* New York: McGraw-Hill, Inc., 1973.

[42] W. Rudin, *Principles of Mathematical Analysis.* New York: McGraw-Hill, Inc., 1976.

[43] G. Tao and P. V. Kokotović, "Adaptive control of plants with unknown deadzones", *IEEE Transactions on Automatic Control*, Vol. 39, No. 1, pp. 59–68, 1994.

[44] G. Tao and P. V. Kokotović, *Adaptive Control of Systems with Acutator and Sensor Nonlinearity.* New York: John Wiley & Sons, Inc., 1996.

[45] J. van Tiel, *Convex Analysis: An Introductory Text.* New York: John Wiley & Sons, Inc., 1984.

[46] M. S. Verma and L. R. Hunt, "Right coprime factorizations and stabilization for nonlinear systems", *IEEE Transactions on Automatic Control*, Vol. 38, No. 2, pp. 222–231, 1993.

[47] M. Vidyasagar, *Nonlinear Systems Analysis*, Second Edition. Englewood Cliffs, NJ: Prentice Hall, 1993.

[48] G. Zames, "On the input-output stability of time-varying nonlinear feedback systems, Part I", *IEEE Transactions on Automatic Control*, Vol. AC-11, No. 2, pp. 228–238, 1966.

[49] G. Zames, "On the input-output stability of time-varying nonlinear feedback systems, Part II", *IEEE Transactions on Automatic Control*, Vol. AC-11, No. 3, pp. 465–476, 1966.

[50] G. Zames, "Feedback and optimal sensitivity: Model reference transformations, multiplicative seminorms, and approximate inverses", *IEEE Transactions on Automatic Control*, Vol. AC-26, No. 2, pp. 301–320, 1981.

BIOGRAPHICAL SKETCH

Rafael J. Fanjul Jr. was born in West Palm Beach, Florida, on May 28, 1963. He received his bachelor's degree in mechanical engineering from Georgia Institute of Technology in 1985. He then entered graduate school at Georgia Institute of Technology and received a master's degree in electrical engineering in 1986. From 1986 to 1992 he was employed by Martin Marietta, Orlando, Florida, as a guidance and control engineer. During his tenure at Martin Marietta, he attended night school at the University of Central Florida and received a master's degree in mathematical science in 1992. He has been a Professional Engineer in the State of Florida since September 1990. In August 1992, he was granted an educational leave of absence from Martin Marietta to pursue a doctoral degree. Since August 1992, he has been a Ph.D. student and pre-doctoral fellow at the University of Florida under the supervision of Professor J. Hammer.

I certify that I have read this study and that in my opinion it conforms to acceptable standards of scholarly presentation and is fully adequate, in scope and quality, as a dissertation for the degree of Doctor of Philosophy.

Jacob Hammer, Chairman
Professor of Electrical and Computer Engineering

I certify that I have read this study and that in my opinion it conforms to acceptable standards of scholarly presentation and is fully adequate, in scope and quality, as a dissertation for the degree of Doctor of Philosophy.

John M. M. Anderson
Assistant Professor of Electrical and Computer Engineering

I certify that I have read this study and that in my opinion it conforms to acceptable standards of scholarly presentation and is fully adequate, in scope and quality, as a dissertation for the degree of Doctor of Philosophy.

Oscar D. Crisalle
Associate Professor of Chemical Engineering

I certify that I have read this study and that in my opinion it conforms to acceptable standards of scholarly presentation and is fully adequate, in scope and quality, as a dissertation for the degree of Doctor of Philosophy.

Jose C. Principe
Professor of Electrical and Computer Engineering

I certify that I have read this study and that in my opinion it conforms to acceptable standards of scholarly presentation and is fully adequate, in scope and quality, as a dissertation for the degree of Doctor of Philosophy.

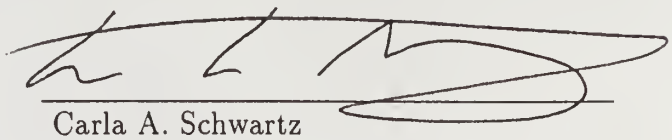

Carla A. Schwartz
Assistant Professor of Electrical and
Computer Engineering

This dissertation was submitted to the Graduate Faculty of the Department of Electrical and Computer Engineering in the College of Engineering and to the Graduate School and was accepted as partial fulfillment of the requirements for the degree of Doctor of Philosophy.

December 1996

Winfred M. Phillips
Dean, College of Engineering

Karen A. Holbrook
Dean, Graduate School